Uncertainty propagation and reliability-based design optimization of wind turbine tower

Hongbo Zhang

Normandie Université

Pour obtenir le diplôme de doctorat

Spécialité Mécanique

Préparée au sein de L'institut National des Sciences Appliquées de Rouen Normandie

Propagation D'incertitudes et Optimisation Fiabiliste D'une Tour D'éolienne.

Présentée et soutenue par
Hongbo ZHANG

Thèse soutenue publiquement le 8 Octobre 2020 devant le jury composé de		
M. GAYTON Nicolas	Professeur - INSTITUT PASCAL-SIGMA Clermont	Rapporteur
M. SCHOEFS Franck	Professeur - Université de NANTES - GeM	Rapporteur
Mme. AUTRIQUE Laurent	Professeur – Université d'Angers	Examinateur
M. BENNIS Fouad	Professeur - École Centrale Nantes	Examinateur
M. YASSINE Adnan	Professeur - Université Le Havre Normandie – LMAH	Examinateur
M. LEMOSSE Didier	Maître de conférences - INSA Rouen Normandie - LMN	Examinateur
M. AOUES Younes	Maître de conférences - INSA Rouen Normandie - LMN	Co-directeur de thèse
M. SOUZA DE CURSI Eduardo	Professeur - INSA Rouen Normandie - LMN	Directeur de thèse

Thèse dirigée par Eduardo SOUZA DE CURSI et Younes AOUES
Laboratoire de Mécanique de Normandie - INSA Rouen

UNIVERSITÉ DE ROUEN NORMANDIE

ED PSIME

LMN

Uncertainty Propagation and Reliability-based Design Optimization of Wind Turbine Tower

by

Hongbo ZHANG

Submitted in Partial Fulfillment of the

Requirements for the Degree

Doctor of Engineering

Supervised by Younes Aoues, Eduardo Souza de Cursi

Laboratoire de Mécanique de Normandie

Institut National des Sciences Appliquées de Rouen Normandie

Saint-Étienne-du-Rouvray, France

2020

May the winds guide you.

Que les vents vous guident.

Acknowledgments

First and foremost, I would like to express my sincere gratitude to China Scholarship Council (CSC) for its financial support during my study in France and to my supervisors: Professor Eduardo SOUZA DE CURSI, Dr. Younes AOUES, Dr. Didier LEMOSSE for their guidance, patience, and encouragements. Their rigorous and responsible attitude towards science and engineering researches will have a great influence in my future researches and daily lives. I've greatly benefited from my PhD study here in INSA-Rouen Normandie, that enhances my ability to think differently and carry out research works independently.

I would like to express my appreciation for my Chinese supervisor Professor Qiuhua Wan, Ms. Shujie Wang from University of Chinese Academy of Sciences, for their supports of my study in France.

I would also to thank my colleagues and friends in INSA-Rouen and CORIA, Changwu HUANG, Bo JIANG, Yahao CHEN, Zelong MA, Hao Bai and Wilson Javier Veloz Parra, for their help and friendship.

Lastly, I offer my sincere thanks to my family members, for their faith in me and encouragements on my study.

Abstract

Wind energy is one of the fastest-growing renewable technologies. The working environments of wind turbines are filled with uncertainties, for example, from foundation vibration, structure degradation, wind turbulence, or ocean waves for offshore wind turbines. Malfunctions or failures may occur during their serving time when facing these uncertainties. To address this problem, Uncertainty Quantification (UQ) and Machine Learning (ML) techniques are widely used for the evaluation of turbine performances. In this thesis, three parts of work are conducted: First, the uncertainty propagation of inflow winds to response loads on the tower is discussed using different surrogate models; Next, the Reliability-based Design Optimization (RBDO) of wind turbine tower is realized with a Kriging assisted Single Loop Approach (KSLA). Last, Time-variant Reliability Optimization (TvRBDO) methodology is achieved using a nested double-loop Kriging approach. The uncertainty propagation results have first shown the mean value and maximum value of response loads under Normal Turbulent Model (NTM) wind condition can be approximated respectively with Normal and Extreme distribution. Then 6 surrogate models are used for the uncertainty propagation of inflow wind, whose results demonstrate the adaptability of Kriging (KRG) surrogate. The results of RBDO using Kring-SLA (KSLA) show that the proposed method needs fewer sample points than other double-loop-based approaches. The accuracy of KSLA is at the same level as other First Order Reliability Methods (FORM). The results of TvRBDO validate the feasibility of the proposed method, after the inner-loop is built, the computational cost for optimization is minimum.

Keywords: Wind turbine energy, uncertainty propagation, machine learning techniques, time-variant reliability design optimization.

Résumé

L'éolien est l'une des énergies renouvelables à la croissance la plus rapide. L'environnement de travail des éoliennes est rempli d'incertitudes, par exemple, les vibrations des fondations, la dégradation de la structure de la turbine, le turbulence du vent. Des dysfonctionnements ou des pannes peuvent survenir durant leur temps de service en raison des incertitudes. Pour quantifier ces problèmes, les techniques de quanlification des incertitudes et d'apprentissage automatique sont largement utilisées pour l'évaluation des performances de l'éolienne. Dans cette thèse, trois parties du travail sont menées: Premièrement, la propagation de l'incertitude (UQ) du vent aux chargements des réponses est discutée en utilisant différents métamodèles; ensuite, l'optimisation, basée sur la fiabilité (RBDO), de la tour de l'éolienne est réalisée avec une approche en boucle-unique assistée par Krigeage. Enfin, la méthodologie d'optimisation de la fiabilité dépendant du temps (TvRBDO) est réalisée en utilisant une approche de Krigeages à double-boucle. Les résultats de l'UQ ont d'abord montré que la valeur moyenne et la valeur maximale des charges des réponses dans des conditions de vent de modèle turbulent normal peuvent être estimées, respectivement, par une distribution Normale et par une distribution Extrême. Les résultats démontrent l'adaptabilité du métamodèle de Krigeage. Les résultats de la RBDO utilisant Krigeage-SLA (KSLA) ont montré que la méthode proposée nécessite moins de points d'échantillonnage que les autres approaches à double boucle. La précision de KSLA atteint le même niveau que les autres méthodes de FORM. Les résultats de TvRBDO ont validé la faisabilité de la méthode proposée. Après la construction de la boucle interne, le coût de calcul pour l'optimisation est minimum.

Mots clés: Energie éolienne, propagation de l'incertitude, les techniques d'apprentissage automatique , optimisation de la fiabilité dépendant du temps.

Résumé étendu

Introduction générale

Le besoin croissant des sociétés modernes en énergie électrique a engendré l'utilisation accrue des combustibles fossiles (pétrole, charbon, etc.). Cependant, ces combustibles fossiles provoquent des dégâts importants à l'environnement. Depuis le protocole de Kyoto en 1995, les États ont pris conscience que la lutte contre le changement climatique est liée à la réduction des gaz à effet de serre. Les énergies renouvelables permettent de réduire le rejet des gaz à effet de serre pour la production de l'électricité. D'ailleurs, l'Union Européenne vise à atteindre la production d'électricité à partir de sources renouvelables à 27 % en 2030. L'énergie éolienne est considérée comme la plus prometteuse et la plus viable des sources d'énergie renouvelable.

Pour augmenter la production d'électricité et éviter l'opposition des résidents, les parcs éoliens sont installés dans des régions éloignées, montagneuses ou au large des mers. Un parc éolien est soumis à des vents violents, à l'usure des turbines et à d'autres incertitudes telles que des pertes de disponibilité. Pour la planification de nouvelles installations ou l'amélioration de parcs éoliens existants, la connaissance des incertitudes liées aux éoliennes est très importante. Le sujet de cette thèse se concentre sur ce sujet, dans cette introduction de premiere partie, la portée et la motivation de cette étude sont abordées, puis un resume étendu de ce travail est présenté.

Motivation

Le secteur des énergies renouvelables et en particulier de l'énergie éolienne est une industrie à croissance rapide [1]. L'éolienne est un système complexe comprenant principalement la fondation de la plate-forme, la tour d'éolienne, les pales et la nacelle, la transmission, le

rotor et le système de contrôle. Ces systèmes sont incorporés pour maximiser la production d'électricité et augmenter la fiabilité des parcs éoliens. Pour améliorer leurs performances (agencement des éoliennes, conception des composants des éoliennes, etc.), certains codes de simulation ont été développés. Cependant, les données d'entrée de ces codes de simulations sont entachées d'incertitudes. Pour cela, un cadre mathématique est nécessaire pour analyser les performances des éoliennes en tenant compte de l'aléa. Ce travail de thèse vise d'une part à mieux comprendre la propagation des incertitudes du vent dans la simulation des systèmes éoliens, d'autre part, à utiliser les approches fiabilistes pour l'optimisation de la conception des tours d'éoliennes.

Objectif

L'objectif de cette thèse est de mieux comprendre la propagation des incertitudes des systèmes d'éoliennes et d'appliquer les méthodes basées sur la fiabilité pour optimiser la conception des tours. Les objectifs de cette thèse sont

1. Propagation de l'incertitude du vent entrant. Pour le vent entrant turbulent, les réponses du système éolien sont également stochastiques, la relation entre l'incertitude d'entrée et la réponse doit être discutée.
2. Optimisation fiabiliste de la conception de la tour de l'éolienne. L'optimisation de la conception basée sur la fiabilité (RBDO Reliability-Based Design Optimization) est largement utilisée dans les problèmes d'ingénierie, qui recherchent un équilibre entre le coût et la fiabilité. Le plus grand inconvénient des méthodes d'optimisation fiabiliste (RBDO) est leur coût de calcul, en particulier lorsque les probabilités de défaillance sont faibles. De nouvelles méthodes ont été développées pour réduire le coût de calcul tout en conservant une précision suffisante.
3. Méthodologie d'optimisation fiabiliste dépendante du temps. En raison de la dégradation des structures (dégradation matérielle ou structurelle) et des incertitudes des paramètres d'entrée, la fiabilité du système dépend du temps. Elle doit être évaluée à l'aide de méthodes de fiabilité dépendante du temps. L'optimisation tenant compte de la fiabilité dépendante du temps doit être proposée.

La première partie sur la propagation de l'incertitude du vent entrant est comme un problème de boîte noire qui est considéré en termes de paramètre d'entrée et de sortie. Dans ce cas, les métamodèles sont largement utilisés. Il existe de nombreux types de métamodèles, donc dans la première partie, plusieurs métamodèles sont comparés, puis appliqués à la quantification de l'effet du vent sur les comportements des éoliennes.

La deuxième partie concerne l'optimisation fiabiliste de la conception de la tour d'éolienne. Les méthodes traditionnelles utilisent une approche en double boucle, où la boucle externe modifie les variables de conception et la boucle interne analyse la fiabilité. Ces méthodes sont très coûteuses en temps de calcul. Dans le cadre de cette thèse, une nouvelle méthode est proposée. Elle utilise une approche en boucle unique couplée au métamodèle de Krigeage pour réduire le coût de calcul.

Dans la troisième partie, une nouvelle méthode pour l'optimisation fiabiliste dépendante du temps est proposée. En raison de la non-linéarité des fonctions de performance, la fiabilité dépendante du temps est calculée en utilisant les simulations de Monte Carlo avec le métamodèle de Krigeage. Deux métamodèles de Krigeage à double boucle sont développés pour réaliser l'optimisation fiabiliste dépendante du temps.

Cette thèse est structurée comme suit:

- Le but et la portée de cette thèse sont résumés dans l'introduction.
- Dans Chapitre 1, les développements récents de l'énergie éolienne sont d'abord revu. Ensuite, les théories fondamentales pour calculer la réponse de l'éolienne: les équations de BEM (BEM: Blade Element Momentum theory) et de Kane sont passées en revue. Enfin, les méthodologies de conception des structures d'éoliennes sont résumées.
- Dans Chapitre 2, les théories de la quantification des incertitudes utilisées dans l'énergie éolienne sont passées en revue, y compris un large éventail de sujets tels que les méthodes de simulation, les métamodèles, l'analyse de sensibilité, l'analyse de fiabilité, etc. Ce chapitre sert de base théorique aux prochains chapitres.
- Dans Chapitre 3, la propagation des incertitudes du vent entrant en utilisant différents métamodèles est discutée. Les caractéristiques probabilistes des réponses des forces sur la tour sont d'abord discutées, puis différents métamodèles sont appliqués pour la propagation des incertitudes du vent stochastique.

- Dans Chapitre 4, l'optimisation fiabiliste de la conception en utilisant l'approche de boucle unique assistée par le Krigeage est discutée. Une nouvelle méthodologie est proposée pour mettre à jour le métamodèle de Krigeage. Cette méthode est d'abord validée sur des problèmes mathématiques puis elle est appliquée à la conception fiabiliste de la tour d'éolienne.
- Dans Chapitre 5, l'optimisation fiabiliste dépendante du temps en utilisant un métamodèle de Krigeage en double boucle est proposée. Cette méthode consiste en deux métamodèles de Krigeage, la boucle interne calcule la fiabilité dépendante du temps et la boucle externe conduit l'optimisation fiabiliste, deux applications numériques sont utilisées pour valider la méthode proposée.

Les dernières parties sont la conclusion et la perspective de la thèse, qui résument les contributions de cette thèse ainsi que les travaux futurs de cette étude.

Organisation de la Thèse

Chapitre 1

Les systèmes d'éoliennes se réfèrent désormais principalement aux appareils qui convertissent l'énergie cinétique du vent en énergie électrique. Les éoliennes peuvent tourner autour d'un axe horizontal (HAWT) ou vertical (VAWT). Basés sur la position d'installation, les systèmes d'éoliennes peuvent être classés comme systèmes d'éoliennes onshore ou offshore. Les éoliennes offshore ont considérablement mûri au cours de la dernière décennie, leur coût diminuant rapidement. La figure 1.3 montre la turbine V164-8.4 Mw pour le programme WindFloat Atlantic à Ferrol (nord de l'Espagne). Comme indiqué, une éolienne horizontale se compose principalement des pales d'éolienne, de la nacelle (y compris le groupe motopropulseur et du générateur), du moyeu (la connexion pour les pieds des pales), de la tour , de la fondation (onshore ou offshore) et des systèmes auxiliaires (système de contrôle et réseau électrique, etc.). Dans les sections suivantes, les théories fondamentales pour des simulations d'éoliennes sont discutées. Ensuite, les méthodologies de conception déterministes et fiabilistes de structures d'éoliennes sont résumées. Pour l'analyse déterministe, les

facteurs de sécurité sont largement adoptés. Cependant, les multiples facteurs de sécurité peuvent entraîner une conception trop conservatrice. Dans ce cas, de nombreux chercheurs ont appliqué des méthodes probabilistes pour caractériser la fiabilité ou optimiser la conception des structures d'éoliennes. L'optimisation de la conception basée sur la fiabilité (RBDO) est ensuite appliquée aux structures sensibles à la fatigue pour réduire la conception trop conservatrice. En raison du coût de calcul pour la réalisation de la RBDO, la méthodes d'approximation par métamodèle de substitution sont largement utilisés. Ceux-ci sont discutés plus en détail dans les chapitres suivants.

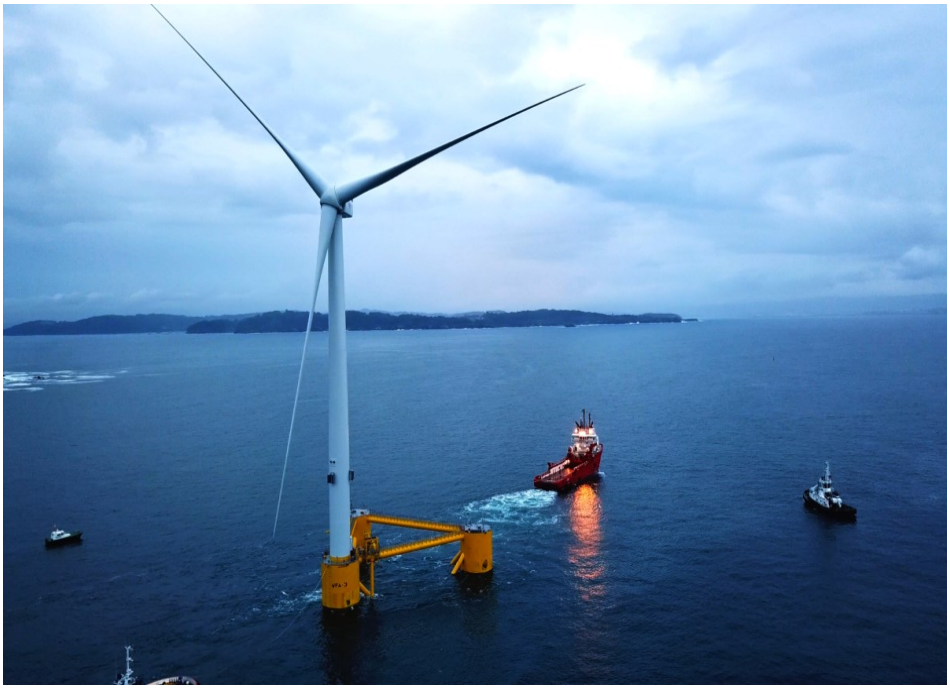

Figure 1: Turbine V164-8,4 MW de MHI Vestas

Chapitre 2

Ce chapitre se concentre sur les théories qui sont largement utilisées pour la quantification des incertitudes dans la modélisation des réponses des structures. Le contexte principal du chapitre est résumé comme suit:

Méthodes de simulation

Pour obtenir les caractéristiques probabilistes de la réponse de $f(X)$, par exemple les moments statistiques de la distribution de X, différentes méthodes peuvent être utilisées. Cette section

donnera une introduction des méthodes de simulation les plus utilisées.

Modèles de substitution par régression

Pour les problèmes d'ingénierie complexes, la réponse précise $Y(X)$ de l'entrée X peut être difficile à obtenir, ou très coûteuse en calcul. Donc l'utilisation d'approximations est très populaire.

Analyse de sensibilité

L'objectif de l'analyse de sensibilité (Sensitivity Analysis: SA) est de décider comment la variabilité de la réponse du modèle est affectée par les variables d'entrée, ou leurs combinaisons. De nombreuses méthodes sont disponibles pour les analyses de sensibilités. Par exemple: la méthode de criblage, la méthode de mesure de l'importance et la méthode d'exploration en profondeur [2].

Analyse de fiabilité

Si nous définissons une fonction d'état limite notée comme $g(\boldsymbol{X})$, par exemple, $g(\boldsymbol{X}) = f(\boldsymbol{X}) - f_{limit}$, f_{limit} est la limite de la réponse. $g(X_f) < 0$, indique le domaine de défaillance D_f, tandis que $g(X_s) > 0$ indique le domaine de sûreté, comme le montre la Figure 2.

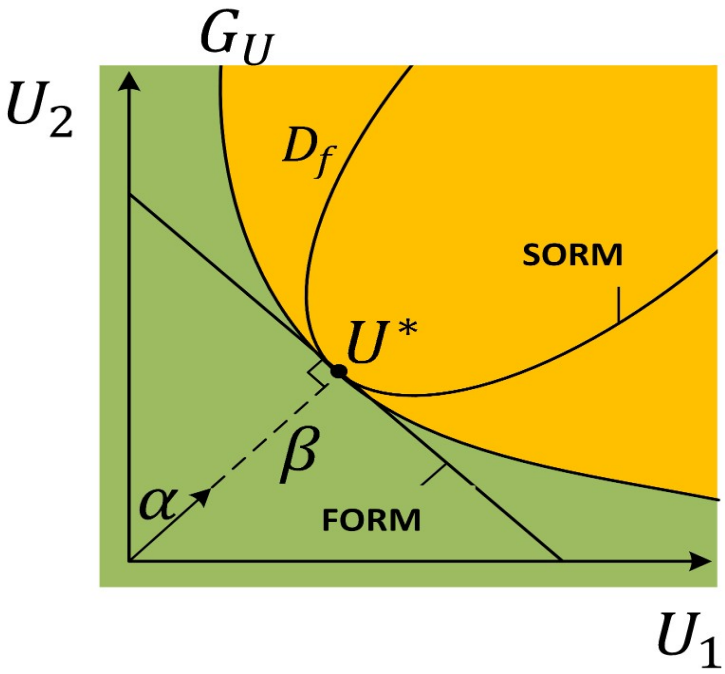

Figure 2: Analyse de fiabilité

La probabilité de défaillance P_f peut être définie comme:

$$P_f = \mathbb{P}(g(X) \leq 0) \tag{1}$$

Des méthodes de simulation basées sur les métamodèles de substitution peuvent être utilisées pour l'évaluation de l'équation (1). Cependant, cela nécessite un très grand échantillon lorsque la probabilité de défaillance est faible. Les méthodes d'approximation sont donc largement utilisées, comme les méthodes de fiabilité du premier ordre (FORM: First Ordre Reliability Method) et du second ordre (SORM: Second Ordre Reliability Method). Avant d'appliquer FORM ou SORM, les variables aléatoires d'entrée X sont transformées de l'espace physique vers les variables U dans l'espace standard à l'aide des transformations isoprobabilistes.

Dans l'espace standard (normé et centré), le problème de fiabilité est simplifié par la recherche de la distance minimale par rapport à l'origine de cet espece et l'état limite:

$$\begin{aligned} &\min_{\mathbf{u}} \beta = \left\|\mathbf{u}^{\mathrm{T}}\mathbf{u}\right\| \\ &st.\mathrm{g}(\mathbf{u}) = 0 \end{aligned} \tag{2}$$

Comme le montre la Figure 2, β est l'indice de fiabilité selon lequel la probabilité de défaillance p_f est approchée par $\Phi(-\beta)$, U^* est le point de défaillance le plus probable (MPP) dans l'espace standard.

Chapitre 3

Dans ce chapitre, la propagation des incertitudes du vent dans les réponses des actions au sommet de la tour de l'éolienne est obtenue en utilisant les outils de simulation d'éoliennes Turbsim et FAST développés par le National Renewable Energy Laboratory (NERL). Les cinq paramètres suivant sont considérés entachés d'incertitudes : la vitesse moyenne du vent entrant (V_{mean}), l'intensité de la turbulence (TI), le coefficient d'exposant de la loi de cisaillement (α), l'angle vertical d'entrée (γ_v) et l'angle horizontal d'entrée (γ_h). Des simulations de Monte Carlo de plusieurs profils du vent conformes au modèle de turbulence normale (NTM) recommandé par l'IEC61400-1 sont effectuées. Les résultats montrent que, pour des simulations indépendantes sous les mêmes variables de profil de vent, en raison des propriétés turbulentes du champ de vent, la valeur moyenne et la valeur maximale des actions sont également stochastiques. Pour mieux étudier la propagation de l'incertitude du vent entrant, 6 métamodèles de substitution aux simulations de FAST sont utilisés et comparés : La méthode des splines de régression adaptative (MARS), le krigeage (KRG), l'expansion du chaos polynomial (PCE), la régression vectorielle de support (SVR), le réseau neuronal profond (DNN) , la régression aléatoire des forêts (RFR). Ces métamodèles de substitution sont d'abord appliqués à plusieurs fonctions mathématiques. Le temps CPU de calcul, l'erreur relative par rapport à la réponse réelle (e_R), le taux de divergence de Kullback-Leibler (d_{KL}) et le coefficient de détermination (R^2) sont utilisés comme critères de validation et de comparaison.

Comparaison des métamodèles

Dans cette section, les modèles de substitution sont comparés à plusieurs problèmes mathématiques basés sur certains critères standard.

Figure 3: Distribution des caractéristiques de réponse

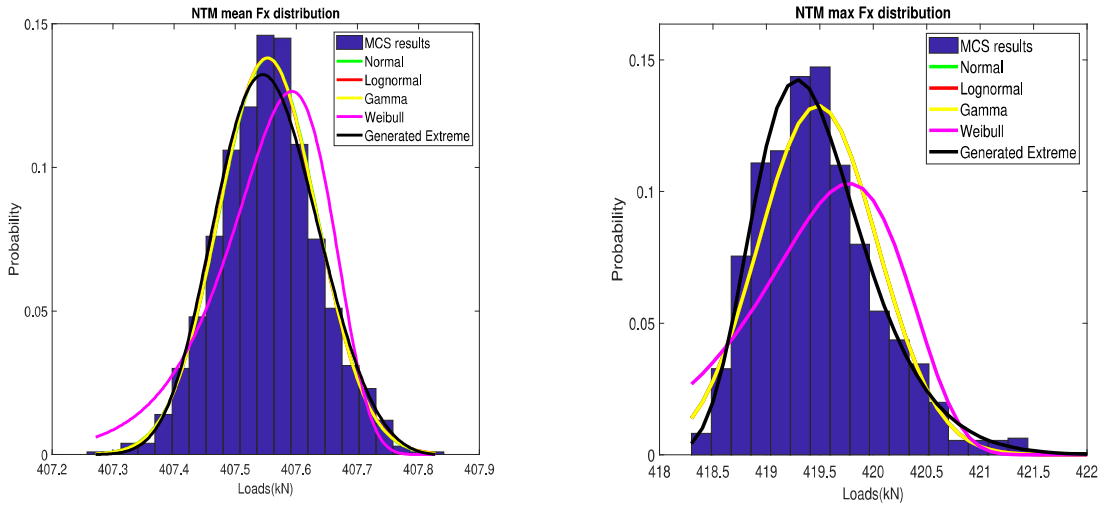

(a) Distribution de la valeur moyenne de Fx

(b) Distribution de la valeur maximale de Fx

Caractérisation de la densité de probabilité des actions du vent

En raison de la propriété stochastique du vent entrant, la distribution de la réponse est d'abord discutée. Les résultats montrent que pour la vitesse du vent turbulent (16m / s dans ce test), la valeur moyenne peut être approximée avec une distribution normale et le maximum avec une distribution extrême de type III . Ensuite, la propagation de l'incertitude du vent entrant est discutée sous cette hypothèse. L'objectif est d'établir une relation entre les paramètres du vent entrant et la valeur moyenne de la distribution de la valeur moyenne et la valeur maximale des forces de réponse au sommet de la tour de l'éolienne.

Propagation de l'incertitude du vent entrant

Les résultats de 500 échantillons d'apprentissage (chacun prenant la valeur moyenne de 100 simulations) pour le Fx moyen et le Fx maximum sont comparés. La comparaison de la distribution de la valeur maximale de Fx est illustrée sur la Figure 4. D'après les résultats, MARS, KRG, PCE et RFR peuvent obtenir une erreur relative plus faible que DNN et SVR avec KRG comme la plus faible. Pour RFR, la divergence Kullback-Leibler (d_{KL}) est élevée, ce qui indique une plus grande différence dans la distribution de sortie, comme le montre la Figure 4. MARS et DNN prennent beaucoup plus de temps à s'entraîner que KRG et PCE pour cette taille de données de 500 échantillon. Donc, après toute les comparaisons, le KRG

est la méthode adaptée pour la propagation des incertitudes du vent entrant.

Figure 4: Distribution et comparaison des différents métamodèles

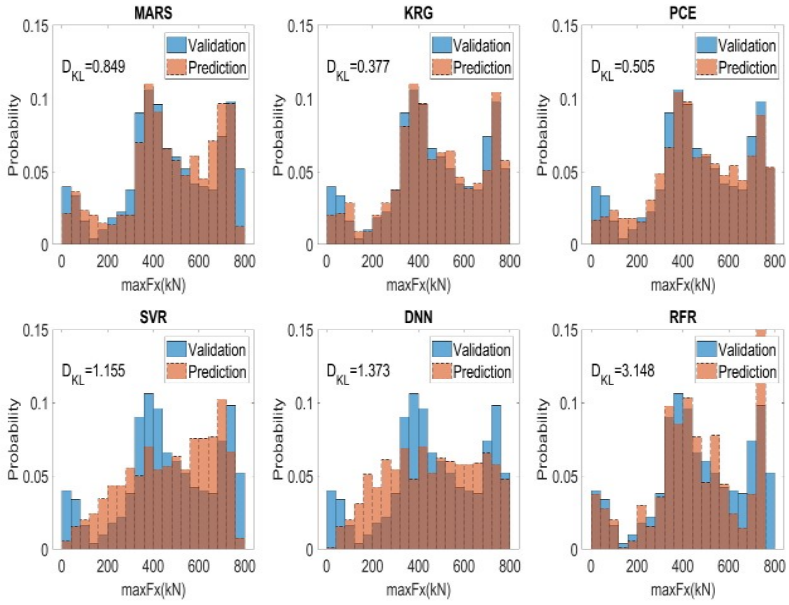

Chapitre 4

Les modèles de substitution ont été largement utilisés dans l'optimisation fiabiliste de la conception (RBDO) pour résoudre des problèmes d'ingénierie complexes. Cependant, la précision et l'efficacité de la RBDO, basées sur les métamodèles de substitution, dépendent en grande partie de la taille de l'échantillon, des méthodes d'échantillonnage et de la probabilité de défaillance à estimer. Pour cette raison, les méthodes d'échantillonnages successifs sont plus prometteuses, qui mettent à jour le métamodèle successivement. De nos jours, plusieurs approches RBDO basées sur le krigeage ont été proposées avec différentes techniques d'échantillonnages successifs. Cependant, ces approches sont basées sur des simulations de Monte-Carlo et des approches à double boucle. La plupart d'entre elles prennent beaucoup de temps de calcul pour un niveau de fiabilité cible élevé ou pour des problèmes à dimension élevée. Pour améliorer l'efficacité de la RBDO basée sur le métamodèle de substitution, cette thèse propose une approche en boucle unique (SLA) combinée avec le métamodèle de substitution de Krigeage. Le métamodèle de Krigeage est mis à jour efficacement en utilisant les points les plus probables (MPP) de la dernière itération de la méthode SLA (Single Loop Approach). Un critère d'arrêt très simple et efficace est proposé. Par rapport à

d'autres méthodes d'échantillonnage, le Krigeage initial peut être démarré avec très peu de points d'entraînement et converge vers l'optimum approprié de manière très efficace. Trois exemples mathématiques et un problème d'ingénierie sont utilisés pour démontrer l'efficacité, les avantages et les limites de cette méthode.

Approche en boucle unique

La formulation du SLA peut être écrite comme suit:

$$\begin{aligned} &\min_{\mathbf{d}} : C(\mathbf{d}, \mu(\mathbf{X})) \\ &\text{s.t.} \ : \begin{cases} \Pr\left[G_i(\mathbf{d},\mathbf{X}) \leq 0\right] \leq P_{f_i}^T & i = 1,\ldots,m \\ h_j(\mathbf{d}) \leq 0 & j = m+1,\ldots,M \end{cases} \end{aligned} \tag{3}$$

RBDO assisté par Krigeage utilisant SLA

L'organigramme peut être résumé comme suit:

Étape 1. Transformation des variables aléatoires $\boldsymbol{X}$ de l'espace physique en variables normées $\boldsymbol{U}$ dans l'espace standard en utilisant la transformation iso-probabiliste $\boldsymbol{U} = T(\boldsymbol{X})$.

Étape 2. Un plan d'expérience de taille N, $\boldsymbol{U}^N$ avec un échantillonnage en grille ou un échantillonnage en latin hypercube (LHS), et les réponses correspondantes $G_i(\boldsymbol{U}^N), i = 1,2,...,m$, sont utilisés pour entraîner le premier Krigeage.

Étape 3. $k_0 = 0$, ou $k = k+1$. Début la boucle SLA, calcul des points les plus probables (MPP) $\boldsymbol{U}_i^{(k)}$, avec $\boldsymbol{U}_i^{(k)} = -\boldsymbol{\alpha}_i^{(k)}\beta_i^t$, où $\boldsymbol{\alpha}_i^{(k)}$ est calculé avec $\boldsymbol{\alpha}_i^{(k)} = \frac{\boldsymbol{\sigma}_U \nabla_{\boldsymbol{U}} \hat{G}_i(\boldsymbol{d}^{(k-1)}, \boldsymbol{\mu}_i^{(k-1)})}{||\boldsymbol{\sigma}_U \nabla_{\boldsymbol{U}} \hat{G}_i(\boldsymbol{d}^{(k-1)}, \boldsymbol{\mu}_i^{(k-1)})||}$ à partir de la dérivée du métamodèle de Krigeage.

Étape 4. $\min f(\boldsymbol{d}, \boldsymbol{\mu}_{\boldsymbol{U}})$, sous les contraintes $G_i(\boldsymbol{d}^k, \boldsymbol{U}^k) \geq 0, i = 1,2...,m$, et calcul du nouveau $\boldsymbol{d}^{(k)}$ et $\boldsymbol{\mu}_{\boldsymbol{U}}^{(k)}$.

Étape 5. Calcul de la réponse $\hat{G}_i(\boldsymbol{U}_i^k), i = 1,2...,m$ à $\boldsymbol{U}_i^k$ à l'aide du modèle Krigeage, utiliser le point $\boldsymbol{U}_i^*$ comme MPP pour la mise à jour du Krigeage, si $[\hat{G}_1(\boldsymbol{U}_i^*), \hat{G}_2(\boldsymbol{U}_i^*), ..., \hat{G}_m(\boldsymbol{U}_i^*)]$ à l'élément le plus proche de zéro.

Étape 6. Calcul de la vraie réponse de $\boldsymbol{U}_i^*$, comme $G_i(\boldsymbol{U}_i^{(*)})$, $i = 1,2,...,m$, ajouter de cet ensemble de données dans l'ensemble d'apprentissage, actualisation du Krigeage.

Étape 7. Comparer $\boldsymbol{d}^{(k)}$, $\boldsymbol{\mu}_{\boldsymbol{U}}^{(k)}$ avec $\boldsymbol{d}^{(k-1)}$, $\boldsymbol{\mu}_{\boldsymbol{U}}^{(k-1)}$, si $||\boldsymbol{d}^{(k)} - \boldsymbol{d}^{(k-1)}|| \leq \varepsilon$ et $||\boldsymbol{\mu}^{(k)} - \boldsymbol{\mu}^{(k-1)}|| \leq$

ε, stop; sinon, passez à l'étape 3 et continuez.

Exemples

Dans cette section, la méthode Krigeage-SLA est d'abord validée à partir de plusieurs problèmes mathématiques utilisées dans la litérature, puis elle est appliquée à l'optimisation d'une tour d'éolienne.

Les résultats de l'exemple de Liang's sont présentés dans la Figure 5:

Figure 5: L'exemple de Liang

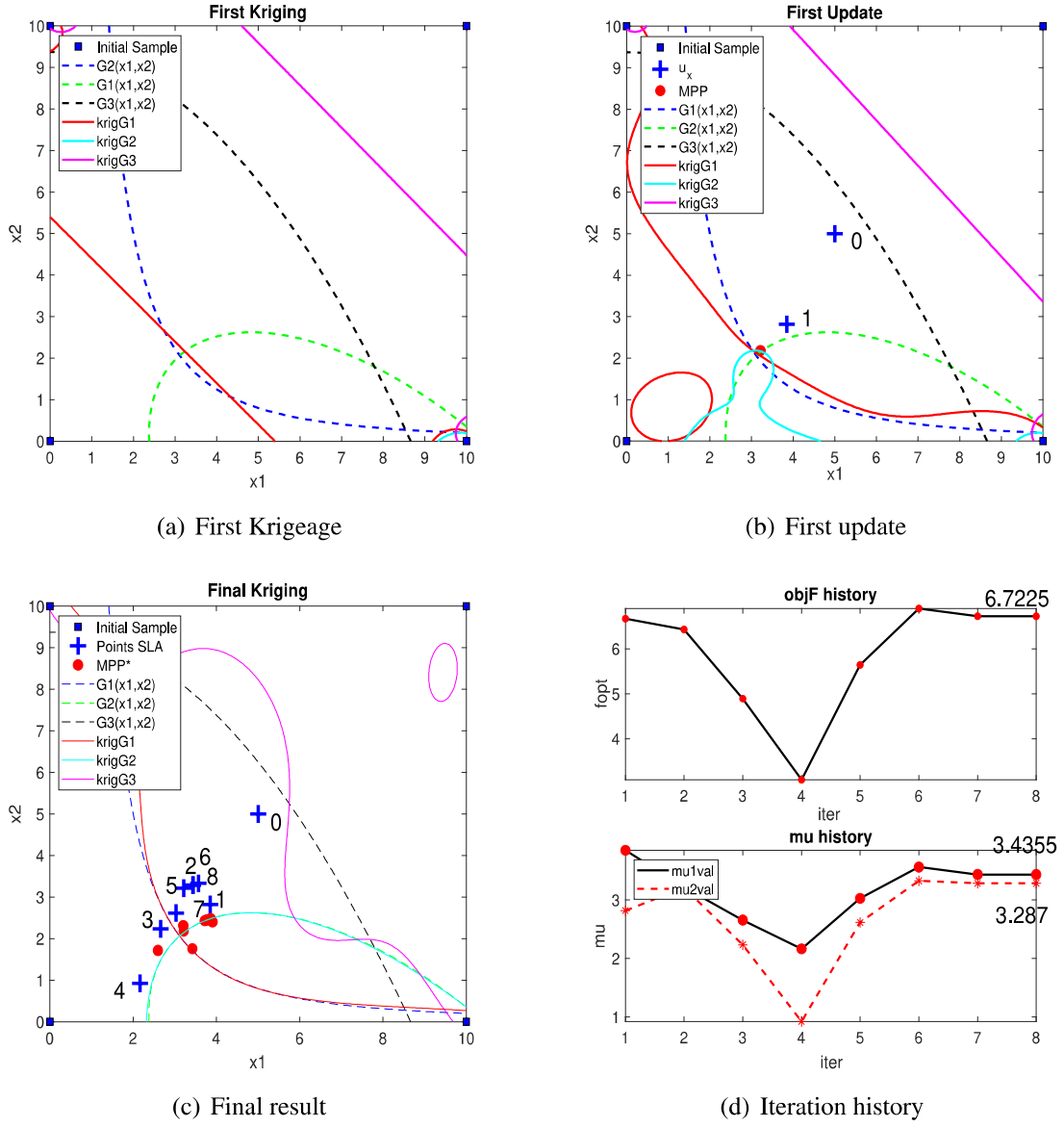

(a) First Krigeage

(b) First update

(c) Final result

(d) Iteration history

RBDO de la tour de l'éolienne

La méthode proposée pour la RBDO (SLA-Krigeage) est utilisée pour l'optimisation de la tour d'éoliennes basée sur une éolienne de référence de 5MW donnée par NREL [3], mais avec plus de détails dans la tour. On peut voir que les résultats de la conception obtenus par l'optimisation déterministe en utilisant les fractiles de 3σ sont beaucoup plus elevés que les résultats de la RBDO pour un indice de fiabilité cible de 4.2.

Chapitre 5

Ce chapitre traite de l'optimisation fiabiliste dépendante du temps à l'aide d'un métamodèle de krigeage à double boucle. Cette méthode utilise la méthode SILK pour l'analyse de fiabilité dépendante du temps [4].

Approche à boucle unique pour une fiabilité dépendante du le temps (SILK)

$$U_{\min}\left(\mathbf{x}^{(i)}\right)=\begin{cases} u_e \begin{cases} \text{if } \hat{G}^{(k)}\left(\mathbf{x}^{(i)},t^{(j)}\right)>0 \\ \text{and } U^{(k)}\left(\mathbf{x}^{(i)},t^{(j)}\right)\geq 2.5, \exists j=1,2,\cdots,N_t \end{cases} \\ \min\limits_{j=1,2,\cdots,N_t}\left\{U^{(k)}\left(\mathbf{x}^{(i)},t^{(j)}\right)\right\}, \text{autrement} \end{cases} \tag{4}$$

TvRBDO utilisant le Krigeage à double boucle

Cette section présente le processus de TvRBDO. Cette méthode consiste à construire deux métamodèles de Krigeage séparés, le Krigeage de la boucle intérieure est utilisé pour effectuer l'analyse de fiabilité dépendant du temps avec la méthode SILK, le Krigeage de la boucle extérieure est utilisé pour conduire l'optimisation. Deux applications numériques sont utilisées pour valider l'efficacité de la méthode. La méthode est simple, précise et facile à mettre en œuvre. Le coût de calcul provient principalement de la recherche de points pour mettre à jour le Krigeage dela boucle intérieure, après la construction du Krigeage externe, le coût de calcul pour l'optimisation est faible.

Table of Contents

General Introduction

Electric energy is essential for the development of modern society, yet over relying on fossil fuels in the past decades have caused serious environmental problems. So clean energy technologies have been increasingly valued, for example, solar, hydro and wind power. Wind energy is considered as a very promising source of energy and has thus attracted growing attention. To increase the power production and avoid the opposition from nearly residents, wind farms are normally installed in remote areas or offshore seas. During their lifetime, wind farms are subjected to many sources of uncertainties such as volatile winds, turbine wear and availability losses. For the planning of new installations or improving the capacities of exiting wind farms, the knowledge of uncertainties related with wind turbines is very important. So this thesis is focusing on the analyses of uncertainties related to wind turbine systems. In this part, the scope and motivation of this study is firstly explained, then a brief outline of this thesis is summarized.

Aim and Scope

The renewable sectors and particularly wind energies have become fast growing industries over the past few years [1]. Wind turbines are wind energy converters that convert the winds' kinetic energy into electrical energy. A large wind turbine is a complex system, mainly consisted of the platform foundation, the wind turbine tower, the blades and the nacelle (including the drive train, the generator, etc) and the control systems. These systems are incorporated to maximize the power production and increase reliability of the wind turbine systems. To better research on the performance of wind turbine system in aspects of the arrangement of wind turbines, structure designs, external uncertainties, some simulation tools have been developed.

The work of this thesis is mostly based on computational simulations. The objective is to have a better understanding of the uncertainty propagation of the wind turbine systems, and apply reliability-based methods to optimize the design of wind turbine tower. The aims of this thesis are:

1. Uncertainty propagation of inflow winds. For turbulent inflow winds, the statistical moments of response loads on the wind turbine tower are also stochastic, the relationship between the input uncertainties and load responses should be discussed.
2. Reliability design optimization of wind turbine tower. Reliability-based Design Optimization (RBDO) is widely used in engineering problems, which seeks a balance between cost and reliability. The biggest traverse for realizing RBDO analyses comes from its high computational cost, especially when the failure rate is low. New methods should be developed to reduce the computational cost while maintaining sufficient accuracy.
3. Time-variant Reliability Optimization (TvRBDO) methodology. Due to system degradation and input uncertainties, the reliability of a system dependent of time (TvR) should be studied. To reduce the calculation time needed for TvRBDO, surrogate models can be added to replace both those physical models and the TvR constraints.

The first part of work is about the uncertainty propagation of inflow winds. This problem is like a black-box problem that is viewed in terms of inputs and outputs. In this case, surrogate models can be used. There exist various surrogate models, so firstly, several popular surrogate models are compared. To establish a relationship between the inputs and outputs, wind uncertainty parameters and output response loads should be characterized. Then those surrogate models are applied to the uncertainty quantification of the response loads.

The second part of work is about the reliability-based design optimization (RBDO) of wind turbine tower. Traditional methods use double-loop approaches, where the outer-loop changes the design variables and the inner-loop calculates their corresponding reliability. These methods are time-consuming when facing high-reliability problems, so in this study a new method is proposed, which utilizes a Kriging-based Single Loop Approach (KSLA) to reduce the computational cost.

The third part of work is about Time-variant Reliability Optimization (TvRBDO). Due to

the high non-linearity of performance functions, the Time-variant Reliability (TvR) is often calculated with simulation methods, which become computational expensive when facing high reliability problems. TvRBDO involves multiple iterations of searching from the design space, so the computational costs are multiplied. To reduce the computational costs, this study utilizes double-loop Kriging surrogates to conduct TvRBDO.

Thesis Outline

This thesis is organised in six chapters:

- In the introduction, the goal and scope of this thesis are summarized.
- In Chapter. 1, the recent developments of wind energy are firstly reviewed. Then the fundamental theories to calculate the wind turbine responses: BEM and Kane's equations are reviewed. Next, deterministic and reliability-based wind turbine structure design methodologies are explained, mentioning the wind turbine classes, the wind conditions, and different design load cases.
- In Chapter. 2, the uncertainty quantification methods applied to wind energy are reviewed, including a wide scope of subjects such as simulation methods, surrogate models, sensitivity analyses, reliability analyses, etc. This chapter serves as the theoretical bases for the latter chapters.
- In Chapter. 3, the uncertainty propagation of inflow wind using different surrogate models are discussed. In this chapter, the probabilistic characteristics of the load responses on the tower are firstly discussed, then different surrogate models are applied for the uncertainty propagation of the stochastic inflow winds.
- In Chapter. 4, Reliability-Based Design Optimization (RBDO) using Kriging-assisted Single Loop Approach (KSLA) is presented. In this chapter, a new updating methodology is proposed for updating the Kriging surrogate. This method is first validated by several mathematical problems and then applied to the RBDO of a 5MW reference wind turbine tower.
- In Chapter. 5, TvRBDO analysis using double-loop Kriging surrogates is proposed. This method consists two Kriging surrogates, the inner-loop calculates the time-variant

reliability and the outer-loop conducts TvRBDO, several mathematical problems are used to validate the method.

The last part are the conclusions and perspectives of the thesis, which summarized the contributions of this thesis and also the future works for this study.

List of Tables

List of Figures

Chapter 1

State of Art of Wind Turbine Simulation

Wind energy is considered to be a very promising source of clean energy and has draw growing attentions in recent years. In this chapter, the state of the art of wind energy is reviewed. In Section.1.1, recent developments of wind energy are firstly introduced, which sees a steady growth in last decades. For a better understanding of the performances of wind turbine structures, in Section.1.2, the simulation methods for wind turbine systems and simulation codes are introduced. Based on these analytical relations or simulation codes, in Section.1.3, the structure design methodologies for wind turbine systems: semi-deterministic and reliability-based methods are discussed and compared. Section.1.4 is the summary.

1.1 General introduction

1.1.1 Wind energy development

Wind energy is the use of wind to provide the mechanical power through wind turbines to turn electrical generators or to do other traditional work like milling or pumping. Wind energy is a sustainable and renewable source of energy, and has much smaller environmental impacts compared to fossil fuels. Wind energy has developed rapidly in recent years that sees a steady increasing of new installations each year. The cumulative installed capacity of top 5 countries is shown in Table. 1.1.

In 2018, global wind power capacity has grown 9.6% to 591 GW [5], reaching 4.8% of the worldwide electric power usage [6] and has provided 15% electricity presumption in European

Table 1.1: Top 5 countries cumulative installed capacity 2014-2018

S. No.	Country	MW (2014)	MW (2015)	MW (2016)	MW (2017)	MW (2018)
1	China	114,609	145,362	168,690	188,232	211,392
2	USA	65,879	74,471	82,184	89,077	96,665
3	Germany	39,165	44,947	50,018	56,132	59,560
4	India	22,456	25,088	28,700	32,848	35,129
5	Spain	22,987	23,025	23,074	23,170	23,484
#	Global	369,695	432,680	487,657	539,581	591,549

Union in 2019 [7]. International Energy Agency (IEA) reported in 2015 that the wind energy supplied more new power generation than any other technologies. China is the leading nation in wind power installed capacity that accounts 35.7% [8], [9]. The top 5 countries contribute more than 50% share of world total installation. 2018 was a solid year with 51.3GW installed, a decrease of 4% compared to last year, with total installed capacity of 591GW (a growth 9% compared to 2017). New installations in the onshore wind market reached 46.8 GW, and global offshore market installed 4.5 GW, bring the share in the global market to 8%.

In Figure.1.1 and Figure.1.2, the cumulative wind energy capacity and the global annually installed capacity are shown respectively.

Figure 1.1: World cumulative installed capacity (GW)

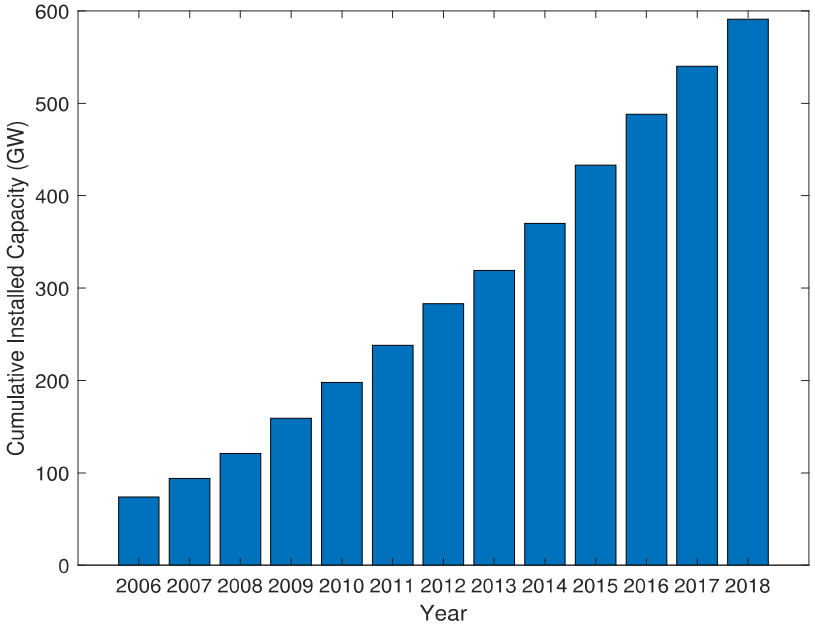

Figure 1.2: World annual installed capacity (GW)

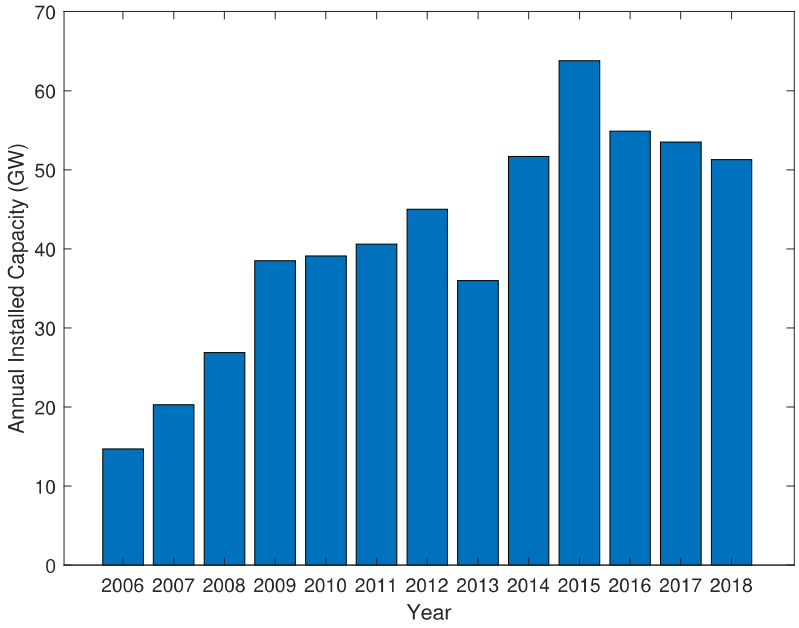

1.1.2 Wind turbine system

Wind turbine hubs can rotate about either a horizontal axis (HAWT) or a vertical axis (VAWT), the former being more common and competent. Based on installation positions, the wind turbine systems can be classified as onshore or offshore wind turbine systems. Offshore wind turbine systems have greatly matured during the last decade, with their cost decreasing rapidly. The average Levelized Cost Of Electricity (LCOE) has decreased from from 120€/MWh in 2000 to about 100€/MWh in 2015 with average anticipation for 2021 reaching 70€/MWh [10]. Figure.1.3 shows the V164-8.4 Mw turbine for Wind-Float Atlantic program in Ferrol (northern Spain). A typical configuration of a modern large scale wind turbine is shown in Figure.1.4. As is shown, a horizontal wind turbine tower system mainly consists of wind turbine blades, a nacelle (including the drive shafts, and the electrical generator), a hub (for the connection for blade roots), the wind turbine tower, the tower foundation (onshore or offshore), and auxiliary systems (such as control systems, power grids, etc.).

Figure 1.3: V164-8.4 MW turbine from MHI Vestas

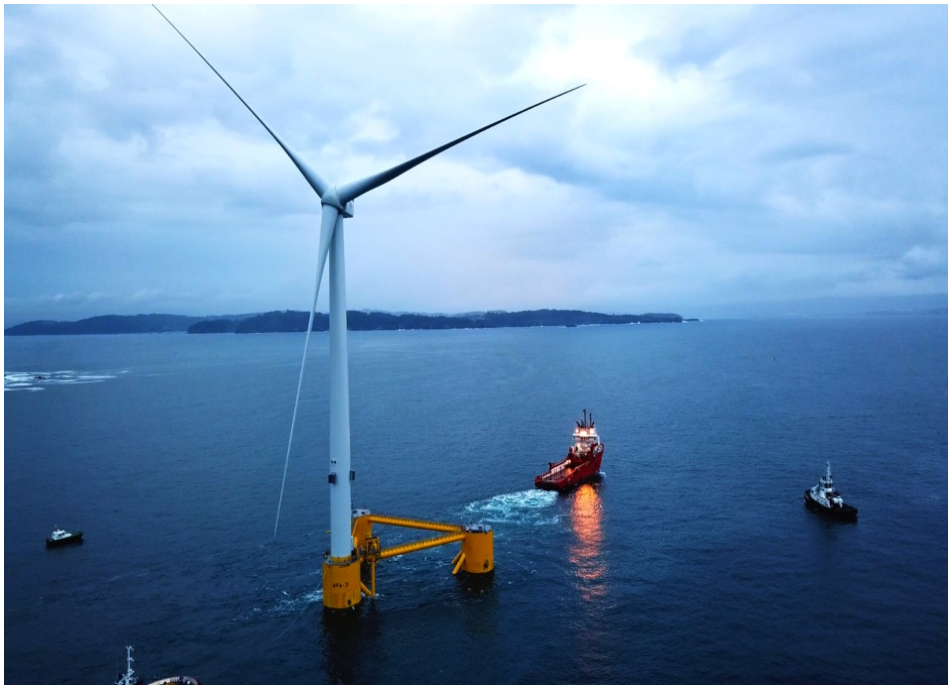

Figure 1.4: A typical configuration of a modern large scale wind turbine.
Source: Tchakoua et al., https://ieeexplore.ieee.org/abstract/document/6618706

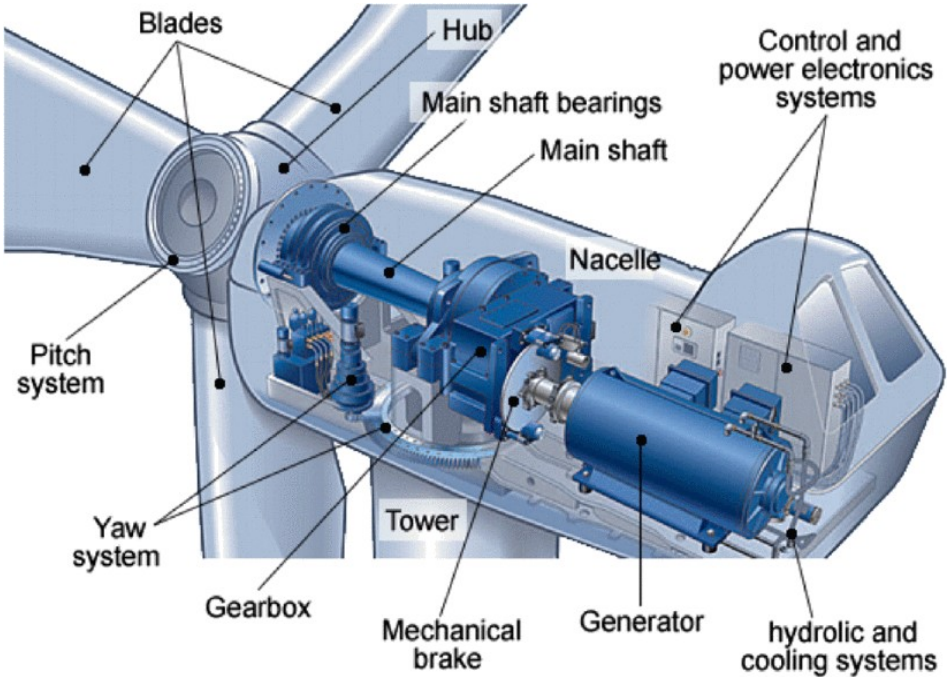

1.2 Wind turbine system simulation

For the analyses of wind turbine systems, Blade Element Momentum theory (BEM) and Kane's equations are widely used for their efficiency and accuracy. In this section, the fundamental

theories for the aerodynamics, support platform kinematics, system kinetic modeling methods are summarized. Based on these methods, and taking into consideration of other auxiliary systems, some simulation codes are developed.

1.2.1 Aerodynamics of wind turbine blades

Though there exist various levels of complexity to calculate the aerodynamics loads on the wind rotor, the BEM is the most commonly used method in simulation codes, for its efficiency and accuracy [11]. BEM was proposed by Glauert [12] by combining the momentum balance theory with blade element theory. The detailed derivation of the theory is shown in Appendix.A.

Momentum balance theory

The momentum balance theory or classical Rankine-Froude theory considers the balance of axial-momentum far-up and downstream of the rotor for a uniformly loaded disc, the theory is established under the following assumptions [13]–[15]:

1. Air is stable, homogeneous, in-compressible without friction.
2. There are infinite number of blades.
3. There is no rotational component of the flow.
4. The velocity through the disc is continuous.
5. The pressure per unit over the disc is constant.

In momentum balance theory, the thrust force and power output are expressed in dimensionless coefficients C_T and C_P:

$$\begin{aligned} C_T &= 4a(1-a) \\ C_P &= 4a(1-a)^2 \end{aligned} \tag{1.1}$$

a is defined as the ratio between the fractional speed decrease at the rotor plane and far downstream. Note that the thrust coefficient C_P has a global optimum C_P^{max} at $a = 1/3$. This C_P^{max} is called Betz limit, indicating the maximum theoretical power output from wind turbine blades.

Generalized momentum theory

The Rankine-Froude actuator disc theory is generalized to include the effect of wake rotation of the wind turbine rotor. The thrust T and torque Q exerted on the rotor are then represented as differentials:

$$\begin{aligned} dT &= 4a'(1+a')\tfrac{1}{2}\rho\Omega^2 r^2 2\pi r dr \\ dQ &= \Delta m \omega r^2 = \rho V_R 2\pi r dr \omega r^2 \end{aligned} \tag{1.2}$$

a' is angular induction factor; r is the radius of the disc; ρ is the density of air; Ω is the angular velocity of inflow air relative to the disc; ω is the angular speed imparted by the rotor; V_R is the horizontal wind speed at the disk position.

Blade element method

The blade element method is another method for analyzing the forces on the turbine blade based on its geometry. As shown in Figure.A.3, along the blade, the blade is divided into small independent sections, with the width of each section being dr, the length of the section being c. α is the angle between inflow wind and the chord line, θ is the sum of the pitch angle and the blade twist angle; ϕ is the angle between inflow wind with respect to plane rotation, which is the sum of θ and α . On an airfoil, the forces are resolved into two forces: drag force F_D and lift force F_L. These forces are then expressed as drag and lift coefficients C_D and C_L :

$$\begin{aligned} C_D &= \frac{F_D/Element}{0.5\rho V_{ref}^2 c} \\ C_L &= \frac{F_L/Element}{0.5\rho V_{ref}^2 c} \end{aligned} \tag{1.3}$$

V_{ref} is the incoming flow velocity relative to the airfoil, which can be derived from the geometry relationship of the blade:

$$\begin{aligned} V_{ref} &= V_\infty(1-a)/\sin(\phi) \\ \tan(\phi) &= \frac{V_\infty(1-a)}{\Omega r(1+a')} \end{aligned} \tag{1.4}$$

For a wind turbine rotor consists of B rotors, the differential thrust dT and differential

torque dQ can be expressed as:

$$\begin{aligned} dT &= B\tfrac{1}{2}\rho V_{rel}^2 \left[C_L\cos(\phi)+C_D\sin(\phi)\right] cdr \\ dQ &= B\tfrac{1}{2}\rho V_{rel}^2 \left[C_L\sin(\phi)-C_D\cos(\phi)\right] crdr \end{aligned} \tag{1.5}$$

Blade element momentum theory

As the name indicates, the blade element momentum theory (BEM) is established by combining the thrust and torque equations from momentum theory and blade element theory (Equation.A.13, Equation.A.14, Equation.A.18). Before applying BEM theory, the thrust and torque of Equation.A.13 and Equation.A.14 are multiplied by a tip-loss factor F that is summarized by Wilson [16] to account for the finite number of blades and finite radius of blades.

$$F = \left(\frac{2}{\pi}\right)\cos^{-1}\left[e^{-\frac{B(R-r)}{2r\sin(\phi)}}\right] \tag{1.6}$$

Then the equations result in:

$$\left(\frac{a}{1-a}\right)\left[\frac{\sin^2(\phi)}{\cos(\phi)}\right] = \left(\frac{Bc}{2\pi r}\right)\left(\frac{C_L}{4F}\right)\left[1+\frac{C_D\sin(\phi)}{C_L\cos(\phi)}\right] \tag{1.7}$$

$$\left(\frac{\Omega r}{V_0}\right)\left[\frac{\sin(\phi)}{\cos(\phi)}\right]\left(\frac{a'}{1-a}\right) = \left(\frac{Bc}{2\pi r}\right)\left(\frac{C_L}{4F}\right)\left[\frac{1}{\cos(\phi)}-\frac{C_D}{C_L\sin(\phi)}\right] \tag{1.8}$$

To derive from the equations above for the induction factor a and a', the drag coefficient C_D is set to zero to simplify the problem. According to Wilson [16], this will add negligible errors. After algebraic manipulation, considering $C_D = 0$, the drag force coefficient C_L and the power coefficient of each blade element C_p are summarized as:

$$C_L = \frac{4F\sin(\phi)}{\sigma}\frac{(\cos(\varphi)-\sin(\phi))}{(\sin(\phi)+\lambda_r\cos(\phi))} \tag{1.9}$$

$$C_P = \frac{8}{\lambda^2}\int_{\lambda_h}^{\lambda}\left[\begin{array}{c} F\sin^2(\phi)\left(\cos(\phi)-\lambda_r\sin(\phi)\right)\left(\sin(\phi)\right. \\ \left.+\lambda_r\cos(\phi)\left[1-\frac{C_D\cos(\phi)}{C_L\sin(\phi)}\right]\lambda_r^2\right. \end{array}\right] d\lambda_r \tag{1.10}$$

here $\sigma = Bc/2\pi r$ is the solidity radio; $\lambda = \Omega R/V_\infty$ is tip speed radio; $\lambda_r = \lambda r/R$ is the local speed ratio.

The lift coefficient and power coefficient are functions of angle attack α, annular radius r, wind speed V_0, number of blades B, blade radius R, pitch, twist, chord distribution c, and rotation speed Ω. These are used to calculate the responses of wind turbine blades.

1.2.2 Structure kinematics of wind turbine system

Once the applied loads on wind turbine structures are calculated, the structural kinematics expressions for wind turbine structure systems can be derived from Kane's equations [17], which are widely used for calculating the system responses with complex structural interactions. In this section, Kane's equation is reviewed.

Kinetic modeling with Kane's equations

Essentially, all methods to derive the equations of motions are equivalent. Newton-Euler method is the most comprehensive to obtain all forces and kinematics for each body. It requires balancing forces and moments for each part by taking consideration of all interactive and external forces. The Newton's law can be expressed as:

$$\mathbf{F}_i - m_i \ddot{\mathbf{r}}_i = 0 \tag{1.11}$$

here $\mathbf{F}_i$ are the total forces on the particle i; $\mathbf{r}_i$ is the position of particle i ; $\ddot{\mathbf{r}}_i$ are corresponding accelerations.

Multiply Equation.1.11 with a infinitesimal displacement $\delta\mathbf{r}_i$, Equation.1.11 becomes:

$$\sum_{i=1}^{v} (\mathbf{F}_i \cdot \delta\mathbf{r}_i - m_i \ddot{\mathbf{r}}_i \cdot \delta\mathbf{r}_i) = 0 \tag{1.12}$$

Equation.1.12 is called principle of virtual work, where v is the number of particles.

By combining virtual work with Newton's law, Lagrange's equations disregard the interactive forces that do not provide work, while requiring evaluations of kinetic energy and preforming differentiation. Compared with Newton's method, Lagrange's method provides a

simpler way to handle complex problems. The Lagrange's equation can be expressed as:

$$\frac{d}{dt}\left(\frac{\partial K}{\partial \dot{q}_s}\right) - \frac{\partial K}{\partial q_s} = Q_s + \sum_{r=1}^{m} \lambda_r A_{rs} \quad (s = 1, 2, \ldots, n) \tag{1.13}$$

here q_i comes from the coordinate transformation that $\sum_{i=1}^{v} \mathbf{F}_i \cdot \delta \mathbf{r}_i = \sum_{s=1}^{n} Q_s \delta q_s$; Q_s are the n generalized forces; K is the kinetic energy; A_{rs} are the $m\,(m < n)$ constraints so that $\sum_{s=1}^{n} A_s \delta q_s = 0$; λ_r are Lagrange multipliers.

For modern engineering problems, like wind turbine structure systems, more complex interactions are involved. To solve these kinds of problems, a modern method is developed by Kane [17]. This method reduces the labor needed to derive equations of motions, so compared with Newton and Lagrange's methods, this method is simpler and more numerically efficient. The Kane's formula is expressed as:

$$F_i + F_i^* = 0 \quad (i = 1, 2, \ldots, n) \tag{1.14}$$

where F_i are the generalized active forces; F_i^* are the generalized inertia forces:

$$F_i = \sum_{k=1}^{N} \left(\vec{\omega}_i^k \cdot \vec{T}_k\right) + \sum_{k=1}^{N} \left(\vec{v}_i^k \cdot \vec{F}_k\right) \tag{1.15}$$

$$F_i^* = \sum_{k=1}^{N} \left[\vec{\omega}_i^k \cdot \left(-I_k \vec{\alpha}_k - \vec{\omega}_k \times \vec{H}_k\right)\right] + \sum_{k=1}^{N} \left[\vec{v}_r^k \cdot (-m_k \vec{a}_k)\right] \tag{1.16}$$

here, $\vec{\omega}_i^k$ is the ith angular velocity in the kth reference frame; $\vec{T}_k$ is the torque; $\vec{V}_i^k$ is the velocity; $\vec{F}_k$ is the force; N is the number of rigid bodies; I_k is the moment of inertia; α is the angular acceleration; $\vec{H}_k$ is the angular momentum; m is the mass, $\vec{a}$ is the acceleration. After regrouping, Kane's equation can be expressed as:

$$\sum_{k=1}^{N} \left[\vec{\omega}_i^k \cdot (\vec{T} - I\vec{\alpha} - \vec{\omega} \times \vec{H})_k\right] + \sum_{k=1}^{N} \left[\vec{v}_i^k \cdot (\vec{F} - m\vec{a})_k\right] = 0 \tag{1.17}$$

It can be seen that in Equation.1.17, the first part and the second part are respectively Euler's law and Newton's law of motion.

Support platform kinematics

The wind turbine system can be simulated with a combination of rigid and flexible components, for example, in FAST simulator [18], a three-bladed HAWT is simulated with 24 degree of freedoms (DOF). These DOFs includes 6 DOFs from the base foundation, 4 DOFs from the tower flexibility, 1 DOF from the nacelle yaw, 2 DOFs from the generator and the rotor speed, 1 DOF from the blade teetering, 6 DOFs from the blade flexibility, 2 DOFs from the rotor-furl and the tail-furl. These DOFs are necessary for characterizing the displacements and forces of the wind turbine components.

For offshore wind turbine systems, hydrodynamic-added forces should be considered to account for the influence of the water mass. So the external forces on the base foundation should be written as [19]:

$$F_i^{\text{Platform}} = -A_{ij}\ddot{q}_j + F_i^{\text{Hydro}} + F_i^{\text{Lines}} \tag{1.18}$$

here A_{ij} is the added-mass from hydrodynamics, F_i^{Hydro} is the ith hydrodynamic load, F_i^{Lines} is the loads from mooring lines.

1.2.3 Simulation tools

The dynamic analysis of wind turbine system relates to flexible multi-body dynamics, aerodynamics, control strategies, mooring and hydrodynamics (for offshore). There exist several simulation codes, for example HAWC2 [20],Bladed [21] and FAST [18] which are widely used by industries and academic researches. Several parts of this thesis are based on FAST simulation code.

FAST code

FAST stands for Fatigue, Aerodynamics, Structures and Turbulence, is a non-linear time-domain simulator developed by the National Renewable Energy Laboratory (NERL). It relates 22 degree of freedoms (DOFs) for two-bladed turbines or 24 DOFs for three-bladed horizontal wind turbines. FAST employs a combined model and multi-body dynamics formulations, such

as Aerodyn, HydroDyn, MAP, etc, as shown in Figure.1.5.

Figure 1.5: FAST workflow

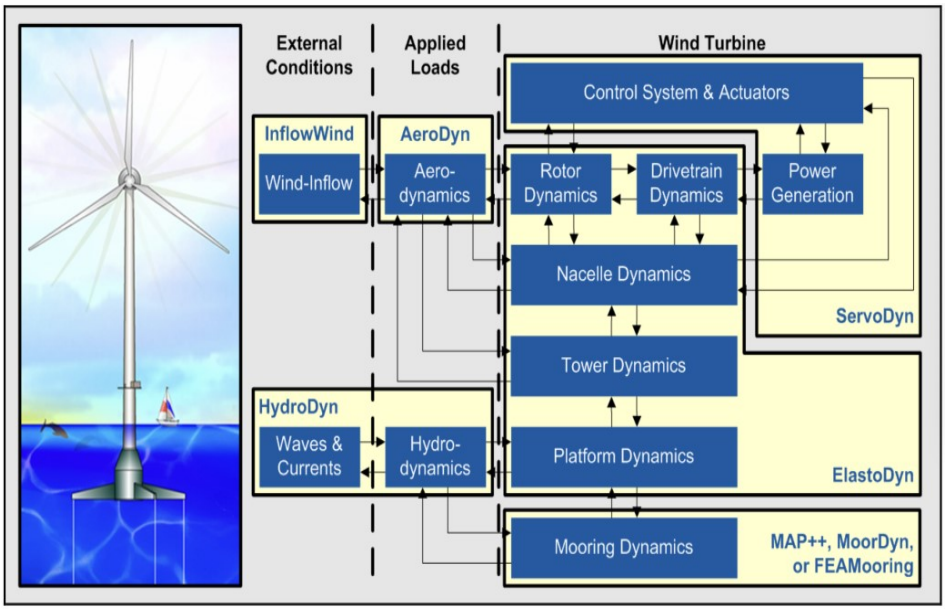

AeroDyn uses (BEM) theory with empirical corrections. HydroDyn is used to analyze the wave loads. Mooring Analysis Program (MAP) is used to analyze the multi-segmented quasi-static cable system. In FAST simulation, aerodynamic and structural responses to the wind inflow conditions are determined in time space. Outputs of the simulations include time-series data for aerodynamics loads, power output, as well as loads and deflections for structural components of wind turbine components.

1.3 Design of wind turbine structures

Based on the analytical relations or simulation codes, this section focuses the design of wind turbine structures. Firstly, the preconditions: wind turbine classes, wind conditions and design load cases are summarized. Two types of design methodologies: semi-deterministic and reliability-based methods are discussed.

1.3.1 Wind turbine class

Depending on installation sites, wind turbine classes are defined in terms of wind speeds and turbulence parameters. The wind turbine classes are intended to cover the most applications

and to represent different installation sites. The basic parameters that defines the wind turbine classes are shown in Table.1.2.

Table 1.2: Basic parameters for wind turbine classes

Wind turbine class		**I**	**II**	**III**	**S**
V_{ref} (m/s)		50	42.5	37.5	Installation
A	I_{ref}		1.6		site
B	I_{ref}		1.4		specified
C	I_{ref}		1.2		value

The wind turbine classes I, II, III and S are defined according to the average reference wind speed V_{ref} . I_{ref} is the expected turbulence intensity at $15m/s$ related with installation sites A-C, that designate high, medium, and low turbulence characteristics respectively.

1.3.2 Wind conditions

Wind condition is the primary consideration for a wind turbine system. A wind turbine system should be resistant to wind conditions defined by wind turbine classes. The wind regimes are classified as normal wind conditions and extreme working conditions based on the frequency of recurrence. The wind conditions include not only a constant mean value but in most cases also turbulent components. The turbulent components should allow random changes in wind speed, shears and directions. Three vector components that are longitudinal, lateral and upward are defined for the wind velocity. For the standard wind turbine classes, the turbulence models should satisfy [22]:

1. The turbulence standard deviation σ_1 is assumed to be independent with height, and the lateral deviation σ_2 and the upward deviation σ_3 component satisfy:

$$\begin{aligned} \sigma_2 &\geq 0.7\sigma_1 \\ \sigma_3 &\geq 0.5\sigma_1 \end{aligned} \tag{1.19}$$

2. The longitudinal turbulence scale parameter $\Lambda_1\,(m)$ is a function of hub height z:

$$\Lambda_1 = \begin{cases} 0.7z & z \leq 60 \\ 42 & z \geq 60 \end{cases} \tag{1.20}$$

The power spectral density of longitudinal $S_1(f)$, lateral $S_2(f)$, and upward $S_3(f)$ components should asymptotically approach the following forms as the frequency f increases:

$$\begin{aligned} S_1(f) &= 00.5\sigma_1^2\,(\Lambda_1/V_{hub})^{2/3}\,f^{-5/3} \\ S_2(f) &= S_3(f) = 0.75S_1(f) \end{aligned} \tag{1.21}$$

V_{hub} is the wind speed at hub height.

Two recommended models are Mann uniform shear turbulent model [23] and Kaimal spectrum and exponential coherence model [24].

Normal wind conditions

The mean value of wind speed at turbine hub height V_{hub} over a time period of 10 minutes should be assumed to follow a Rayleigh distribution given by:

$$P(V_{\text{hub}}) = 1 - \exp[-\pi(V_{\text{hub}})/(0.4V_{\text{ref}})] \tag{1.22}$$

where V_{ref} is the reference wind speed of wind turbine. Figure.1.6 is an example of Rayleigh distribution with the mean value of V_{hub} being 13m/s.

The normal wind conditions include normal wind profile model (NWP) and normal turbulence model (NTM). For NWP, the average wind speed is given as a function of height z:

$$V(z) = V_{\text{hub}}(z/z_{\text{hub}})^{\alpha} \tag{1.23}$$

For NTM, the standard deviation of turbulence σ_1 is given as:

$$\sigma_1 = I_{\text{ref}}(0.75V_{\text{hub}} + 5.6) \tag{1.24}$$

Figure 1.6: Rayleigh distribution

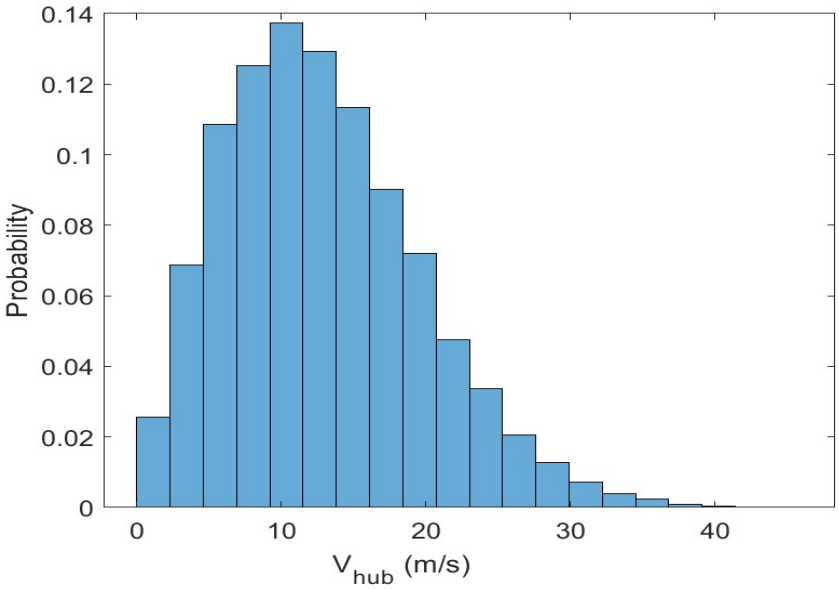

Extreme wind conditions

The extreme wind conditions include wind shear events, peak wind speeds, rapid changes in wind speed and direction. 6 types of extreme wind conditions are specified in IEC61400-1 design requirements for wind turbines, which are extreme wind speed model (EWM), extreme operating gust (EOG), extreme direction change (EDC), extreme coherent gust with direction change (ECD), extreme wind shear (EWS), and extreme turbulence model (ETM). For ETM, the wind profile uses the same profile of NWP, while the standard deviation of the longitudinal component σ_1 is given by:

$$\sigma_1 = cI_{\text{ref}}[0,072(V_{\text{ave}}/c+3)(V_{\text{hub}}/c-4)+10]; c = 2\text{m/s} \tag{1.25}$$

To generate the random wind field, there are also simulation codes available. This thesis uses Turbsim also developed by NREL [25]. TurbSim is a stochastic, full-field, turbulent-wind simulator. It numerically simulates time series of three dimensional wind velocity vectors at points in vertical rectangular grids. TurbSim output can then be used as input into aerodynamic-based codes such as FAST.

1.3.3 Design load cases

The design lifetime for wind turbine classes *I*, *II*, *III* should at least last 20 years. Besides wind conditions, other environmental conditions should also be taken into account to guarantee the integrity and safety of wind turbines during their serving time. For example, thermal, photo-chemical, corrosive, mechanical, electrical conditions.

The design load cases (DLCs) are used to verify a wind turbine can withstand the most significant conditions during its lifetime with reasonable probability of occurrence. The design situations of a wind turbine can be summarized in Figure.1.7.

Figure 1.7: Wind turbine lifetime design situations

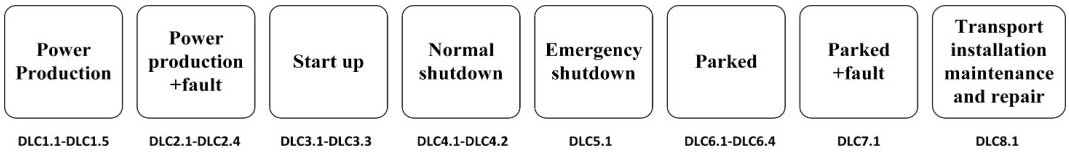

For each phase of design situation, DLCs are defined according to environmental conditions. For example, in the phase of power production, 5 DLCs are defined, which requiring different types of analyses as shown in Table. 1.3.

Table 1.3: Design load cases for power production

DLC	Wind condition	Other conditions	Type of analysis
1.1	NTM	For extrapolation of extreme events	U
1.2	NTM		F
1.3	ETM		U
1.4	ECD		U
1.5	EWS		U

Here, U denotes analysis of ultimate strength, F denotes the analysis of fatigue .

1.3.4 Wind turbine semi-deterministic analysis

The wind turbine structures should be verified for all DLCs in Figure.1.7. To account for uncertainties and variations in loads and materials, the design values of applied loads F_d are

multiplied by partial safety factors for loads γ_f. And the design values for materials f_d are divided by safety factors for materials γ_m:

$$\begin{aligned} F_d &= \gamma_f F_k \\ f_d &= f_k/\gamma_m \end{aligned} \tag{1.26}$$

For different types of analyses, the safety factors γ_f, γ_m may take different values. Four types of mechanical analyses are used according to the IEC-61400 standards [22]:

1. Ultimate strength: For turbine structure design, the resistance of structure materials R should be larger than the highest response S multiplied by a failure consequence factor γ_n:

$$\gamma_n S(F_d) \leq R(f_d) \tag{1.27}$$

   γ_n is designated by the importance of the structure component, that whether the failure of this component will result in the failure of a major part of the wind turbine.

2. Fatigue failure: Fatigue damage should be estimated with appropriate fatigue damage calculation. For example, by adopting Miner's rule, the cumulative damage M should be less than 1.

$$\gamma_n M(F_d) \leq 1 \tag{1.28}$$

3. Stability: Stability indicates that the structure components should not buckle or resonate under design loads F_d.
4. Critical deflection: It should be verified that no structure deflections will affect the integrity or functionality of wind turbine systems. For example, the maximum elastic deflection in unfavourable direction should be examined to avoid interference between blades and tower.

The flowchart of semi-deterministic analyses for wind turbine structures is summarized in Figure.1.8:

Giving environmental conditions (Section.1.3.1), turbine classes (Section.1.3.2), design load cases (Section.1.3.3) , the characteristic loads F_k can be obtained from experimental data, analytical results, or simulation codes (Section.1.2). This step of load characterization will be further discussed in Chapter.3. The design load effects S_d of wind turbine structures are

Figure 1.8: Semi-deterministic analyses of turbine structures

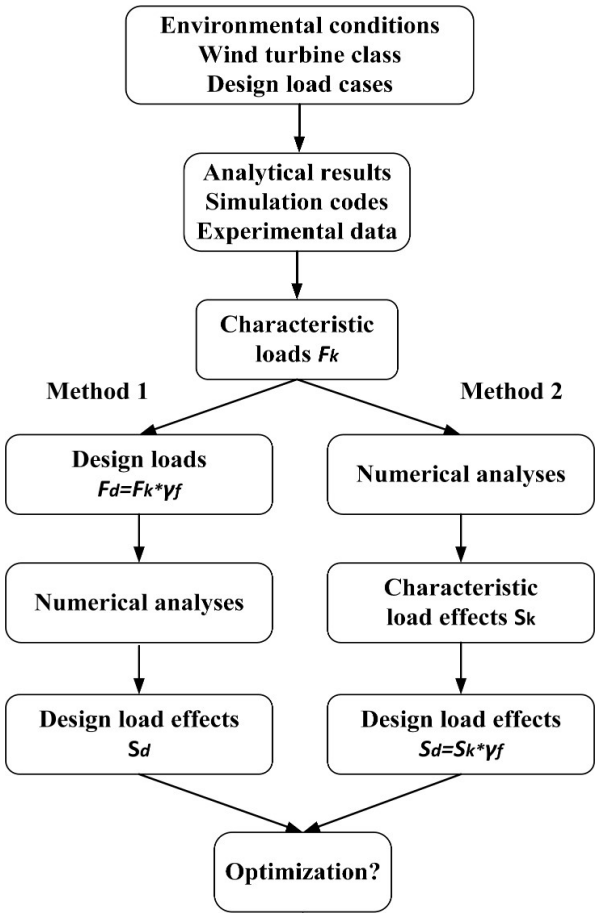

calculated with numerical analyses or simulation codes such as finite element method (FEM). For method 1, the safety factor γ_f is applied to the characteristic loads F_k, so method 1 is more suitable for non-linear analysis. While for method 2, the safety factor γ_f is applied to the characteristic load effects S_k, so this method is more suitable for precise dynamic reaction analysis. Based on the constraints of design load effects, semi-deterministic optimization can be conducted, to achieve the lowest installation cost or highest annual profit, etc.

1.3.5 Wind turbine reliability analysis

Although using the partial safety factors is convenient to account for wind uncertainties, the spatial and temporal wind load variations are not represented accurately. Besides, using multiple safety factors may result in over conservative design. In this case, many researchers [26]–[29] have applied probabilistic methods to characterize reliability and optimize the design of the wind turbine structures. The flowchart for reliability analysis is shown in Figure.1.9.

Figure 1.9: Reliability analyses of turbine structures

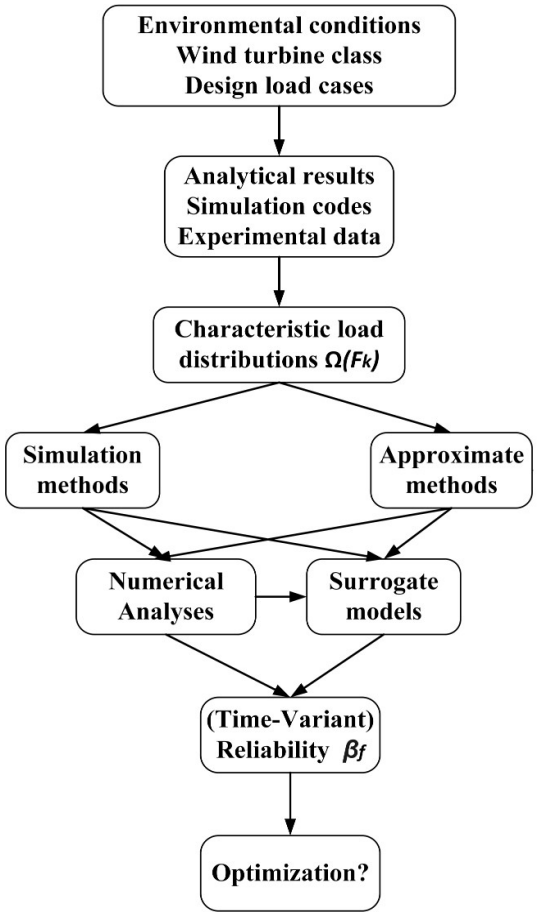

In reliability analysis, the characteristic loads in semi-deterministic loads F_k is replaced with load distributions $\Omega(F_k)$; the characteristic load distributions $\Omega(F_k)$ are not multiplied with safety factors γ_f. The performance of a structure design is indicated by its reliability index β_f, which is an indicator of failure.

The failure rates are defined as the probability of limit state of a turbine structure $G(\Omega(F_k))$ is smaller than zero:

1. Ultimate strength: For turbine structure materials, the highest response S_k from characteristic loads, is bigger than the resistance of structure materials R :

$$G^U(F_k) = R(f_k) - S(F_k) < 0 \tag{1.29}$$

2. Fatigue failure: The cumulative damage M is bigger than 1.

$$G^F(F_k) = 1 - M(F_k) < 0 \tag{1.30}$$

3. Stability: The characteristic loads F_k lead to buckling of wind turbine components or resonance of wind turbine system ($G^S_{F_k} < 0$).
4. Critical deflection: The characteristic loads F_k lead to deflections that affect the integrity or functionality of wind turbine systems ($G^D_{F_k} < 0$).

To calculate reliability, the most straightforward way is using crude Monte Carlo Simulation (MCS), this however requires large sample sets, which may become prohibitive for high reliability problems (where failure rates are low). To alleviate this problem, different simulation methods or approximation methods can be used. The surrogate models can also be utilized to replace the complicated time consuming numerical analyses. These are further discussed in Chapter.2. After getting the reliability, reliability-based design optimization (RBDO) can be conducted, this part is focused in Chapter.4. If time is considered as a variable in the analyses, then this reliability problem becomes time-variant reliability (TvR), and the optimization becomes Time-variant Reliability Optimization problem (TvRBDO), which will be further discussed in Chapter.5.

1.4 Summary

This chapter gives a brief introduction of wind energy, in Section.1.1, recent developments of wind energy are introduced, which sees the cumulative installed capacity continuously increasing. To better understand the responses of wind turbine systems under uncertainties, simulation codes are developed based on the theories from Section.1.2. With the simulation tools, in Section.1.3, researchers have tried to optimize the wind turbine structure design, different methodologies are presented, such as semi-deterministic or reliability-based methods. Reliability-based methods have the advantage of finding the most cost-effective design while satisfying reliability expectation. In the next parts of the thesis, the objective is to focus on the uncertainty effects of wind turbine systems and design optimization based on reliability.

Chapter 2

Uncertainty Quantification Theory

The working environments of wind turbines are filled with uncertainties. Uncertainty quantification (UQ) methods are powerful tools to analyze such problems. This chapter gives a overview of UQ methods that are widely applied in wind turbine systems. In Section.2.1, the framework or steps of UQ are firstly introduced. For the quantification of the probability of certain rare events, in Section.2.2, reliability analysis is discussed. To characterize the impact level of each input uncertainty to output responses, in Section.2.3, sensitivity analysis is discussed. For calculating reliability and sensitivity, the most direct way is using the simulation methods which are summarized in Section.2.4. To reduce computational cost, surrogate models can be used. So in Section.2.5, the theories of different surrogate models are reviewed; Section.2.6 is the summary.

2.1 Uncertainty quantification framework

All problems explicit or otherwise, can be mathematically represented by f, with their input variables X belonging to a probability space (Ω, P). Ω is its sample space; P is its probability measure. $\boldsymbol{x}(x_1, x_2, ..., x_m)$ is the realization of X with dimension m, length n. The responding output is represented with $Y(y_1, y_2, ..., y_n)$. The relation can be described as Equation.2.1, with ε as the discrepancy between model prediction and real world reality:

$$Y(X) = f(X) + \varepsilon, X \in \Omega \subset \mathbb{R}^m, Y \subset \mathbb{R}^n \tag{2.1}$$

If the inputs of the system are perfectly known, this can be classified as deterministic problems. If the inputs contain uncertainties, like uncertainties in material properties, or incomplete knowledge of the systems, these kinds of problems should be treated as uncertainty problems. The advantage of UQ over deterministic methods is that it can provide more information on the trend and variability of a system state [30].

The working environments of wind turbine systems are filled with uncertainties due to uncertainties in material properties, manufacturing processes and external loads [31]. So uncertainty quantification (UQ) methods have been widely used to analyze the wind turbine problems [28], [32], [33]. The framework or steps of uncertainty quantification discussed in this thesis are shown in Figure.2.1. This framework is summarized as:

Figure 2.1: Uncertainty quantification framework

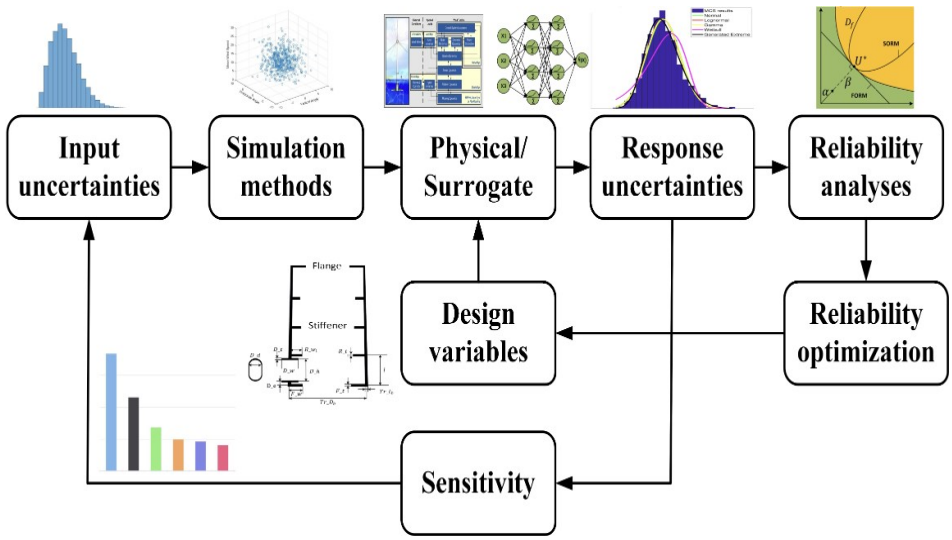

1. **Identifying the sources of input uncertainties.** This step consists in identifying the number of uncertainty sources and finding the parameters of their joint distributions. For wind turbine systems, the input uncertainties mainly comes from wind uncertainties.
2. **Select simulation methods**. This step involves drawing samples from the uncertainty joint distributions. This part will be presented in Section.2.4.
3. **Evaluate physical models**. In this step, the samples are evaluated by physical models, such as FAST simulation code or Finite Element (FE) analysis. If the physical models are time-consuming and the sample size is large, to save time, the physical models are widely replaced by trained surrogates. Several popular surrogates are reviewed in

Section.2.2.

4. **Characterize the output responses**. This step consists in the uncertainty propagation of the input uncertainties. For example, in this thesis, the uncertainty propagation of inflow winds to the load responses on the top of the wind turbine tower is discussed in Chapter.3.
5. **Conduct reliability analysis**. This step consists in defining failure modes, and calculating corresponding reliability. For wind turbine structures, the failure modes are discussed before in Section.1.3. Reliability analysis is discussed in Section.2.2.
6. **Conduct sensitivity analysis**. Sensitivity analysis can provide information of the impact levels of input uncertainties to response uncertainties. Sensitivity analysis is discussed in Section.2.3.
7. **Realize Reliability-based Design Optimization (RBDO)**. This step consists in optimizing design variables (wind turbine tower geometry, for example) under reliability constraints. This part is further discussed in Chapter.4 and Chapter.5.

The following sections will give more detailed introductions of UQ methods that are widely used in wind turbine uncertainty analyses.

2.2 Reliability analysis

Reliability analysis of wind turbine systems often target specific wind sub-assemblies [31], for example, rotor blades [34]–[39], gear box [40]–[43] or turbine tower [44], [45], etc.

The reliability problem is defined as follows: $g(X)$ is the limit state of a component under uncertainty X, for example, $g(X) = f(X) - f_{limit}$, f_{limit} is the limit for the component. $g(X_f) < 0$, indicates the failure domain D_f, while $g(X_s) > 0$ indicates the safe domain, as shown in Figure.2.2. In the figure, the yellow part represents the failure domain and the green part represents the safe domain. The meaning of α, β, U^*, FORM and SORM will be explained below in this section.

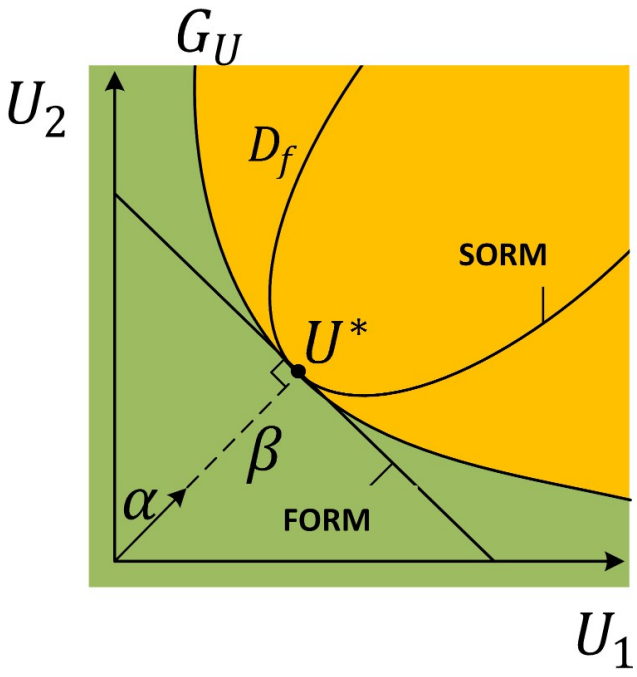

Figure 2.2: Reliability analysis

The failure probability P_f can be defined as:

$$P_f = \mathbb{P}(g(X) \leq 0) \tag{2.2}$$

For the evaluation of Equation.2.2, simulation methods or surrogate model based simulation methods can be used, which are mentioned later in Section.2.4 and Section.2.5. This however, requires a very large sample size when failure rate is low. So approximation methods are widely used, for example, first order reliability method (FORM) and second order reliability method (SORM). Before applying FORM or SORM, the input variables X are first transformed from physical space to standard normal space with isoprobabilistic-transformation T.

$$U = T(X) \tag{2.3}$$

In standard normal space, the reliability problem is simplified to find the minimum distance to the limit state:

$$\begin{aligned} \min \beta &= \left\| \mathbf{u}^{\mathrm{T}} \mathbf{u} \right\| \\ st.\mathrm{G}(\mathbf{u}) &= 0 \end{aligned} \tag{2.4}$$

As shown in Figure.2.2, β is the reliability index that the probability of failure p_f is calculated with $\Phi(-\beta)$, where Φ is the cumulative density function (CDF) of standard normal distribution; U^* is the so-called 'Most Probable Point' (MPP) in standard space.

2.2.1 First order reliability method

Many methods are available to solve Equation.2.4 that is a optimization problem. A dedicated iterative method, called HLRF method is proposed by Rackwitz and Fiessler [46]. In HLRF, at each iteration k, the limit state function G_U is approximated by its tangent hyper-plane at current MPP U^k:

$$\tilde{Z}^{FORM} = G(U^k) + \nabla G_{|U_k}(U^k)(U - U^k) \tag{2.5}$$

In the next iteration, an improved MPP U^{k+1} is calculated with:

$$\mathrm{U}^{k+1} = \frac{1}{\left\|\nabla G_{|U_k}(\mathrm{U}^k)\right\|^2}\left[\nabla G^T_{|U_k}(\mathrm{U}^k)\mathrm{U}^k - G(\mathrm{U}^k)\right]\nabla G_{|U_k}(\mathrm{U}^k) \tag{2.6}$$

2.2.2 Second order reliability method

Second Order Reliability Method (SORM) is a refinement of FORM [47], as shown in Figure.2.2. The tangent hyper-plane in Equation.2.5 is replaced with second order Taylor expansion at the MPP:

$$\tilde{Z}^{SORM} = G(U^*) + \nabla G^T_{|U^*} \cdot (U - U^*) + \frac{1}{2}(U - U^*)^T H (U - U^*) \tag{2.7}$$

Then Breitung [48] proposed a simple closed-form solution for the probability computation using the theory of asymptotic approximation as:

$$P_f \approx \Phi(-\beta_{\mathrm{FORM}}) \prod_{i=1}^{n-1} (1 + \beta_{\mathrm{FORM}}\, \kappa_i)^{-1/2} \tag{2.8}$$

where β_{FORM} is the reliability from FORM method; i is the number of variables, κ_i are the principal curvatures at MPP.

2.3 Sensitivity analysis

The working conditions of wind turbine systems consist in multiple sources of uncertainties. To characterize the impact level of each input uncertainty to the response concerned, for example, output power or fatigue of components, Sensitivity Analysis (SA) is widely used by researchers [49]–[54]. The objective of sensitivity analysis is to characterize how the variability of the model response is affected by each input variable or their combinations. Many methods are available for SA, for example: screening method, importance measure method, and deep exploration method, etc [2]. In this subsection, the widely used Morris method and Sobol's indices are reviewed.

2.3.1 Screening

Screening methods are based on discretization of inputs in levels, allowing a fast exploration, which can be used before other finer yet more costly methods. There are also different kinds of screening methods, the most widely used is Morris method [55], this method can be expressed as:

$$d_i(x) = \frac{Y(x_1,\ldots,x_i+\Delta,\ldots,x_m) - Y(x)}{\Delta} \tag{2.9}$$

where Δ is a perturbation parameter $\frac{c}{p-1}$, p is the grid level parameter, $c \in \{1,\ldots,p-1\}$ is a predetermined fixed number. The sensitivities are indicated by the mean value $\widehat{\mu}_i$ and standard deviation $\widehat{\sigma}_i$ of $d_i(x)$:

• Mean value $\widehat{\mu}_i$: is a measure of importance of this input. A big mean value indicates that the input x_i is important, or otherwise if the mean value is small.

• Standard deviation $\widehat{\sigma}_i$: is a measure of interaction. A big value suggests a linear relationship, while a small value suggests a non-linear effect for interactions with itself or other input variables.

2.3.2 Sobol's indices

Sobol's indices [56] are based on the expansion of the response into sum of increasing dimensions. Consider $f(\bullet)$ is a square-integratable function, defined on a d dimensional unit hyper-cube $[0,1]^d$, and the input variables are independent, then the Sobol's decomposition can be expressed as:

$$f(X) = f_0 + \sum_{i=1}^{d} f_i(x_i) + \sum_{i<j}^{d} f_{ij}(x_i, x_j) + \cdots + f_{12\ldots d}(x) \tag{2.10}$$

This expansion is unique if the integrals with respect to their own variables equals to zero :

$$\int_0^1 f_{i_1\ldots i_s}(x_{i_1}, \ldots, x_{i_s})\, dx_{i_k} = 0, 1 \leq k \leq s, \{i_1, \ldots, i_s\} \subseteq \{1, \ldots, d\} \tag{2.11}$$

and all the margin cumulative distribution function (CDF) of the expansion can be computed using integrals:

$$\begin{aligned} f_0 &= \textstyle\int_{\Omega_X} f(x)dx \\ f_i(x_i) &= \textstyle\int_0^1 \ldots \int_0^1 f(x)dx_{\sim i} - f_0 \\ f_{ij}(x_i, x_j) &= \textstyle\int_0^1 \ldots \int_0^1 f(x)dx_{\sim(ij)} - f_0 - f_i(x_i) - f_j(x_j) \end{aligned} \tag{2.12}$$

where $\sim$ indicates that variables are excluded. The total variance is defined as:

$$D = \int_{\Omega_X} f^2(x)dx - f_0^2 \tag{2.13}$$

and partial variance is computed from the marginal CDF:

$$D_{i_1,\ldots,i_s} = \int_0^1 \ldots \int_0^1 f^2_{i_1,\ldots,i_s}(x_{i_1}, \ldots, x_{i_s})\, dx_{i_1} \ldots dx_{i_s}$$
$$1 \leq i_1 < \ldots < i_s \leq d; s = 1, \ldots, d \tag{2.14}$$

then the Sobol's Indices are given by:

$$S_{i_1,\ldots,i_s} = \frac{D_{i_1,\ldots,i_s}}{D} \tag{2.15}$$

There are many methods to evaluate Equation.2.14 and Equation.2.15 [57], for example, Simulation-based methods, see Section.2.4, or surrogate-basd methods, see Section.2.5.

2.4 Simulation methods

To conduct reliability analysis and sensitivity analysis in Section.2.2 and Section.2.3, or to get the probabilistic characteristics of the response of $f(X)$ given in Equation.2.1, for example the statistical moments of the response $Y(X)$, different methods can be used. This section will give a introduction of the mostly straightforward simulation methods.

2.4.1 Monte Carlo simulation

Monte Carlo simulation (MCS) is the most straightforward simulation method, which simply draws large data samples following the input distribution $X \in (\Omega, P)$ as:

$$\mathbb{E}(f(X)) = \int_X f(X)P(X)d_X \approx \frac{1}{N}\sum_{x_i \sim P, i=1}^{N} f(x_i) \tag{2.16}$$

MCS can be very accurate if the sample size is large enough, according to the *law of large numbers*, though it requires high computation cost, it still serves as the fundamental tool or benchmark for various problems [58].

2.4.2 Importance sampling

To reduce the number of samples needed for MCS, or when sampling from P is difficult, Important Sampling (IS) [59] can be used, which by its definition, focuses on more of the input samples that have larger importance to the parameter being estimated. For the problem in Equation.2.16, in stead of $P(X)$, a well defined distribution $Q(X)$, which assembles the shape of $Q(X)$ is chosen, so Equation.2.16 turns into:

$$\mathbb{E}(f(X)) = \int_X f(X)\frac{P(X)}{Q(X)}Q(X)d_X \approx \frac{1}{N}\sum_{x_i \sim Q, i=1}^{N} \frac{P(x_i)}{Q(x_i)}f(x_i) \tag{2.17}$$

By using Equation.2.17, data sets can be sampled from $Q(X)$, avoiding from $P(X)$.

Table 2.1: Metropolis-Hastings Procedure

1. Initialise x^0, $t = 0$.
2. For i=0 to N-1
   - Generate a sample $x^{'}$ from $Q(x|x^t)$
   - Calculate $\alpha(x^{'}|x^t) = \min(1, \frac{P(x^{'})Q(x^t|x^{'})}{P(x^t)Q(x^{'}|x^t)})$
3. Accept or Reject
   - Generate u from Uniform distribution $\mathscr{U}(0,1)$
   - If $u \leq \alpha(x^{'}|x^t)$, accept the candidate and $x^{t+1} = x^{'}$, $t = t+1$
   - If $u > \alpha(x^{'}|x^t)$, reject the candidate and $x^{t+1} = x^t$

2.4.3 Subset sampling

When trying to find out the probability of a rare event of the response $f(X)$, subset simulation (SS) can be a very powerful tool, especially for high dimensional problems. Subset simulation attempts to convert the rare event problem into a more frequent one. For example, a rare event $P(Y(X > b)$ has to be decided, with the theories of condition probability:

$$\begin{aligned} P(Y > b) =& P(Y > b_m | Y > b_{m-1}) P(Y > b_{m-1} | Y > b_{m-2}) \cdots \\ & P(Y > b_2 | Y > b_1) P(Y > b_1) \end{aligned} \tag{2.18}$$

where $b_1 < b_2 < \cdots < b_m = b$ is a increasing sequence of intermediate threshold. The $P(Y > b)$ can be evaluated using MCS, for calculating the conditional probabilities in Equation.2.18, Metropolis–Hastings Markov Chain Monte Carlo (MCMC) sampling can be used. The Metropolis-Hastings step can be summarized in Table.2.1.

2.5 Surrogate models for regression

For wind turbine system problems, the accurate response $Y(X)$ of input X may be hard to get or very computationally expensive, such as Finite Element (FE) analysis. So using surrogate models, for example $\hat{Y}(X)$ of the global performance based on some training sets, has been very popular. In this section, several popular surrogate models are presented. Note that the choice for these surrogates are quite problem oriented, so it's not suitable trying to figure out

which one is the best for all situations.

2.5.1 Multivariate adaptive regression splines

Multivariate adaptive regression splines (MARS) was first proposed by JH Friedman [60], the MARS model can be described as:

$$\hat{Y}^{MARS}(X) = a_0 + \sum_{m=1}^{M} a_m B_m(X) \tag{2.19}$$

where M is the number non-constant basis; a_0 is the constant term; a_m are the coefficients; B_m are the base functions also called as hinge functions, taking the form of:

$$B_m^{(q)}(X) = \prod_{k=1}^{K_m} \left[\pm \cdot \left(x_{v(k,m)} - t_{km} \right) \right]_+^q \tag{2.20}$$

K_m is the interaction order; $x_v(k,m)$ is the vth variable; t_{km} is the knot location; q is the order of the basis function with $q = 1$ as linear model and $q = 2$ as cubic model; the $+$ sign means taking the positive part.

The optimal MARS is built in two stages: forward pass (selection) and backward pass (pruning), in the selection phase, a pre-determined maximum number of basis functions are added to model, which is normally larger than the optimal. In the pruning phase, the basis functions that are associated with the smallest increase in the least square goodness-of-fit are removed. The goodness of fit is measured by the so-called Generalized Cross Validation (GCV):

$$\begin{aligned} &\mathrm{GCV}(M) = \frac{(1/N)\sum_{i=1}^{N}\left[y_i - \hat{Y}(x_i)\right]^2}{[1-(C(M)/N)]^2} \\ &\text{with } C = M + cd \end{aligned} \tag{2.21}$$

where N is the number of cases in data set; d is number of independent basis functions; c is a user-defined penalty for adding a basis.

2.5.2 Response surface method

Response Surface Method (RSM) is first proposed by George E. P. Box and K. B. Wilson [61] as:

$$\hat{Y}^{RSM}(X) = M(X)\beta + \varepsilon \tag{2.22}$$

here β is the vector of coefficients to be determined; ε is the error to be minimized; and the components of M is formed by quadratic products of $\boldsymbol{x}$:

$$M(\mathbf{x}) = \begin{bmatrix} 1 & x_{11} & x_{12} & \dots & x_{1m} \\ 1 & x_{21} & x_{22} & \dots & x_{2m} \\ \vdots & \vdots & \vdots & \vdots & \vdots \\ 1 & x_{n1} & x_{n2} & \dots & x_{nm} \end{bmatrix} \tag{2.23}$$

where $x_{12} = x_1 x_2$, m is the dimension of $\boldsymbol{x}$, n is the length of $\boldsymbol{x}$:

The mean square error is:

$$L = \sum_{i=1}^{n} \varepsilon_i^2 = \varepsilon'\varepsilon = (Y - M\beta)'(Y - M\beta) \tag{2.24}$$

By minimizing the square error, the best $\hat{\beta}$ is deduced as:

$$\hat{\beta} = \left(M'M\right)^{-1} M'Y \tag{2.25}$$

So the approximation is given as:

$$\hat{Y}^{RSM} = M\hat{\beta} \tag{2.26}$$

2.5.3 Polynomial chaos expansion

Polynomial Chaos Expansion (PCE) was first proposed by Norbert Wiener [62], the random response $Y(X)$ is represented in a suitable functional space, like Hilbert space L^2. Assume a physical model with a finite second order measure, such that $\mathbb{E}\left(\|Y(X)\|^2\right) < +\infty$, then PCE

Table 2.2: Distributions and associated orthonormal families

Distribution	Support	Polynomial
Normal $\mathscr{N}(0,1)$	$\mathbb{R}$	Hermite
Uniform $\mathscr{U}(-1,1)$	[-1,1]	Legendre
Gamma $\Gamma(k,1,0)$	$(0,+\infty)$	Laguerre
Beta $B(\alpha,\beta,-1,1)$	(-1,1)	Jacobi
Poisson $\mathscr{P}(\lambda)$	$\mathbb{N}$	Charlier
Binommial $\mathscr{B}(m,n)$	$\{0,...,m\}$	Krawtchouk

approximation of this model can be expressed as:

$$\hat{Y}^{PCE}(X) \approx \sum_{\alpha \in \mathscr{A}} y_\alpha \Psi_\alpha(X) \tag{2.27}$$

$\Psi_\alpha(X)$ is the given basis; y_α is the finite subsets of coefficients from a truncated basis $\mathscr{A} \subset \mathbb{N}^M$. Different truncation plan, with parameters p and q can be used:

$$\mathscr{A}^{n,p,q} = \left\{ \alpha \in \mathscr{A}^{n,p} : \|\alpha\|_q \leq p \right\} \tag{2.28}$$

here n is the number of inputs and p is the maximum degree. For $q = 1$, this corresponds a standard truncation, and for $q < 1$, this corresponds a hyperbolic truncation which includes high-degree terms in each single variables, while avoiding high order interaction terms [63]. The basis can adopt different types, and their supported distributions are summarized as Askey-Scheme [64] listed in Table.2.2.

Due to the orthonormality of the polynomial basis as respect to their joint probability density function (PDF), the inner product of the basis satisfy:

$$\left\langle \Psi_\alpha(x), \Psi_\beta(x) \right\rangle = \mathbb{E}(\Psi_\alpha(x), \Psi_\beta(x)) = \delta_{\alpha\beta} \tag{2.29}$$

where $\delta_{\alpha\beta} = 1$, only if $\alpha = \beta$; otherwise, $\delta_{\alpha\beta} = 0$.

For the calculation of coefficients, two types of methods are available, referred as intrusive stochastic collocation method (SC) and non-intrusive Galerkin projection method, the performance of these two methods are quite similar [65], and non-intrusive method is more used for

its easier implementation. The projection method can be expressed as:

$$y_\alpha = \mathbb{E}\left[\Psi_\alpha(x)\cdot\hat{Y}(x)\right] \tag{2.30}$$

This expectation of Equation.2.30 can be evaluated using Gaussian quadrature:

$$y_\alpha \approx \sum_{i=1}^{N} w^{(i)}\mathscr{M}\left(x^{(i)}\right)\Psi_\alpha\left(x^{(i)}\right) \tag{2.31}$$

The weights in Equation.2.31 can be calculated using Golub-Welsch algorithm [66]. For higher dimensional integration, the weights are derived from Smolyak' sparse quadrature:

$$A(l,d) = \sum_{l+1\le|\mathbf{i}|\le l+d}(-1)^{l+d-|\mathbf{i}|}\begin{pmatrix} d-1 \\ l+d-|\mathbf{i}| \end{pmatrix}\left(U^{i_1}\otimes\cdots\otimes U^{i_d}\right) \tag{2.32}$$

where d is the dimension of inputs; $\mathbf{i} = (i_1,\cdots,i_d)\in\mathbb{N}_d$ is the multi-index that $|\mathbf{i}|$=$i_1+\cdots+i_d$; U^{i_j} is the univariate linear operator; $\otimes$ is the tensor product operation; l is the level parameter.

2.5.4 Gaussian regression

Gaussian Regression or Kriging is a surrogate model based on regression using observed data sets [67]. Kriging tries to give a Gaussian estimation of an unmeasured location as well as an estimate square error (MSE) of this point. The Kriging model can be described as:

$$\widehat{Y}^{KRG}(X) = \sum_{i=1}^{k}\beta_i h_i(X) + Z(X) \tag{2.33}$$

where $\widehat{Y}(X)$ is the estimation of input X, which is assumed to be a regression model. It's a linear combination of base function $h_i(X)$ and their coefficients β_i plus a stochastic process $Z(X)$. $Z(X)$ is assumed to be zero mean and the covariance between two points from $Z(x_i)$ and $Z(x_j)$ is defined as:

$$Cov(Z(x_i),Z(x_j)) = \sigma_z^2 R_z(\theta,x_i,x_j) \tag{2.34}$$

here θ is the parameter to be defined; σ_z^2 is the variance of Z; R_z is the correlation function that can adopt different forms, such as, linear correlation, exponent correlation, cubic correlation, etc. The Gaussian correlation is very commonly used, which is defined as [68]:

$$R_z(\theta, x_i, x_j) = \exp[-\sum_{j=1}^{n} \theta_j (x_i - x_j)^2] \tag{2.35}$$

To determine the value of θ, β_i and σ_z^2 from observed data set $[\mathbf{x}, \mathbf{Y}(\mathbf{x})]$, maximum likelihood estimation (MLE) can be used. The likelihood function of Equation.2.33 is expressed as [69]:

$$L(\theta, \beta_i, \sigma_z^2 | \mathbf{x}, \mathbf{Y}(\mathbf{x})) = -\frac{n}{2}\ln(2\pi\sigma_2) - \frac{1}{2}\ln(|R|) - \frac{1}{2\sigma^2}(Y - F\beta)^T R^{-1}(Y - F\beta) \tag{2.36}$$

where R is a $n \times n$ correlation matrix with its elements $R_z(\theta, x_i, x_j)$; F is a $n \times 1$ regression matrix with its elements $h_i(x)$. The maximum likelihood estimates of β_i and σ_z^2 by taking the derivative equation with respect to β_i and σ_z^2, thus:

$$\hat{\beta} = (F^T R^{-1} F)^{-1} F^T R^{-1} Y \tag{2.37}$$

$$\hat{\sigma}^2 = \frac{1}{n}(Y - F\hat{\beta})^T R^{-1}(Y - F\hat{\beta}) \tag{2.38}$$

The post Bayesian MLE Kriging predictor at x is give as:

$$\hat{Y}(x) = h^T(x)\hat{\beta} + \Psi^T(x) R^{-1}(Y - F\hat{\beta}) \tag{2.39}$$

where $\Psi^T(x)$ is the correlation vector between observed value and the new prediction.

2.5.5 Support vector machine

Support Vector Machine (SVM) is developed by Vapnik [70] for classification and regression. It is marked with significant generalization capacities, making them less likely to over-fit data.

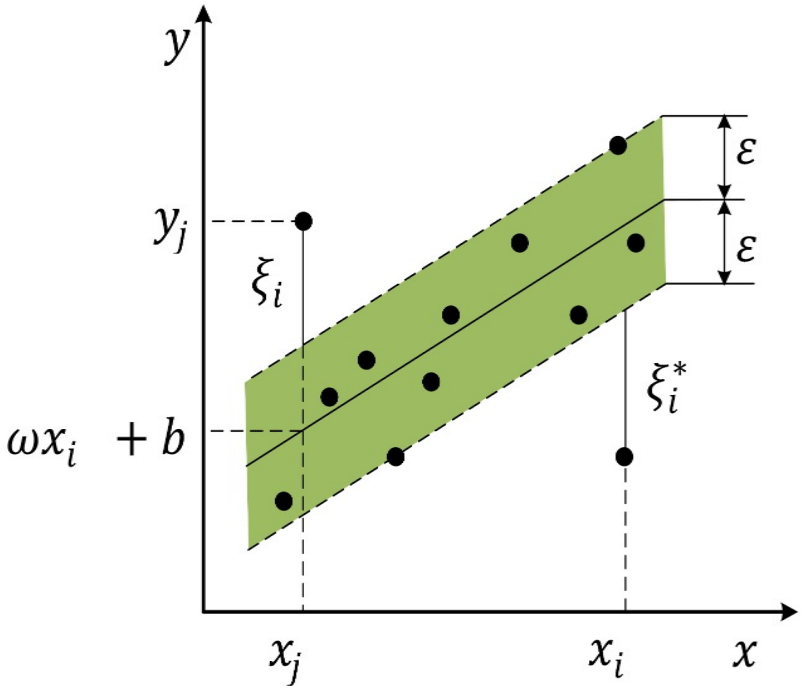

Figure 2.3: Illustration of SVM and penalty function

The simplest linear SVM is expressed as:

$$\hat{Y}^{SVM}(X) = w^T X + b \tag{2.40}$$

where w and b are weight coefficients and offset parameters to be determined. The best w and b should be the robustest, which allows the largest distance possible for the separation of the training points. This is achieved by minimizing loss functions, such as the most popular ε-insensitive loss function [71] given as:

$$L^{\varepsilon}(x;y) = \begin{cases} 0 & \text{if } \left|\hat{Y}^{\text{SVM}}(x) - y\right| < \varepsilon \\ \left|\hat{Y}^{\text{SVM}}(x) - y\right| - \varepsilon & \text{otherwise} \end{cases} \tag{2.41}$$

where ε is the distance between the points and the separation surface. The points within this tube will not be penalized, as shown in Figure.2.3.

Then this problem is transformed into an optimization problem [72]:

$$\begin{aligned} \min_{w} \quad & \tfrac{1}{2}\|w\|^2 + c\sum_{i=1}^{N}(\xi_i + \xi_i^*) \\ \text{st.} \quad & y_i - w^T x_i - b \le \varepsilon + \xi_i \\ & w^T x_i + b - y_i \le \varepsilon + \xi_i^* \\ & \xi_i, \xi_i^* \ge 0 \end{aligned} \tag{2.42}$$

where c is a regularization parameter, and ξ_i, ξ_i^* are deviations from the insensitive tube. Equation.2.42 is generally solved by its dual form by introducing Lagrange multipliers as:

$$\begin{aligned} \min_{\alpha,\alpha^*} \quad & \tfrac{1}{2}\sum_{i=1}^{N}\sum_{j=1}^{N}(\alpha_i\alpha_i^*)\left(\alpha_j - \alpha_j^*\right)x_i^T x_j + \sum_{i=1}^{N}(\alpha_i + \alpha_i^*)\,\varepsilon - \sum_{i=1}^{N}(\alpha_i - \alpha_i^*)\,y_i \\ \text{st.} \quad & \sum_{i=1}^{N}(\alpha_i - \alpha_i^*) = 0 \\ & 0 \le \alpha_i, \alpha_i^* \le C \end{aligned} \tag{2.43}$$

here α_i and α_i^* are Lagrange multipliers. Equation.2.43 can be easily solved with Quadratic Programming (QP) method. After α_i, α_i^* and b are decided, the SVM for regression can be expressed as:

$$\hat{Y}^{\mathrm{SVM}}(x) = w^T x + b = \sum_{i=1}^{n}(\alpha_i - \alpha_i^*)\,x_i^T x + b \tag{2.44}$$

For a better accuracy and efficiency of SVM for highly non-linear or high-dimensional problems, SVM are extended to non-linear SVM. The extension from linear SVM to non-linear SVM is very simple, by mapping x in Equation.2.40, into a higher dimensional space $\Phi(x)$, so $x_i^T x$ becomes $\Phi(x_i)^t\Phi(x)$; or more conveniently, by using a kernel $k(x_i, x)$. The kernel function can adopt different forms [73], as long as they satisfy Mercer's condition [74], similar with Kriging surrogate, such as Polynomial, Sigmoid, Gaussian, Exponential, etc.

Then the linear SVM in Equation.2.44 can be written as:

$$\hat{Y}^{\mathrm{SVM}}(x) = w^T x + b = \sum_{i=1}^{n}(\alpha_i - \alpha_i^*)\,k(x_i, x) + b \tag{2.45}$$

Table 2.3: k-Means Algorithm Procedure

1. Select k points as the initial clustering centers
2. *repeate*
   - classify all the points into their nearest clustering centers
   - use the mean value of each group as the new clustering center

until converge

2.5.6 Radial basis function network with k-Means

In the last subsection, SVM is discussed, with special interest on SVM with Gaussian kernel, in fact, the Gaussian kernel SVM can be treated as a special case of Radial Basis Function (RBF), the RBF Network can be expressed as [75]:

$$\hat{Y}^{RBF}(x) = \sum_{i=1}^{n} \beta_i RBF(x, x_m) \tag{2.46}$$

The $RBF(x, x_m)$ is a function that only relies on the distance between x with x_m, that $r = \|x - x_m\|$, with x_m being the center, for example, the Gaussian kernel in Equation.2.35. Other types of basis can be used, like linear r, cubic r^3, Multi-quadratic$(r^2 + \sigma^2)^{1/2}$, etc.

If all the training points are seen as the centers, this kind of RBF network is called uniform full RBF network. In reality, data are firstly divided into homogeneous classes or clusters and to reduce the number of centers. k-Means [76] is one of the simplest and most widely used clustering method. The step of k-Means can be summarized in Table.2.3.

After getting k centers from k-Means method, RBF can use these centers to reduce the cost of calculation or avoid over-fitting.

2.5.7 Deep neural network regression

Deep Artificial Neural Networks (DNN) are computing systems inspired by the biological neural networks. They are parts of a broader family of machine learning methods based on artificial neural networks [77]. These tools are very versatile and powerful for solving complex problems. For regression problems, the DNN structure can be described in Figure.2.4.

Figure 2.4: Illustration of DNN

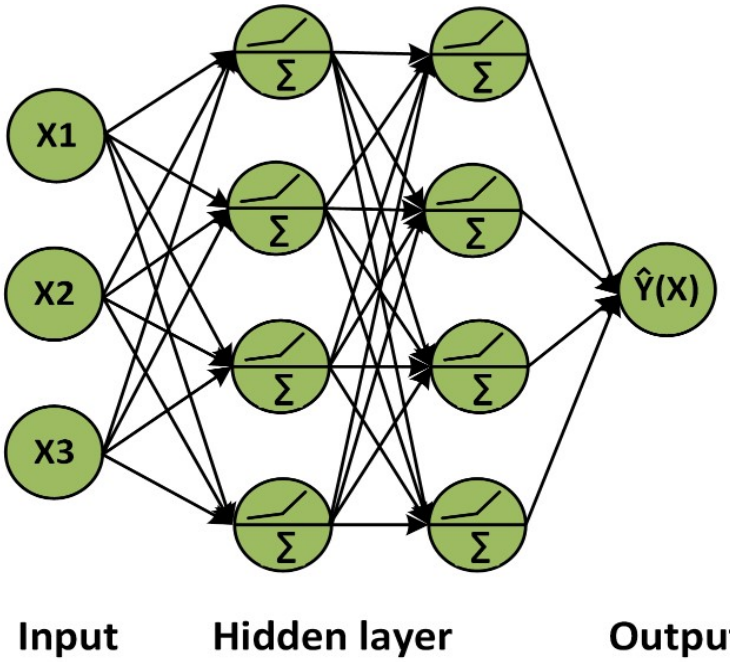

The first column represents the inputs; the middle columns represent the neurons; the last column is the output. The structure of DNN can adopt different forms, by changing the number of layers and nodes, the way of the nodes are connected, and activation function types, etc. The neurons can be binary or in more general cases a weight sum of their inputs associated with a weight w_k, and use a activation function $\varphi(\cdot)$ to output a value. The activation function can adopt different forms, for example, LTU, Relu, Sigmoid, leakyReLU etc. In Figure.2.4, LeakyRelu is used, which is both efficient while avoiding the problem of dying neurons (stop outputting anything other than 0) [77], the leakyReLu is given as:

$$\text{LeakyRelu} = \max(\alpha z, z) \tag{2.47}$$

where α define the slope angle.

The weights of the neurons for DNN are calculated with a so-called back-propagation method, and to improve the efficiency, Adaptive moment estimation (Adam) optimization method [78] is widely used to update the weights.

2.5.8 Random forest

A Random Forest is an ensemble technique capable of performing both regression and classification tasks with the use of multiple decision trees and a technique called Bootstrap Aggregation, commonly known as bagging. An example of random forest regression is shown in Figure.2.5.

Figure 2.5: Illustration of random forest

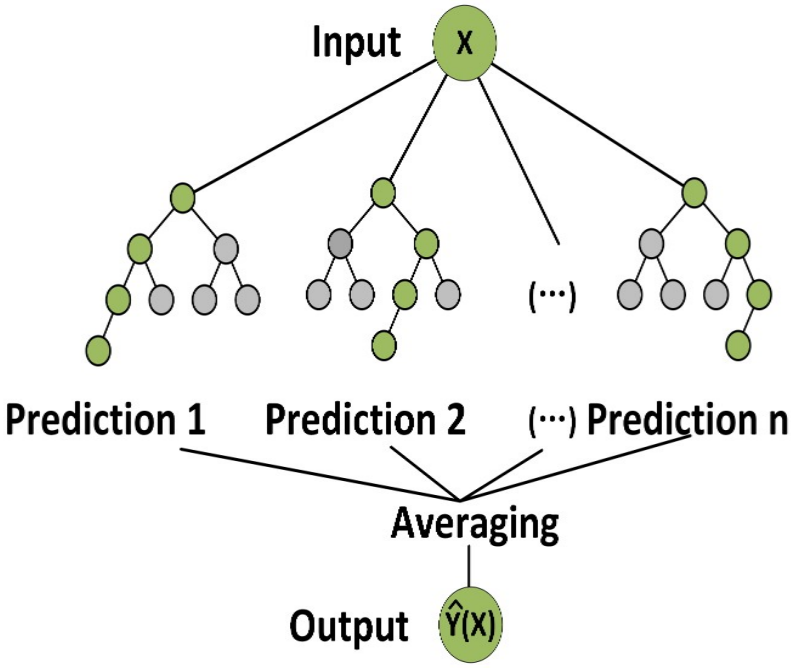

There are many ways available for building a decision tree, for example, the Classification And Regression Tree (CART) [79] is widely used. The CART algorithm splits the training set into two subsets using a single feature k and a threshold t_k, so that this pair (k, t_k) produces the purest subsets. The node's impurity (performance of separation) is measured by mean square error of the separation, so the cost function of CART for regression to minimize is given as [77]:

$$J(k, t_k) = \frac{m_{\text{left}}}{m}\text{MSE}_{\text{left}} + \frac{m_{\text{right}}}{m}\text{MSE}_{\text{right}} \tag{2.48}$$

where

$$\begin{cases} \text{MSE}_{\text{node}} = \sum_{i \in \text{ node}} \left(\hat{y}_{\text{node}} - y^{(i)}\right)^2 \\ \hat{y}_{\text{node}} = \frac{1}{m_{\text{node}}} \sum_{i \in \text{ node}} y^{(i)} \end{cases}$$

here $m_{left/right}$ is number of instances of left/right instances. The subsets will continue to split using the same logic until predetermined max depth is reached.

2.6 Summary

Uncertainty is omnipresent in engineering problems. To deal with problems with uncertainties, various uncertainty quantification methods have been proposed. In this chapter, the methods of uncertainty quantification are summarized. To characterise the properties of uncertainties, most straightforward methods are using simulation methods, but their convergence rely on large data size, which may become unrealistic for complex engineering problems. Sensitivity analysis can be used to find out which input parameters have the largest influence to the response, this can be useful when facing high-dimensional problems. Reliability gives a quantitative measure of system performance under uncertainties. Based on reliability analysis, reliability-based design optimization can be realized. Surrogates are used to replace expensive engineering simulations, which are widely used in sensitivity and reliability analyses. The objective of chapter is to provide the theoretical bases for the following chapters.

Chapter 3

Uncertainty Propagation of Inflow Wind

For Reliability-based Design Optimization (RBDO) of wind turbine structures, the knowledge of the probabilistic characteristics of applied loads on the structures is indispensable. This is possible with the help of simulation codes, such as Turbsim and FAST codes. In FAST simulation, the load responses under given stochastic wind conditions are output in form of time-history sequences. This chapter focuses on the mean values and maximum values of these load histories under different wind uncertainty parameters. To get the statistical characteristics of the load responses, each set of wind uncertainty parameters are run multiple times with different random seeds in Turbsim. This however is very computationally expensive. it's impossible to run all wind scenarios for more comprehensive analyses. So surrogate models are used to replace the time-consuming Turbsim and FAST simulations. There exist many kinds of surrogate models, as reviewed in Chapter.2. Before applying the surrogates, the performance of these surrogates should be compared. So this chapter is structured as follows: in Section.3.1, the introduction of this study is firstly presented, in Section.3.2, the mean values and maximum values of response loads of repeated FAST simulations under different random seeds in Turbsim are discussed; next, in Section.3.3 the performance of 6 popular surrogate models are compared with several mathematical problems; lastly, in Section.3.4, these surrogates are applied to the uncertainty propagation of inflow winds; Section.3.5 is the conclusion.

3.1 Introduction

There have already been very extended studies on the structural modeling of wind turbine tower components, such as the wind turbine blades, the turbine tower, the base foundation, and the control system.

P.J, Schubel and R.J, Crossley [80] have discussed the blade design considering aerodynamics design principles, for example, the optimal blade shape and attack angle. K.J, Smith and D, Griffin [81] have studied the challenges associated with manufacturing and deploying large, land-based wind turbine blades. X.D, WANG, W.Z, Shen [82] have optimized the blade design based on structural dynamics of the blades using the Blade Element Momentum (BEM) theory. P, Fuglsang, H.A, Madsen [83] have optimized the blade to minimize the unit cost of energy. I, Lavassas, G, Nikolaidis [84] have discussed the design of an 1MW-wind turbine tower. H.M, Negm and K.Y, Maalawi [85] have compared the tower optimization designs based on different objectives such as light weight, high stiffness,etc. M, Muskulus, S, Schafhirt [86] have optimized the tower considering different constraints, like static loads, transit loads and fatigue of the tower,etc.

Besides the mechanical components, the control system also play an important role in the performance of wind turbine systems. F.D, Bianchi, De, Battista [87] have introduced the role of control system in wind turbine systems to increase turbine capacities and protect the turbine systems.

To better understand the overall behavior of wind turbine systems, taking into consideration of the turbulent wind fields, component structure properties, and control strategies, several wind turbine system simulators are developed. For example, A.D, Hansen [88] from National Laboratory for Sustainable Energy have developed simulation tool DIgSILENT. J, Jonkman, et al [18] from National Renewable Energy Laboratory (NREL) have developed a simulation tool called Fatigue, Aerodynamics, Structures, and Turbulence code (FAST), which have been widely used by researchers for wind turbine simulations [89], [90].

With the help of simulation codes, many researchers have tried to study the uncertainty propagation of random input variables, for example, J.P, Murcia, P.E, Réthoré [91] have used polynomial chaos expansion (PCE) to characterize the energy production and lifetime

equivalent fatigue loads by taking the mean wind speed, turbulence intensity, yaw misalign, and shear law exponent as input random variables. J, Velarde, C, Kramhøft [92] have investigated the sensitivity of fatigue loads with respect to structural, geotechnical and metocean parameters using Morris screening method, the results show that the uncertainty in fatigue is highly influenced by turbulence intensity. J, Quick, P.E, Hamlington [93] have conducted multilevel, multi-fidelity Monte Carlo sampling considering the uncertainties in the inflow wind conditions, and have reduced the variance of lift expectation over an airfoil. V, Keshavarzzadeh, R.G, Ghanem [94] have presented a computation framework for the shape optimization of blades under uncertainties, where Polynomial Chaos Expansion (PCE) is used to estimate the stochastic performance. Its optimization result under uncertainties are compared with deterministic optimization.

These researchers try to build a relationship between the input stochastic variables and the responses of the turbine system. The goals of building such a relationship are eventually to maximize wind turbine capacities with the lowest cost. However, there exist two problems:

1. **The statistical characteristics of the response loads under stochastic wind fields are not well characterized.**

   This study focuses on the mean values and maximum values of the time-history of the response load sequences under different wind uncertainty parameters. The stochastic wind fields are generated by Turbsim code with uncertainty wind parameters. For each set of the wind uncertainty parameters, 1000 stochastic wind fields are generated with different random seeds which are then input to FAST. The mean value and maximum value distributions of the response load sequences are then characterized.

2. **The accuracy and efficiency of different surrogate models are not compared.** Due to the stochastic wind fields and limited simulation time, the statistical characteristics of response loads are very noisy. This noise will affect the performance of surrogate predictions. A comparison should be made before apply these surrogates for the characterization of the wind responses.

In this chapter, five sources of wind uncertainties: the mean inflow wind speed (V_{mean}), the turbulence intensity (TI), the shear exponent (α), vertical inflow angle (γ_v), and horizontal inflow angle (γ_h) are investigated. Monte Carlo simulations of wind profiles accordant with

IEC61400-1 Normal Turbulence Model (NTM) and Extreme Turbulence Model (ETM) are conducted. To better study the uncertainty propagation of the inflow wind, 6 popular and representative surrogates: Multiple Adaptive Regression Splines (MARS), Kriging (KRG), Polynomial Chaos Expansion (PCE), Support Vector Regression (SVR), Deep Neural Network(DNN), Random Forest Regression (RFR) are used. These surrogates are first tested with several mathematical functions, the computational CPU time, generalized Relative Error (e_R) and Kullback-Leibler Divergence (d_{KL}) are used as criteria to compare their capacities. Then these models are applied for the uncertainty propagation of inflow wind. The flowchart of this chapter is shown in Figure. 3.1.

Figure 3.1: Flowchart of uncertainty propagation of inflow wind

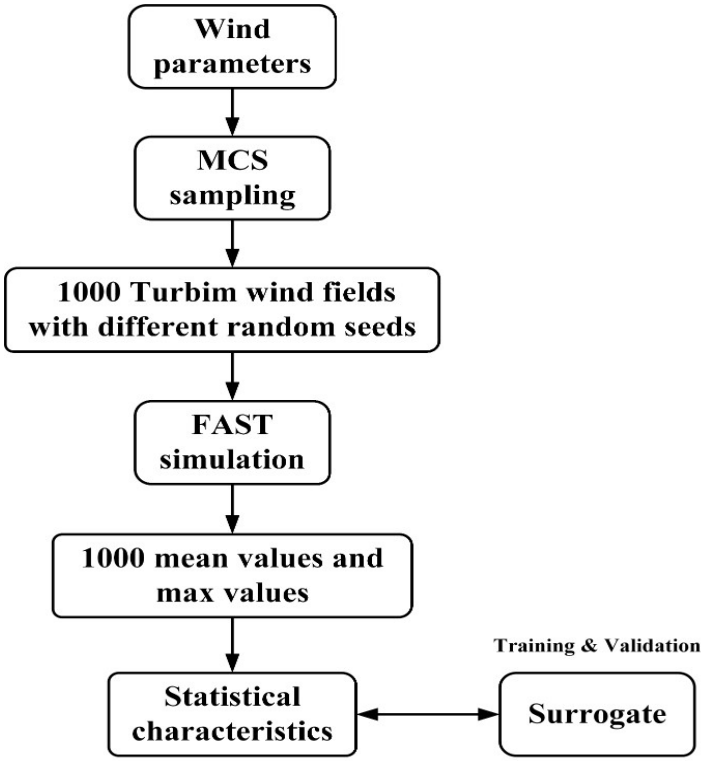

MCS sampling is used to draw samples from the joint distribution of wind uncertainty parameters. For each set of wind parameters, 1000 stochastic wind fields with different random seeds generated by Turbsim. These stochastic wind fields are then input to FAST code, and the mean values and maximum values of response loads on top of wind turbine tower are drawn from the output time-history sequences. Next, distributions of the mean and maximum values from the 1000 simulations are characterized. Then with the statistical parameters of these distributions, a relationship can be established between the input wind parameters with

the statistical response characteristics of the mean value and maximum value distributions. Surrogates can also be trained using this relationship. Lastly, the prediction of the surrogates are then validated with the Turbsim-FAST simulations.

3.2 Characterization of load responses on top of the tower

Due to the stochastic properties of the input wind fields, the probabilistic properties of the corresponding response loads are discussed in this section. First, the reference 5MW wind turbine system used in this study and the correlations between wind uncertainty parameters are presented. Next, the mean value and maximum value distributions of the load responses under stochastic wind parameters (different Turbsim random seeds) are fitted with several common probabilistic distributions. Chi-square goodness-of-fit is used to test the fittings of the distributions.

3.2.1 Reference 5MW wind turbine and wind uncertainty parameters

The wind turbine tower is based on a 5MW reference wind turbine [3] from NREL, the gross properties are shown in Table.4.6.

Table 3.1: Gross Properties of 5MW baseline wind turbine

Rating	5 MW
Rotor orientation, configuration	upwind, 3 blades
Control	variable speed, collective pitch
Drivetrain	high speed, multiple-stage gearbox
Rotor, hub diameter	126 m, 3 m
Hub height	90 m
Cut-in, rated, cut-out wind speed	3 m/s, 11.4 m/s, 25 m/s
Cut-in, rated rotor speed	6.9 rpm, 12.1 rpm
Rated tip speed	80 m/s
Overhang, shaft tilt, precone	5 m, 5°, 2.5°
Rotor mass	110,000 kg
Nacelle mass	240,000 kg
Tower mass	347,460 kg
Coordinate location of overall CM	(-0.2 m, 0.0 m, 64.0 m)

The wind profile is generated using a turbulence simulator Turbsim [25] from NREL consistent with IEC-61400 [95] Normal Turbulence Model (NTM) and Extreme Turbulence

Model with occurrence of 1 year (ETMx1) . In this study, Mann's uniform shear turbulence model [23] is used. As mentioned in Chapter.1, according to IEC61400 standards, the mean value of the wind speed over a time period of 10 min shall be assumed to follow a Rayleigh distribution at hub height given by:

$$P_r(V_0) = 1 - \exp\left[-\pi\left(V_0/2V_{ave}^2\right)\right] \tag{3.1}$$

where, $P_r(V_0)$ is the cumulative probability function, V_0 is the limit wind speed, V_{ave} is the average wind speed.

The wind speed is considered as a function of height given by the power law exponent α :

$$V(z) = V_{hub}(z/z_{hub})^{\alpha} \tag{3.2}$$

where $V(z)$ is the wind speed at height z, V_{hub} is the wind speed at hub height.

The dependency between wind speed and turbulence intensity is given by the local statistical moments based on ICE61400 standards. The turbulence intensity is considered to follow Log-Normal distribution. Its mean value μ_{TI} and standard deviation σ_{TI} are given as:

$$\sigma_{TI} = \left(\ln\left(\frac{1.4^2}{(0.75V_{mean}+3.8)^2}+1\right)\right)^{1/2} \tag{3.3}$$

$$\mu_{TI} = \ln\left(\mathrm{TI}_{\mathrm{ref}}(0.75\mathrm{V}_{\mathrm{mean}}+3.8)\right) - \frac{\sigma_{\sigma_{TI}}^2}{2} \tag{3.4}$$

where TI_{ref} is the reference turbulence intensity. For class 1A wind turbine tower, $TI_{ref} = 0.16$.

The power law exponent α is considered to follow normal distribution. Its mean value μ_α and standard deviation σ_α are given as:

$$\mu_\alpha = 0.088(\ln(\mathrm{V}_{\mathrm{mean}})-1) \tag{3.5}$$

$$\sigma_\alpha = 1/\mathrm{V}_{\mathrm{mean}} \tag{3.6}$$

3.2.2 Distribution of response loads on top of the tower

This study uses FAST [18] and Turbsim [25] codes from NERL to simulate the response loads on top of wind turbine tower. In one simulation example, the response wind history (mean speed 13m/s NTM, in x direction) and the response load (the force on top of tower in x direction) from FAST are shown in Figure.3.2.

Figure 3.2: History of turbulent wind speed and response load

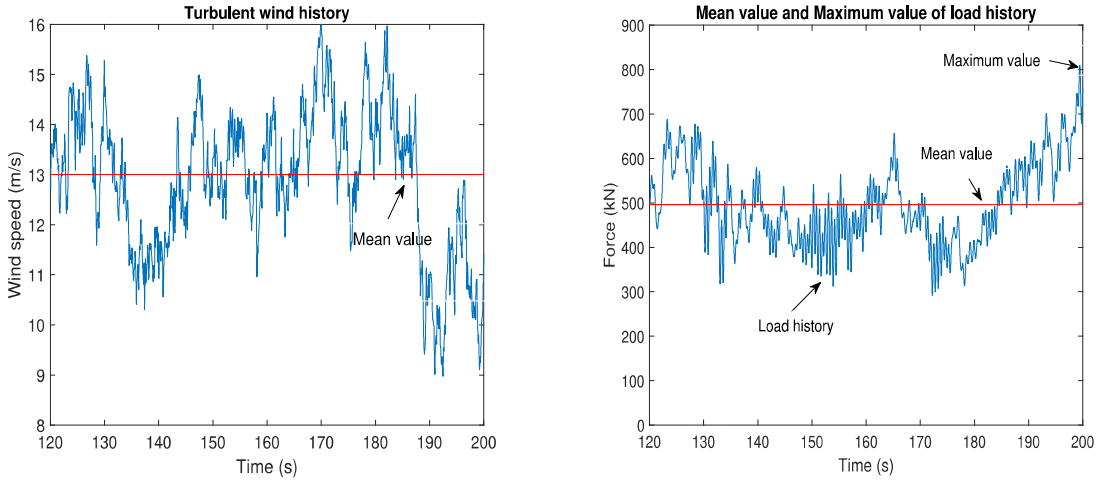

(a) Turbulent wind history W_x (m/s)

(b) Response F_x (kN) on top of tower

The first 120 seconds of FAST simulation are ignored due to the instability of starting simulation phase. In Figure.3.2(b), the mean value and maximum value of the load history are shown.

For each set of wind parameters, 1000 repeated FAST simulations with different Turbsim random seeds are conducted, to get the distribution of the mean and maximum values. Figure.3.4 shows the mean value distributions for NTM and ETM wind conditions with wind speed being 16m/s (wind simulated time 10 minutes, other parameters of Turbsim are set to be default). Figure.3.2 shows the maximum value distributions for NTM and ETM wind conditions with wind speed being 16m/s (wind simulated time 10 minutes, other parameters of Turbsim are set to be default).

Figure 3.3: Mean Fx distribution

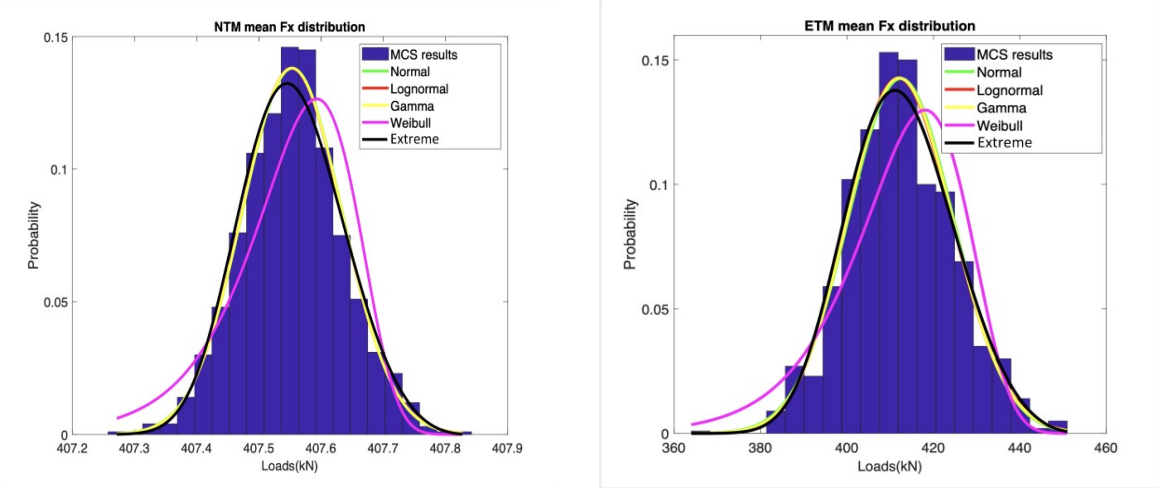

(a) Distribution of NTM mean value of F_x

(b) Distribution of ETM mean value of F_x

Figure 3.4: Max Fx distribution

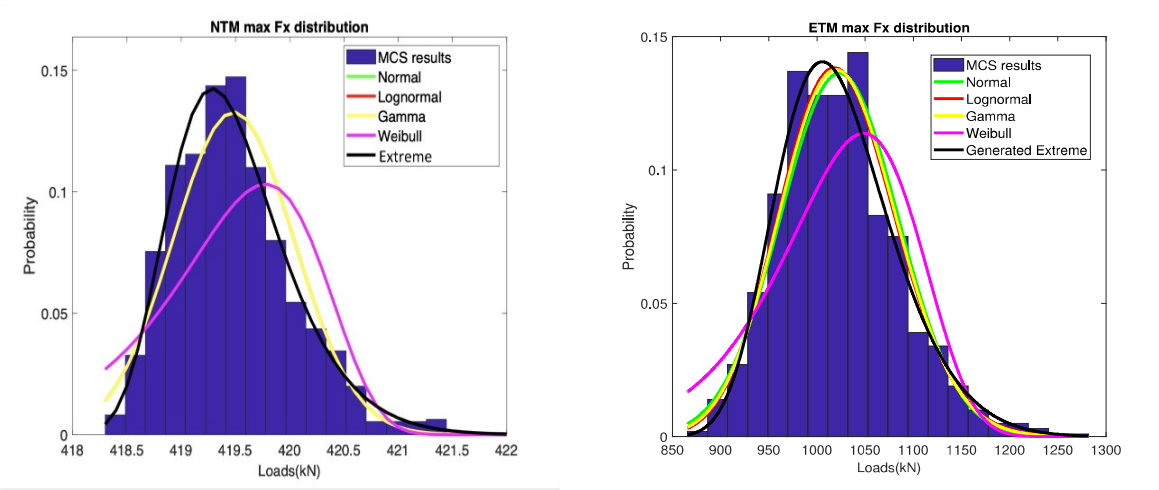

(a) Distribution of NTM max value of F_x

(b) Distribution of ETM max value of F_x

These distributions are then fitted with 5 common distributions, that are Normal distribution, Log-normal distribution, Gamma distribution, Weibull distribution, and Generalized Extreme distribution . Chi-Square Goodness-of-fit is used to test the fittings with a parameter called p-value. The p-value is used in hypothesis testing to help supporting or rejecting the distribution hypothesis. A smaller p-value will support the rejection of this hypothesis. In this study, the threshold p-value for rejecting a hypothesis is chosen to be 0.05. The p-values of Chi-Square Goodness-of-fit of the distributions in Figure.3.4 and Figure.3.3 are shown in Table. 3.2.

Though the hypnosis test can only reject Weibull distribution for both NTM and ETM

Table 3.2: p-value of Chi-Square Goodness-of-fit

	Normal	Lognormal	Gamma	Weibull	Extreme
NTM mean	0.38	0.29	0.23	0	0.20
NTM max	0	0	0	0	0.16
ETM mean	0.24	0.17	0.14	0	0.22
ETM max	0	0.02	0	0	0.37

mean distributions, this study will assume the mean value distributions follow normal distribution. While the maximum value distributions of NTM and ETM can only be fitted well by generalized extreme distribution (Type III).

If the wind speed is taken as the only input variable (by setting other parameters default, and the inflow angles to be zero), the relationship between the wind speed with the forces and moments on top of the tower are shown in Figure.3.5 and Figure.3.6.

Figure 3.5: Forces on top of tower with different wind speeds

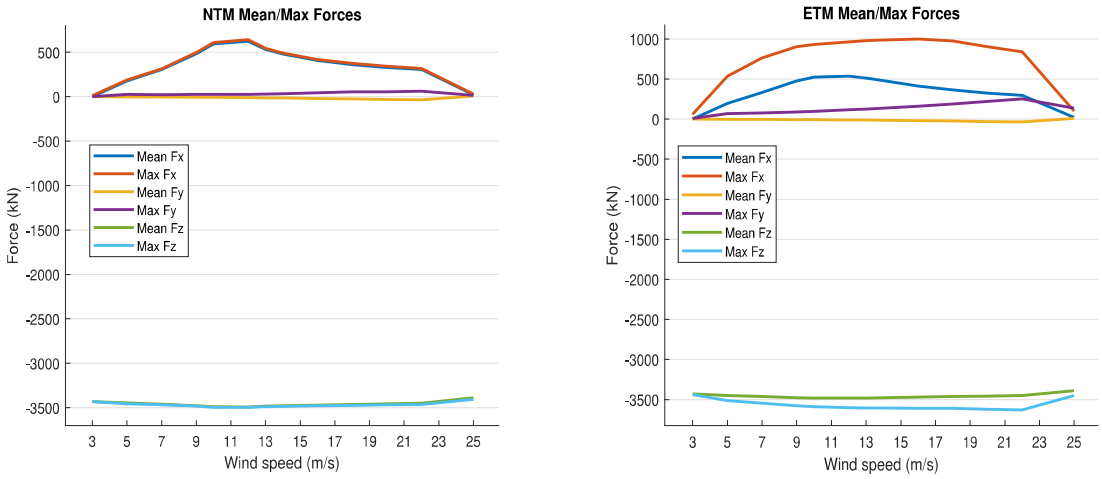

(a) NTM forces on top of the tower

(b) ETM forces on top of the tower

Figure 3.6: Moments on top of tower with different wind speeds

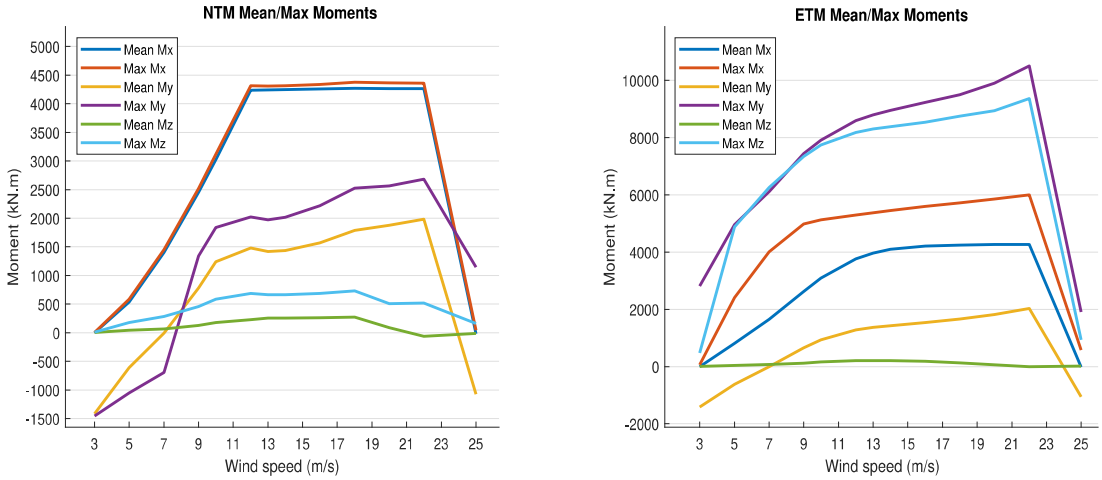

(a) NTM moments on top of the tower

(b) ETM moments on top of the tower

As can be see, the forces and moments steadily increase before reaching wind turbine rated wind speed. Then these loads will be stabilized by control system via adjusting the pitch and yaw. The loads will quickly decrease when the wind speed surpass wind turbine cut-out speed, when the turbine is shut down.

After the mean values and maximum values of response loads are fitted with normal and generalized extreme distributions, relationships can be built between the input wind uncertainty parameters and the statistical moments of the mean value and maximum value distributions. However, getting the statistical moments of these distributions is very time-consuming, it's impossible to simulate all combinations of wind parameters. So surrogate models are used. Before applying the surrogates, their performances are firstly compared.

3.3 Comparison of surrogates

As reviewed in Section.2.5, there exist different types of surrogates. The choice for these surrogates are quite problem oriented, it's not suitable trying to figure out which one is best for all situations. So in this section, 6 surrogate models mentioned in Section.2.5: MARS, KRG, PCE, SVR, RFR, and DNN are compared. Their performances are firstly tested with several mathematical problems.

3.3.1 Performance measure of surrogates

After the surrogates are built, measures are taken to evaluate their performance, in this section, 3 performance measures are used.

Generalized relative error

The error of the surrogate predictions can be assessed by generalized relative error (e_R), the generalized relative error is given by:

$$e_R = \frac{\sum_{i=1}^{n}(Y(\boldsymbol{x}^{(i)}) - \hat{Y}(\boldsymbol{x}^{(i)}))^2}{\sum_{i=1}^{n}(Y(\boldsymbol{x}^{(i)}) - \mu_Y)^2} \tag{3.7}$$

where μ_Y is the mean value of the validation data $Y(\boldsymbol{x})$, $\hat{Y}(\boldsymbol{x})$ is the prediction of $Y(\boldsymbol{x})$.

Kullback-Leibler divergence

Kullback-Leibler divergence (d_{KL}) is used to measure the difference between the true distribution and the predicted distribution. $Y(X)$ and $\hat{Y}(X)$ follow the same distribution when $d_{KL} = 0$. The d_{KL} is calculated as:

$$d_{KL}(Y(X)||\hat{Y}(X)) = \sum_{i=1}^{n} Y(\boldsymbol{x}^{(i)}) \log\left(\frac{Y(\boldsymbol{x}^{(i)})}{\hat{Y}(\boldsymbol{x}^{(i)})}\right) \tag{3.8}$$

CPU time

To compare the computational cost, the CPU time for building the surrogates are compared on a Intel®Core™ 6700hq CPU.

3.3.2 Hyper-parameters of the surrogates

The MARS surrogate is implemented in ARESLab toolbox[96]; the Kriging, PCE and SVR are implemented in UQlab [97], the RFR is implemented in scikit-learn [98], DNN is implemented in Tensorflow [99]. The hyper-parameters will have a great impact for the performance of the surrogate models, the hyper-parameters are shown in Table.3.3.

Table 3.3: Hyper-parameters

Methods	Hyper-parameters	Values
MARS	Order q, Penalty c	$q = 2$, $c = 0$
KRG	Correlation, Estimation method	matern-5/2, ML
PCE	Optimization method, Degree	LARS, 2:15
SVR	Order, QPsolver, Kernel	1, SMO, matern-5/2
RFR	Max depth, Num trees, Validation	range(2,6), range(200,800), CV
DNN	Type, Activation, Optimizer, Layers, Nodes, Early-stop	Sequential fully-connected, LeakyRelu, Adam, 3, 75, True

3.3.3 Comparison on mathematical problems

A simple one-dimensional problem

The surrogates are first tested with a non-noisy sinuous function of Equation.3.9. $\boldsymbol{x} \sim U(0, 15)$ is uniformly distributed over [0 15].

$$y = x\sin(x) \tag{3.9}$$

10 uniformly distributed points are firstly used to train the surrogates, the prediction tracks from the 6 surrogates are shown in Figure.3.7(a). In the figure, the training points are marked with red dots, and the true curve is marked with the blue dash line. It's obvious that PCE and RFR have bigger error compared with other models. The boxplot of the logarithm generalized relative error($\log_{10}(e_R)$) over 50 simulations is shown in Figure.3.7(b). For each box, the central mark indicates the median, and the bottom and top edges of the box indicate the $25th$ and $75th$ percentiles, respectively. The outliers are plotted individually using the '+' symbol. It can be seen that for this example, the KRG has the lowest relative error when data size is small, which is shown in Table.3.8.

Figure 3.7: Surrogate prediction curve comparison

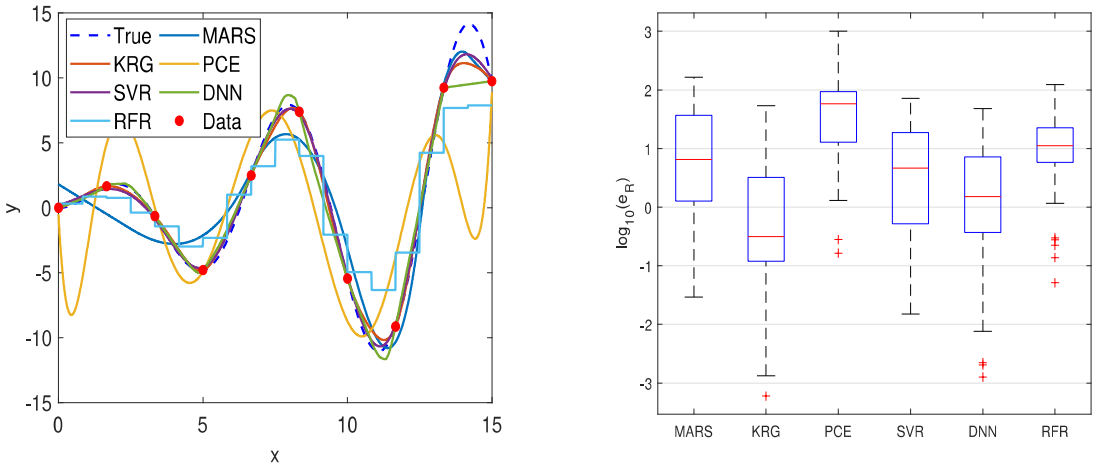

(a) 10 training points without noise

(b) Generalized error comparison

Table 3.4: Comparison of mean log_{10} generalized relative error

Methods	MARS	KRG	PCE	SVR	DNN	RFR
$\mu(log_{10}(e_R))$	0.73	-0.32	1.51	0.49	0.08	0.97

If there exists noise in the training data, and the training set is comparably large, the performance of the surrogates may be worsened by over-fitting. So in this test, a arbitrary noise ε that follows $N(2,1)$ is added into the response, and 32 training points are used to train the surrogates.

Figure.3.8(a) shows the fitting curves of different surrogates. The box-plot of generalized error comparison (e_R) over 50 simulations is shown in Figure.3.8(b). Table.3.5 shows the average e_R values. It can be observed that PCE has the best performance when facing noisy data in this example, while the accuracy of KRG is strongly affected by over-fitting.

Table 3.5: Comparison of mean generalized relative error

Methods	MARS	KRG	PCE	SVR	DNN	RFR
e_R	0.027	0.085	0.019	0.052	0.039	0.037

Figure 3.8: 32 training points with noise

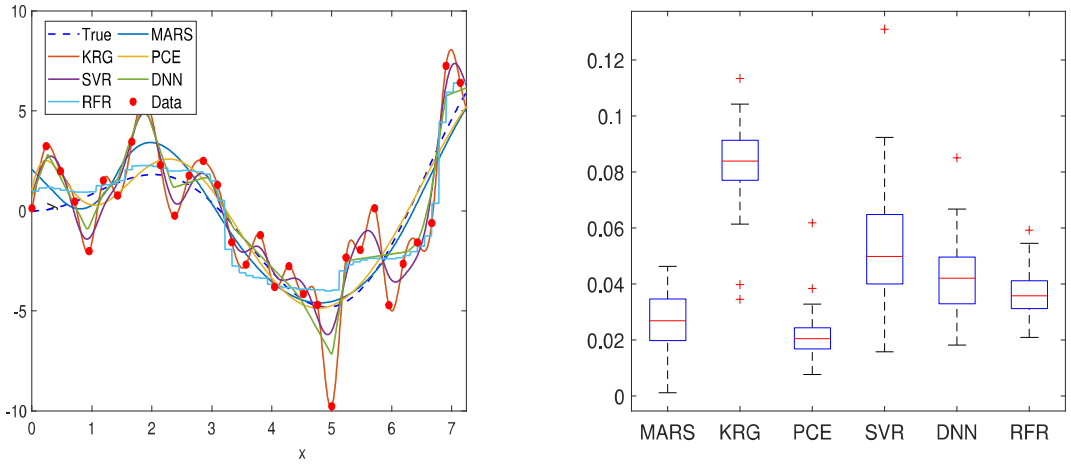

(a) Surrogate prediction curve comparison

(b) Generalized error comparison

Sobol's function

This example uses a 8-dimension Sobol's function, and X is uniformly distributed over the interval [0, 1]. The Sobol's function is given by:

$$f_2(\boldsymbol{X}) = \prod_{i=i}^{8} \frac{|4X_i - 2| + c_i}{1 + c_i} \tag{3.10}$$

where $c = (1, 2, 5, 10, 20, 50, 100, 500)^\top$

First, 128 training points sampled by Latin Hyper-cube Sampling (LHS) are used to train the surrogates, and the predictions are shown in Figure.3.9(a). In the figure, the x axis represents the true values Y_t while the y axis represents the predictions from the surrogates Y_p .

For 50 simulations, the $log10$ Kullback-Leibler divergence (d_{KL}) is shown in Figure.3.9(b) and their average are given in Table.3.6. It can be seen that MARS, KRG, and PCE have comparably better performance than SVR, DNN, and RFR.

Table 3.6: Comparison of mean Kullback-Leibler divergence

Methods	MARS	KRG	PCE	SVR	DNN	RFR
$log_{10}(d_{KL})$	-0.902	-0.718	-0.818	-0.119	-0.6630	0.334

Figure 3.9: Sobol's function

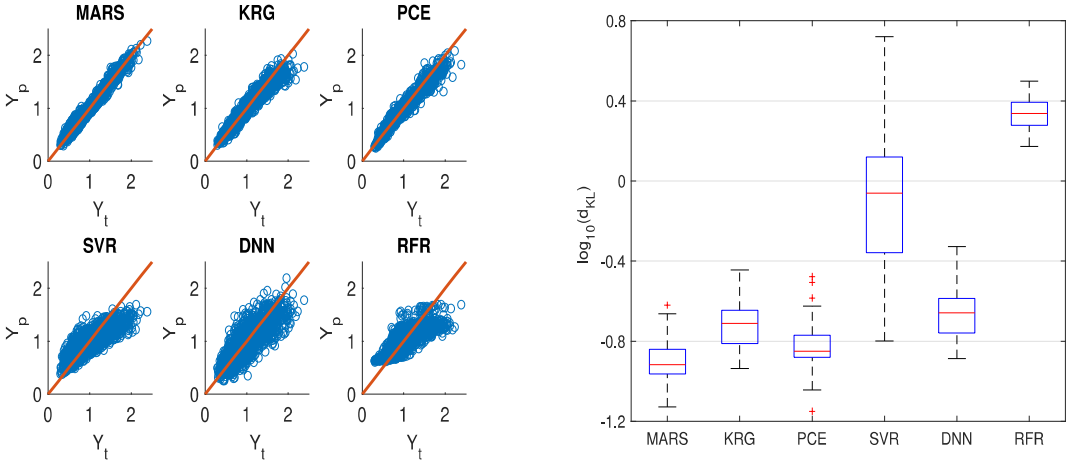

(a) Prediction of surrogates

(b) Kullback-Leibler divergence comparison

Next, the CPU time and error comparisons with different sample size are shown in Figure.3.10. It can be seen that all the surrogate models take more time to train when the sample size increases, however, SVR, PCE, and KRG increase more dramatically, as shown in Figure.3.10(a). As shown in Figure.3.10(b), for small data size, KRG has the best accuracy. By increasing the data size, the accuracy for MARS and PCE surrogates may catch up, while DNN will be advantageous when facing larger data sets for its lower computational cost as shown in Figure.3.10(a).

Figure 3.10: Sobol's function with different data size

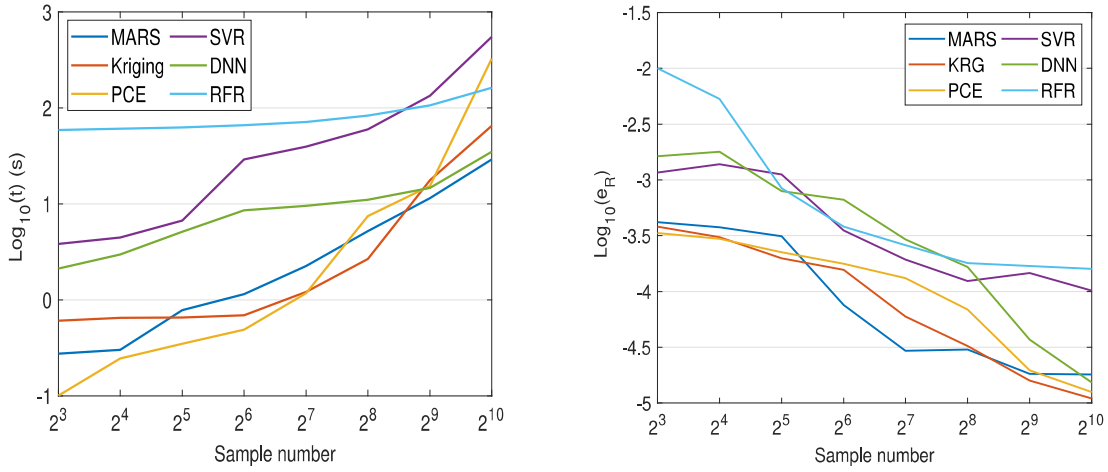

(a) CPU time comparison

(b) Generalized relative error comparison

3.4 Uncertainty propagation of inflow wind

To evaluate the uncertainty propagation of wind uncertainties to the characteristics of response loads, 5 wind uncertainty variables mentioned in Section.3.2 are used to represent the turbulent wind profile, namely, the mean inflow wind speed (WS, V_{mean}), the turbulence intensity (TI), the shear law exponent(SE, α), the vertical inflow angle (VA, γ_v), and the horizontal inflow angle (HA, γ_h). The vertical inflow angle and the horizontal inflow angle are considered to be independent with other variables, and are assumed to follow Beta distribution. The range of the Beta distribution are set to be -15 degrees to 15 degree, and the shape parameter is chosen to be [4, 4]. The wind speed is considered to follow Rayleigh distribution, with the mean value chosen to be 13m/s. These turbulence intensity and the shear law exponent are assumed to follow log-normal distribution and normal distribution respectively. Their moments are calculated with Equation.3.3 to Equation.3.6 in Section.3.2. The wind conditions are summarized in Table.3.7.

Because the turbulence intensity and shear exponent are correlated with wind speed, Rosenblatt transformation [100] is first used to transform the correlated input variables into

Table 3.7: Variables of wind condition

Variable	Distribution	Moments
Wind Speed (v_{mean})	Rayleigh	$\mathbb{E}(\mathrm{v_{mean}}) = 13\mathrm{m/s}$
Turbulence Intensity (TI)	Log-normal	μ_{TI}, σ_{TI}
Shear Exponent (α)	Normal	$\mu_{\alpha}, \sigma_{\alpha}$
Vertical Inflow Angle (γ_v)	Beta	shape [4 ,4] Range[-15, 15]
Horizontal Inflow Angle(γ_h)	Beta	shape [4 ,4] Range[-15, 15]

uncorrelated standard Gaussian variables:

$$\mathbf{u} = R(\mathbf{w}) \tag{3.11}$$

where R is the Rosenblatt transformation. Wind uncertainty parameters are then sampled with LHS method. Each wind sample are run 1000 repeated times with different random Turbsim seeds. The statistical mean of the response distributions that are discussed in Section.3.2.2 are seen as target response loads. 500 samples are used to train the surrogates, and 1000 samples are used to validate their performance.

The predictions for the mean Fx and maximum Fx from surrogates trained by 500 samples are shown in Figure.3.11(a), and Figure.3.11(b) respectively. In the figures, the x axis represents the validation sets, while the y axis represents the predictions from the surrogates.

Figure 3.11: Comparison of surrogate prediction of load responses

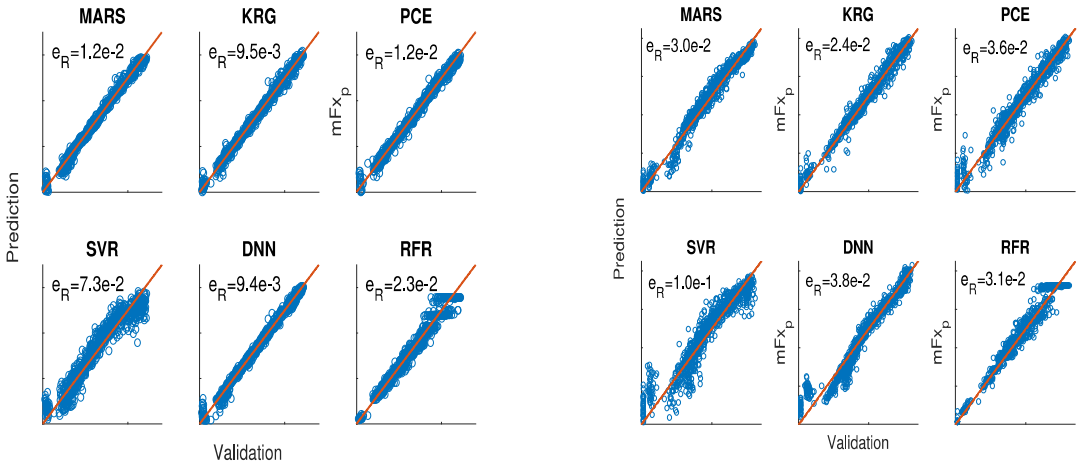

(a) Surrogate prediction for mean Fx

(b) Surrogate prediction for max Fx

Their performances for the prediction are shown in Table.3.8 and Table.3.9.

Table 3.8: Comparison of surrogates for wind loads of 500 samples for mean Fx

Criteria	MARS	KRG	PCE	SVR	DNN	RFR
$e_R(\rightarrow 0)$	1.2e-2	9.5e-3	1.2e-2	7.3e-2	9.4e-3	2.3e-2
$d_{KL}(\rightarrow 0)$	0.7788	0.3610	0.3854	1.5041	1.1437	2.6242
CPU_{time}	17.41	9.73	9.32	52.65	30.61	93.09

Table 3.9: Comparison of surrogates for wind loads of 500 samples for maximum Fx

Criteria	MARS	KRG	PCE	SVR	DNN	RFR
$e_R(\rightarrow 0)$	0.0303	0.0236	0.0363	0.0999	0.0377	0.0316
$d_{KL}(\rightarrow 0)$	0.8486	0.377	0.5053	1.5041	1.2626	3.1355
CPU_{time}	23.14	11.37	6.75	60.66	31.61	96.36

The histogram of maximum Fx generated by surrogate predictions are compared with validation sets in Figure.3.12.

Figure 3.12: Histogram comparison of different surrogates for max Fx

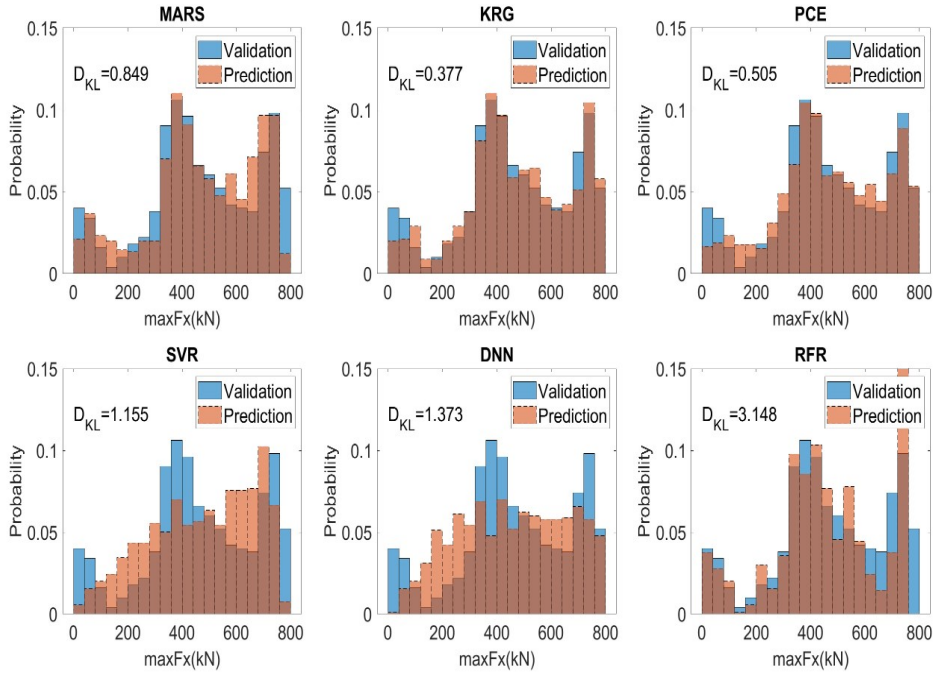

From the results, MAR, KRG, PCE, and RFR can achieve lower relative error than DNN and SVR.

For RFR and DNN, the Kullback-Leibler divergence(d_{KL}) is comparably high, which indicates bigger difference in the output distribution, as shown in Figure.3.12. MARS and DNN take much more time to train than KRG and PCE for this data size of 500. KRG and

PCE have similar performance, KRG has lower e_R (9.5e-3 and 2.4e-2 compared to 1.2e-2 and 3.6e-2), and smaller d_{KL} (0.361 and 0.377 compared to 0.385 and 0.505). So after all the comparison, KRG is the best for the uncertainty propagation of inflow wind.

3.5 Conclusion

This chapter uses Turbsim and FAST to simulate response loads on top of the wind turbine tower. In the first step, the distributions of the mean and the maximum of the response load sequences are characterized. It is shown that, for a given wind condition, the mean value, the maximum of the response loads on the top of tower can be approximated with normal and extreme distribution respectively. In the second step, 6 types of regression surrogates are used to regenerate the characteristics of the distributions. These surrogates are first applied to several mathematical functions, the computational CPU time, generalized Relative Error(e_R), and Kullback-Leibler Divergence (d_{KL}) are used as performance measures. These surrogates are then applied to the uncertainty quantification of wind loads. The results show that, it's possible to build a relationship between input wind uncertainties and the statistical characteristics of response loads on top of the tower. The surrogate comparison shows KRG can achieve lower generalized relative error e_R and smaller Kullback-Leibler divergence d_{KL} for the wind uncertainty propagation problem.

Chapter 4

Reliability-based Design Optimization of Wind Turbine Tower

To conduct reliability-based design optimization (RBDO), traditional methods use double-loop approach where the outer-loop changes the design variable, and the inner-loop calculate the reliability. This is computational expensive for high reliability problems. For complex engineering applications, surrogate models are widely used to replace the time-consuming limit states. So this chapter focuses on the reliability-based design optimization (RBDO) of wind tower using Kriging-assisted double-loop approach. In Section.4.1, the state of the art of RBDO is reviewed; in Section.4.2, the traditional RBDO, single -loop approaches and decoupled methods are summarized; in Section.4.4, the procedures of single loop approach (SLA) coupled with Kriging surrogate is proposed; in Section.4.5, the proposed method is firstly applied to several mathematical problems and then to RBDO of wind turbine tower. Section.4.6 is the conclusion.

4.1 States of the art

Structural optimization is considered as modern design, where is usually applied to find the best design with reducing costs and improving structural performances. The optimal design is generally searched by minimizing the structural cost while checking performance criteria and particular design requirements [101]. However, Uncertainty is omnipresent in real applications. For that purpose, a rational structural design involves considering uncertainty

parameters related to design parameters due to manufacturing tolerances, material properties or imperfect knowledge of the material behaviors, environmental conditions, operating conditions including future degradation and model analyzes. All these uncertainties contribute to making the structural performances different from the expected ones. The probability theory offers a suitable framework for modelling such uncertain parameters [102]. The pioneers in this new approach date from the last century [103], [104]. The concept of the reliability of structures was first proposed by Freudenthal [105] that a rational structural design requires to consider uncertainties, nowadays the safety of structures has become an indispensable part of designing structures, such as industrial, civil engineering, automotive, spatial domains,etc. [106]. For complex structures, the reliability and performance of mechanical system may be impacted by several failure modes, such as ultimate limit states (stress, buckling, etc.), service limit states (displacements, frequency, etc.) and fatigue.

The deterministic optimization does not lead to reliable solutions. When the deterministic optimal design is significantly affected by uncertainties, optimization procedures often lead to designs at the limits of some constraints, so their remaining margins are reduced to their lower bounds. To alleviate this situation, the deterministic design optimization uses safety factors to reduce the effects of uncertainty parameters. These safety factors are defined by standard specifications or by engineering feedback. Nevertheless, the use of the safety factors in optimizing the structural design is not adapted to determine the optimal with appropriate reliability, as these factors are not directly linked to uncertainties and to the target safety level [107]. Moreover, these safety factors often lead to either risky or over-conservative designs.

To address such shortcomings, the design optimization is formulated by considering the probabilistic constraints. The Reliability-Based Design Optimization (RBDO) was developed since the 1960's. Hilton and Feigen [108], then Moses and Kinser [109] are considered as the first works that are proposed the formulation of the design optimization under reliability constraints. The RBDO considers uncertainties in the design optimization procedure, with a way that the safety requirements are fulfilled. It consists in finding the best design ensuring safety, where the performance constraints are replaced by failure probability constraints with respect to these performance functions. Thus, the RBDO methodology involves the evaluation of probabilistic constraints performed by reliability analysis, which can be done by

moment methods, Monte-Carlo simulations or by approximation methods [110]. Optimization procedures and reliability analysis demand the repeated evaluation of the structural response for different sets of design variables and uncertain parameters, where the evaluation of the structural response is often obtained by numerical models with costly computation. (e.g. Finite Element models). Thereby, the approach to practical problems obviously involves several difficulties, most of them related to the practical evaluation of probabilities of failure and their sensitivities. Four difficulties of the RBDO methodology can be addressed: (i) The computational cost required by the RBDO methodology and especially the reliability analysis methods; (ii) The numerical convergence of the optimization procedure and the reliability approach employed; (iii) The accuracy of the reliability analysis methods; (iv) Efficiency of the optimization procedure to deal with complex problems [111].

To solve the RBDO problem, 3 levers have been used: (i) Several tools have been developed for reducing the computational demand of the reliability analysis, as the development of the moment methods and approximation methods for the reliability analysis [112]–[114]; (ii) The development of new strategies to deal the RBDO, single loop methods and decoupled methods [115], [116] and parallel computing techniques [117] are proposed in this way; (iii) The application of surrogate models in order to replace the costly numerical models by less expensive ones [118].

The classical formulation of the RBDO approach is the double-loop methods, that consists to solve the RBDO problem in two loops, the outer loop tries to solve the optimization problem by changing the design variables, while the inner loop solves the reliability constraints. The constraints can be evaluated with Monte-Carlo Simulations (MCS), which is straightforward, but it needs large sample sets and becomes prohibitive when the probability of failure is low [119]. Approximation methods are proposed to reduce the computation cost. The reliability index defined by Hasofer and Lind [120] is widely used in the first formulation of the RBDO, called the Reliability index approach (RIA) [112], [113]. Tu, Choi, and Park [114] have proposed the performance measure approach (PMA), which has proven to be more robust and efficient in evaluating inactive probabilistic constraints. These two first-order reliability methods (FORM) are easy to implement but are time-consuming for complex constraints, because for each time the design variables are changed, the inner loop must

calculate the reliability constraints separately. Recently, new methods have been proposed, using new sampling methods to reduce the number of simulations, Rashki, Miri, and Azhdary Moghaddam [121] have proposed a new simulation method to approximate the probability of failure and the most probable failure point, then this method is applied for RBDO [122]. Other simulation approaches are also proposed for RBDO, like the weighted average simulation techniques [123]. To reduce the computational cost of the double loop approach, single loop approach methods and decoupled approaches have been proposed. Madsen and Hansen [124] have proposed a method based on the Karush-Kuhn-Tucker(KKT) optimality conditions, where the RBDO problems are transformed into KKT optimality conditions. Liang, Mourelatos, and Tu [125] have based on KKT method, and have further developed a Single Loop Approach (SLA) where, the nested RBDO problem is transformed into equivalent deterministic single-loop processes. Du and Chen [126] have proposed the Sequential Optimization and Reliability Assessment (SORA) method. Cheng, Xu, and Jiang [127] have proposed a Sequential Approximate programming (SAP) method, these methods all try to separate the reliability analysis from the optimization loop and transform the RBDO problem into deterministic optimization loops to improve efficiency.

For complex engineering problems, metamodels are widely used to substitute complex reliability constraints. Hyeon Ju and Chai Lee [128] have used Kriging metamodel and moment method to solve RBDO problem. Lee and Jung [119] have proposed a constraint boundary sampling(CBS) method, that adds more training points on the limit state functions and have used MCS to solve the reliability problems. Chen, Qiu, Gao, *et al.* [129] have proposed a local adaptive sampling (LAS) method, that will add points around current design points to update the Kriging metamodel, and have used FORM to perform the reliability analysis. Dubourg and Sudret [130] have used important sampling (IS) method to build the Kriging model and have used MCS to perform the reliability analysis. Lv, Lu, and Wang [131] have proposed a sequential sampling for Kriging using PMA method and add samples using expected relative improvement (ERI) criterion, which focuses more points on current most probable point (MPP). Zhang, Xiao, and Gao [132] have used **U** function to update the Kriging and calculate the reliability using subset simulation(SS). These sampling methods separate the processes of training the Kriging metamodels and the reliability analysis, they

use double loop methods to solve RBDO problems. Several authors have found that the single loop approach is more suitable for RBDO [115], [133], [134]. To further improve the efficiency of Kriging-based RBDO, this section tries to combine the Kriging surrogate with the Single Loop Approach (SLA). The Kriging metamodel is updated by using the Most Probable Points (MPPs) calculated at each iteration of SLA [135]. This section is structured as follows, in part 1, previous works of RBDO are discussed, in part 2, the theory of Kriging metamodel is briefly introduced, in part 3 the Kriging-SLA method is introduced, in part 4, three well-known benchmark examples and an practical engineering problem are used to demonstrate the efficiency and the limitations of the proposed method. The last part is the conclusion.

4.2 Reliability-based design optimization methods

Reliability-based design optimization seeks to find the best compromise between cost and reliability.

4.2.1 Classical RBDO

The classical RBDO consists in minimizing the objective function using double loop approach, where the outer-loop minimizing the objective function and the inner-loop calculate the reliability, the formulation can be written as:

$$\begin{aligned} &\min : C(\mathbf{d}, \mu(\mathbf{X})) \\ &\text{s.t.} \ : \begin{cases} \Pr[G_i(\mathbf{d}, \mathbf{X}) \leq 0] \leq P_{f_i} & i = 1, \ldots, m \\ h_j(\mathbf{d}) \leq 0 & j = m+1, \ldots, M \end{cases} \end{aligned} \tag{4.1}$$

here. $\mathbf{d}$ is the design variables, G_i is the ith performance function, P_r is the probability of failure, h_j is the jth constant constraint, P_{f_i} is the allowable probability of failure. The failure rate Pr can be calculate with simulation methods shown in Section.2.4 or approximation methods shown in Section.2.2.

4.2.2 Single-loop and decoupled methods

To reduce the computational cost for the classical RBDO methods of double-loop approaches in Section.4.2.1, single-loop and decoupled methods are proposed. In single loop methods,the reliability constraints are transformed into equivalent optimality conditions such as SLA. While, the decoupled methods seek to transform the reliability problems into sequences of deterministic optimization problems such as SORA. So in section, these two representative methods are summarized.

Single loop approach (SLA)

Single loop approach (SLA) is developed from FORM method (In Section.2.2), by adopting the Karush-Kuhn-Tucker (KKT) condition of Equation.2.4:

$$\nabla G(\boldsymbol{U}) + \lambda \nabla H(\boldsymbol{U}) = 0 \tag{4.2}$$

Where $\boldsymbol{U}$ is $\boldsymbol{X}$ transformed in standard normal space, $\nabla H(\boldsymbol{U}) = ||\boldsymbol{U}|| - \beta_i^t$, is the equality constraint of PMA, λ is the Lagrangian multiplier.

By considering $\nabla H(\boldsymbol{U}) = 2\boldsymbol{U}$, the relation Equation 4.2 yields:

$$\boldsymbol{U} = -[||\nabla G(\boldsymbol{U})||/(2\lambda)](\nabla G(\boldsymbol{U})/||\nabla G(\boldsymbol{U})|| \tag{4.3}$$

The length of vector of $\boldsymbol{U}$ in the normal space is equal to β_i^t, Equation 4.3 is transformed as:

$$\boldsymbol{U} = -\beta_i^t \boldsymbol{\alpha} \tag{4.4}$$

Where $\boldsymbol{\alpha}$ are the normalized gradient of the constraints. Finally, the formula of SLA can

be summarized as:

$$\min C(\boldsymbol{d}^{(k)}, \boldsymbol{\mu}_U^{(k)})$$
$$st. \begin{cases} G_i(\boldsymbol{d}^{(k)}, \boldsymbol{U}^{(k)}) \geq 0 \\ \boldsymbol{U}_i^{(k)} = -\boldsymbol{\alpha}_i^{(k)} \beta_i^t \\ \boldsymbol{\alpha}_i^{(k)} = \frac{\boldsymbol{\sigma}_U \nabla_{\boldsymbol{U}} G_i(\boldsymbol{d}^{(k-1)}, \boldsymbol{\mu}_i^{(k-1)})}{||\boldsymbol{\sigma}_U \nabla_{\boldsymbol{U}} G_i(\boldsymbol{d}^{(k-1)}, \boldsymbol{\mu}_i^{(k-1)})||} \\ \boldsymbol{d}^L \leq \boldsymbol{d} \leq \boldsymbol{d}^U, \boldsymbol{\mu}^L \leq \boldsymbol{\mu} \leq \boldsymbol{\mu}^U \end{cases} \quad i = 1, 2, ...m \tag{4.5}$$

Where $\boldsymbol{U}_i^{(k)}$ is the random design variables in the normalized space, $\boldsymbol{\mu}_U^{(k)}$ is the statistical mean of $\boldsymbol{U}_i^{(k)}$, k is the iteration number of SLA, $\boldsymbol{d}^{(k)}$ is the deterministic design variables, $G_i(\boldsymbol{d}^{(k)}, \boldsymbol{U}^{(k)})$ is the ith constraint, β_i^t is the target reliability index for the ith constraint, $\boldsymbol{\alpha}_i^{(k)}$ is the normalized gradient vector of the ith constraint. $f(\boldsymbol{d}^{(k)}, \boldsymbol{\mu}_U^{(k)})$ is minimized under the deterministic constraints $G_i(\boldsymbol{d}^{(k)}, \boldsymbol{U}^{(k)}) \geq 0$.

Sequential optimization and reliability assessment (SORA)

The SORA method belongs to the kinds of decoupled methods, where the RBDO problem is transformed into a sequence of deterministic optimizations. In each iteration, the design variables are shifted under the deterministic constraints as:

$$\min : C\left(\mathbf{d}^k\right)$$
$$\text{s.t.} : \begin{cases} G_i\left(\mathbf{d}^k - \delta_i^{k-1}, \check{\mathbf{x}}_i^{k-1}\right) \geq 0 & i = 1, \ldots m \\ h_j\left(\mathbf{d}^k\right) \leq 0 & j = m+1, \ldots, M \end{cases} \tag{4.6}$$

here $\mathbf{d}^k$ is the design variable in the kth iteration, $\check{x}_i^{k-1}$ is the minimum performance target point (MPTP) in the physical space, δ_i^{k-1} is the shift parameter, that are calculated as:

$$\begin{aligned} \check{\mathbf{x}}_i^{k-1} &= T\left(\mathbf{u}^{*T}\right) \\ \delta_i^{k-1} &= \mathbf{d}^{k-1} - \check{\mathbf{x}}_i^{k-1} \end{aligned} \tag{4.7}$$

4.3 Surrogate assisted RBDO

For complex problems, where the evaluation of performance function involves computational expensive simulations, surrogate models are widely used as summarized in Section.2.5. Hyeon Ju and Chai Lee [128] have used Kriging metamodel and moment method to solve RBDO problem. Lee and Jung [119] have proposed a constraint boundary sampling (CBS) method, that adds more training points on the limit state functions and have used MCS to solve the reliability problems. Similarly, Bichon, Eldred, Swiler, *et al.* [136] uses Expected Feasible Function (EFF) to find new points that are expected to better satisfy the equality constraints. Echard, Gayton, and Lemaire [137] have proposed an active learning reliability method combining Kriging and Monte Carlo simulation (AK-MCS). The AK-MCS method utilizes EFF or $\boldsymbol{U}$ function to update the Kriging iteratively and uses the coefficient of variation (Cov) of the probability of failure as its stopping criteria. Wang and Wang [138] have defined a Cumulative Confidence Level (CCL) measure to search the points that increase the confidence level. Sadoughi, Li, Hu, *et al.* [139] has proposed a high-dimensional reliability analysis (HDRA) that employs sequential exploration-exploitation with dynamic trade-off method (SEEDT) to alleviate the curse of dimensionality for conducting surrogate-based reliability problems. Chen, Qiu, Gao, *et al.* [129] have proposed a local adaptive sampling (LAS) method, that adds new points using Constraint Boundary Sampling (CBS) around current design points which are calculated with MCS from last iteration. Li, Qiu, Chen, *et al.* [140] have proposed a similar method that searches new sampling points around the current MPP. The current MPP is calculated with reliability index approach (RIA). Dubourg and Sudret [130] have used important sampling (IS) method to build the Kriging model and have used MCS to perform the reliability analysis. Lv, Lu, and Wang [131] have proposed a sequential sampling for Kriging using PMA method and add samples using expected relative improvement (ERI) criterion, which focuses more points on current most probable point (MPP). Zhang, Xiao, and Gao [132] have used **U** function to update the Kriging and calculate the reliability using subset simulation(SS). In this section, The mostly commonly used EIF and EFF update methods are introduced. The prediction that Gaussian surrogates give of a untrained point can be expressed

as:

$$\hat{Y}(\mathbf{x}) \sim N\left[\mu_Y(\mathbf{x}), \sigma_Y(\mathbf{x})\right] \tag{4.8}$$

After the surrogate is built, measures should be taken to improve the accuracy of the surrogate, especially at the optimum point.

4.3.1 Expected Improvement Function (EIF)

The EIF is defined as the expectation that a point that has the better solution than the current optimum. To update the surrogate, the EIF should be maximized, the EIF can be expressed as[141]:

$$EI(\hat{g}(\mathbf{x})) = (g^* - \mu_g)\,\Phi\left(\frac{g^* - \mu_g}{\sigma_g}\right) + \sigma_g \phi\left(\frac{g^* - \mu_g}{\sigma_g}\right) \tag{4.9}$$

here g^* is the current best solution, u_g and σ_g are the mean and standard deviation of the prediction.

4.3.2 Expected Feasibility function (EFF)

The expected feasibility function (EFF) provides an indication of the well the function is expected to have the value of z^*, the EFF function is given by:

$$\begin{aligned} EF(\hat{g}(\mathbf{x})) = (\mu_g - \bar{z})\left[2\Phi\left(\frac{\bar{z} - \mu_g}{\sigma_g}\right) - \Phi\left(\frac{z^- - \mu_g}{\sigma_g}\right) - \Phi\left(\frac{z^+ - \mu_g}{\sigma_g}\right)\right] \\ - \sigma_g\left[2\phi\left(\frac{\bar{z} - \mu_g}{\sigma_g}\right) - \phi\left(\frac{z^- - \mu_g}{\sigma_g}\right) - \phi\left(\frac{z^+ - \mu_g}{\sigma_g}\right)\right] \\ + \varepsilon\left[\Phi\left(\frac{z^+ - \mu_g}{\sigma_g}\right) - \Phi\left(\frac{z^- - \mu_g}{\sigma_g}\right)\right] \end{aligned} \tag{4.10}$$

where z^- denotes $z^* - \varepsilon$,z^+ denotes $z^* + \varepsilon$ and ε can be set to be $2\sigma_g$[142].

4.4 Kriging-based RBDO using SLA

Kriging is widely used for replacing reliability constraints, to update Kriging, EIF and EFF can be used, however, these two methods still need more unnecessary points far away from the optimum. To further reduce the number of sample points, in the next part the Kriging is connected with SLA, in each loop of the SLA, the MPPs for each constraint are calculated. For Kriging-SLA, these MPPs of each iteration are used to update the Kriging metamodel, and the program will move the design value iteratively, until final convergence.

The flowchart can be summarized as:

Step 1. Transform $\boldsymbol{X}$ from physical space to standardized space $\boldsymbol{U}$ using iso-probabilistic transformation $\boldsymbol{U} = T(\boldsymbol{X})$.

Step 2. A design of experiment of size N, $\boldsymbol{U}^N$ sampled with grid sampling or Latin Hypercube Sampling (LHS), and correspondent responses $G_i(\boldsymbol{U}^N), i = 1,2,...,m$, are used to train the first Kriging.

Step 3. $k_0 = 0$, or $k = k+1$. Start the SLA loop, calculate the Most Probable Points(MPPs) $\boldsymbol{U}_i^{(k)}$, with $\boldsymbol{U}_i^{(k)} = -\boldsymbol{\alpha}_i^{(k)}\beta_i^t$, where $\boldsymbol{\alpha}_i^{(k)}$ is calculated with $\boldsymbol{\alpha}_i^{(k-1)} = \frac{\boldsymbol{\sigma}_U \nabla_{\boldsymbol{U}} \hat{G}_i(\boldsymbol{d}^{(k-1)}, \boldsymbol{\mu}_i^{(k-1)})}{||\boldsymbol{\sigma}_U \nabla_{\boldsymbol{U}} \hat{G}_i(\boldsymbol{d}^{(k-1)}, \boldsymbol{\mu}_i^{(k-1)})||}$ from the derivative of the Kriging metamodel.

Step 4. $\min C(\boldsymbol{d}, \boldsymbol{\mu}_{\boldsymbol{U}})$, under SLA constraints $G_i(\boldsymbol{d}^k, \boldsymbol{U}^k) \geq 0$, $i = 1,2...,m$, and calculate new $\boldsymbol{d}^{(k)}$ and $\boldsymbol{\mu}_{\boldsymbol{U}}^{(k)}$.

Step 5. Calculate the responses $\hat{G}_i(\boldsymbol{U}_i^k), i = 1,2...,m$ at $\boldsymbol{U}_i^k$ using Kriging surrogate, choose $\boldsymbol{U}_i^*$ as the MPP to update the Kriging, if $[\hat{G}_1(\boldsymbol{U}_i^*), \hat{G}_2(\boldsymbol{U}_i^*), ..., \hat{G}_m(\boldsymbol{U}_i^*)]$ has the element that is closest to zero.

Step 6. Calculate the true responses of $\boldsymbol{U}_i^*$, as $G_i(\boldsymbol{U}_i^{(*)})$, $i = 1,2,...,m$, add this set of data into training set, $N = N+1$, and retrain Kriging.

Step 7. Compare $\boldsymbol{d}^{(k)}$, $\boldsymbol{\mu}_{\boldsymbol{U}}^{(k)}$ with $\boldsymbol{d}^{(k-1)}$, $\boldsymbol{\mu}_{\boldsymbol{U}}^{(k-1)}$, if $||\boldsymbol{d}^{(k)} - \boldsymbol{d}^{(k-1)}|| \leq \varepsilon$ and $||\boldsymbol{\mu}^{(k)} - \boldsymbol{\mu}^{(k-1)}|| \leq \varepsilon$, stop; else go to step 3 and continue.

The size N of the initial data set for building the Kriging can be very small, because, though the first surrogate may failed to capture the main characteristics of the constraints, and the SLA loop may converge in the infeasible domain, the point of the current MPP will be added to the training set to update the metamodel, the program will continue moving forward, until

the metamodel is trained better and better around the right optimum. The originality of the proposed Kriging-SLA method resides in: 1) the use of gradient-based approach to estimate the probabilistic constraints, without using Monte Carlo simulations, importance sampling method, RIA and PMA approaches; 2) the updating procedure of the Kriging surrogate performed only by using the MPPs of the previous iteration of SLA, it doesn't require additional searching points with the learning functions. The proposed Kriging-SLA is different to the approach proposed in Li, Qiu, Chen, *et al.* [140], where the MPPs are estimated by the reliability index approach (RIA) and the RBDO is realized by the double-loop approach.

4.5 Wind turbine optimization using Kriging-SLA

In this section, the Kriging-SLA method is first applied to several mathematical problems, then it is applied to the optimization of wind turbine tower.

4.5.1 Mathematical benchmark problems

4.5.2 Liang's example

This is a well-known benchmark example [125], where there are two variables, their standard deviations are same as $\sigma_1 = \sigma_2 = 0.3$, the target reliability index β_t for all three constraints are set to be 3. The reference result with only SLA method is $\mu = [3.4391; 3.2864]$, the optimum objective function value is 6.7255.

The problem is given as:

$$\begin{aligned}
&\min C(\boldsymbol{\mu}_X) = \mu_1 + \mu_2 \\
&G_1(\boldsymbol{x}) = -x_1^2 x_2/20 - 1 \\
&G_2(\boldsymbol{x}) = (x_1 + x_2 - 5)^2/30 + (x_1 - x_2 - 12)^2/12 - 1 \\
&G_3(\boldsymbol{x}) = 80/(x_1^2 + 8x_2 + 5) - 1
\end{aligned}$$

The results are shown in Figure.4.1:

In Figure.4.1(a), only 4 points using grid sampling method are used to train the first

Figure 4.1: Liang's example

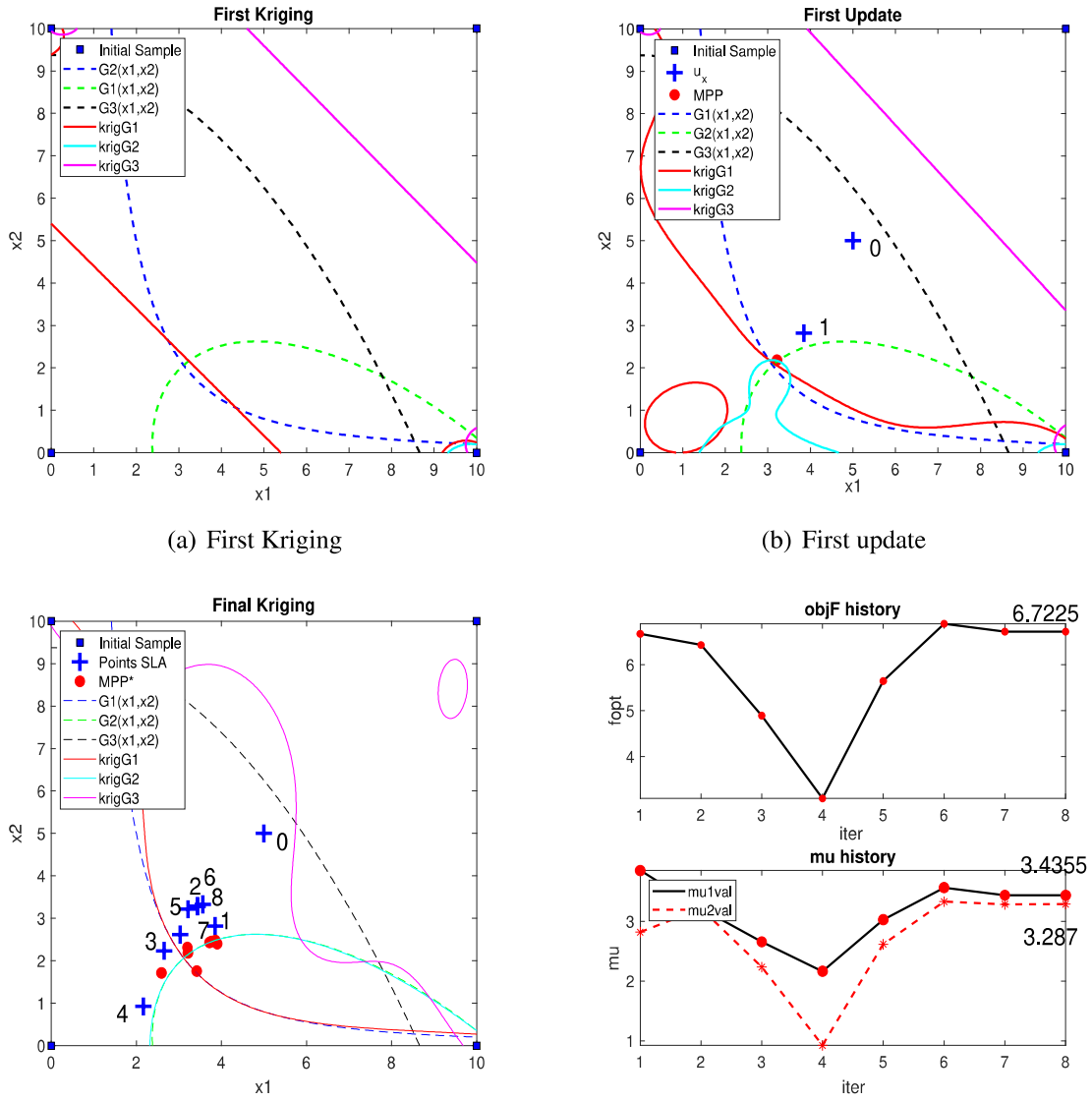

(a) First Kriging

(b) First update

(c) Final result

(d) Iteration history

Kriging. The true constraints are marked as dash lines, while the mean value of Kriging predictions $\mu(\hat{G})$ are marked as solid lines. It can be seen that the first Kriging has a very poor prediction for these three constraints.

In Figure.4.1(b), after the first iteration, a sample of the MPP point is added in the Kriging model (marked with solid red dot). The mean values of the random variables μ_x is marked with $+$ in the figure, μ_x^0 is the starting point.

The final result is shown in Figure.4.1(c). The program converges with 8 iterations, with 8 added points. The history of μ_x and objective function is shown in Figure.4.1(d). It is shown that, the program has moved μ_x to the right optimum gradually. The active constraints G_1 and

G_2 is very accurate around the final MPP.

In Table.4.1, the Kriging-SLA results are compared with simple SLA method (without Kriging), the relative error is calculated with$||\hat{f} - f^{\star}||/||f^{\star}||$, where $\hat{f}$ is the result from Kriging-SLA method, $f^{\star}$ is from the simple SLA result, it can be seen that the relative error for Kriging-SLA is lower than 0.04%.

Table 4.1: Comparison of SLA and kriging-SLA results of Liang's example

Method	$\boldsymbol{\mu}$	$f(\boldsymbol{\mu})$	Points	$[\beta^1, \beta^2, \beta^3]$	R-Error
SLA (Liang et al. 2014)	[3.4391; 3.2864]	6.7255	\	[2.97 3.05 Inf]	\
Kriging-SLA	[3.4355; 3.2870]	6.7225	12	[2.97 3.05 Inf]	0.04%

Note the Relative error is compared with simple SLA method. Because the SLA is a gradient-based FORM approximation method, it consists error in itself, as shown in Table.4.1, the target reliability [2.97, 3.05, Inf], is not the accurate optimum. This may become a more serious problem when facing highly nonlinear and non-convex problems, which will be shown in example 3. The influence of different initial sampling size for the first Kriging is show in Table.4.2. It's shown that the program converges faster if the first Kriging is trained with more sample points. However, the larger sample size will not reduce the final relative error, which comes mainly from FORM approximation.

Table 4.2: Influence of initial sample number of Liang's example

Initial Sample	$\boldsymbol{\mu}$	$f(\boldsymbol{\mu})$	Points	$[\beta^1, \beta^2, \beta^3]$	R-Error
4	[3.4355; 3.2870]	6.7225	$4+8$	[2.97 3.05 Inf]	0.04%
9	[3.4354; 3.2869]	6.7223	$9+4$	[2.97 3.05 Inf]	0.05%
16	[3.4390; 3.2889]	6.7280	$16+3$	[2.97 3.06 Inf]	0.04%

4.5.3 Cho and Lee's example

This is a speed reducer benchmark problem [143]. It is a 7-dimension problem, the objective is to minimize the weight, which is a function of the parameters of the bearings $d_1, d_2, ..., d_7$. There are 11 constraints related to physical quantities, such as limit stress and maximum

displacement. The random design variables are gear width(X_1), gear module(X_2), the number of pinion teeth(X_3), distance between bearings (X_4, X_5), and diameter of each shaft(X_6, X_7). All random variables are statistically independent and follow Normal distribution $N(0, 0.005^2)$. The target reliability index β^t for all constraints are set to be 3. The RBDO problem can be summarized as:

$$\boldsymbol{d} = [d_1, d_2, d_3, d_4, d_5, d_6, d_7]^T$$

$$\min C(\boldsymbol{d}) = 0.7854 d_1 d_2 (3.3333 d_3^2 + 14.9334 d_3 - 43.0943)$$

$$- 1.5080 d_1 (d_6^2 + d_7^2) + 7.4770 (d_6^3 + d_7^3) + 1.5080 d_1 (d_6^2 + d_7^2)$$

$$st.prob[G_i(\boldsymbol{X}) < 0] \leq \boldsymbol{\Phi}(-\beta^t), i = 1, 2, .., 11$$

$$G_1(\boldsymbol{X}) = X_1 X_2^2 X_3 - 27$$

$$G_2(\boldsymbol{X}) = X_1 X_2^2 X_3^2 - 397.5$$

$$G_3(\boldsymbol{X}) = X_2 X_3 X_6^4 - 1.93 X_4^3$$

$$G_4(\boldsymbol{X}) = X_2 X_3 X_7^4 - 1.93 X_5^3$$

$$G_5(\boldsymbol{X}) = 110 X_6^3 - \sqrt{(745 X_4 / (X_2 X_3))^2 + 16.9 \times 10^6}$$

$$G_6(\boldsymbol{X}) = 85 X_7^3 - \sqrt{(745 X_5 / (X_2 X_3))^2 + 157.5 \times 10^6}$$

$$G_7(\boldsymbol{X}) = 40 - X_2 X_3$$

$$G_8(\boldsymbol{X}) = X_1 - 5 X_2$$

$$G_9(\boldsymbol{X}) = 12 X_2 - X_1$$

$$G_{10}(\boldsymbol{X}) = X_4 - 1.5 X_6 - 1.9$$

$$G_{11}(\boldsymbol{X}) = X_5 - 1.1 X_7 - 1.9$$

$$2.6 \leq d_1 \leq 3.6, 0.7 \leq d_2 \leq 0.8, 17 \leq d_3 \leq 28, 7.3 \leq d_4 \leq 8.3,$$

$$7.3 \leq d_5 \leq 8.3, 2.9 \leq d_6 \leq 3.9,$$

$$5.0 \leq d_7 \leq 5.5$$

$$X_j \sim N(d_j, 0.005^2), j = 1, 2, ..., 7$$

$$\beta_1^t = \beta_2^t = ... = \beta_{11}^t = 3.0$$

Table 4.3: Comparison of RBDO results of Cho and Lee's example

Methods	Design variables $\boldsymbol{\mu}^{opt}$	$f(\boldsymbol{\mu})^{(opt)}$	Points	Error
MCS[129]	[3.5765;0.70;17.0;7.3;7.7542;3.3652;5.3017]	3038.6347	\	\
K-SLA	[3.5765;0.70;17.0;7.3;7.7542;3.3652;5.3017]	3038.6234	41.6	0.004%
CBS[129]	[3.5765;0.70;17.0;7.3;7.7541;3.3653;5.3017]	3038.6234	80	0.17%
SS [129]	[3.5778;0.70;17.0;7.7;7.9371;3.3447;5.2993]	3040.6091	72	6.9%
LAS[129]	[3.5765;0.70;17.0;7.3;7.7543;3.3651;5.3017]	3038.6244	46	0.004%

Table 4.4: Comparison of reliability index at the optimum of Cho and Lee's example

Methods	β^1	β^2	β^3	β^4	β^5	β^6	β^7	β^8	β^9	β^{10}	β^{11}
Kriging-SLA	Inf	Inf	Inf	Inf	2.9942	2.9951	Inf	3.0012	Inf	Inf	2.9895
MCS[129]	Inf	Inf	Inf	Inf	2.9946	2.9948	Inf	3.0016	Inf	Inf	2.9895
CBS[129]	Inf	Inf	Inf	Inf	3.4316	3.0045	Inf	2.9995	Inf	Inf	3.0136
SS [129]	Inf	Inf	Inf	Inf	-1.2848	2.5114	Inf	3.0490	Inf	Inf	Inf
LAS [129]	Inf	Inf	Inf	Inf	2.9826	3.0122	Inf	2.9900	Inf	Inf	2.9922

The first Kriging is built with 36 points sampled by LHS method. The program is run for 20 times, to consider the randomness of the LHS sampling . The optimum results and correspondent target reliability indices are compared with Chen et al. (2014)'s reference in Table.4.3 and Table.4.4. Note the iteration number and optimum design point is the average of the 20 simulations.

For this example, the proposed Kriging-SLA method is very accurate and efficient, it needs the least number of sampling points compared to the other methods. It should also be noted that, for CBS, SS, and LAS method, after building the surrogate, double loop approach RBDO is needed to get the optimum design, which will increase the computational cost, especially when the failure rate is low.

4.5.4 Lee and Jung's example

Due to the fact that the SLA method is based on gradient method, as mentioned before, it may not work well for highly-nonlinear problems or non-convex problems. As it is pointed out [125], it may converge to a wrong minimum or even fail to converge. For example, in this benchmark problem [144], it includes a highly nonlinear constraint around the MPP. This problem is described as follows:

$$\min C(\boldsymbol{\mu}_X) = (\mu_1 - 3.7)^2 + (\mu_2 - 4)^2$$
$$G_1(\boldsymbol{x}) = x_1 + x_2 - 3$$
$$G_2(\boldsymbol{x}) = -x_1 \sin(4x_1) - 1.1x_2 \sin(2x_2)$$

$\boldsymbol{x}$ is the realization of random variable $\boldsymbol{X}$, composed of two independent normal variables, their standard deviation are $\sigma_1 = \sigma_2 = 0.1$. The objective function and constraints are given below. The target reliability index for both constraints are set the same as $\beta_1^t = \beta_2^t = 2$. For the comparison of the Kriging-SLA method, a reference result of simple SLA method is used. The optimum value from simple SLA is 1.3040 and the optimum design variables are $[2.8162; 3.2769]$.

In Figure.4.2(a), 4 points using grid sampling method are used to train the first Kriging. It can be seen that the first Kriging has a comparably better prediction of the linear constraint $G_1(\boldsymbol{x})$, but has a very poor prediction of the nonlinear constraint $G_2(\boldsymbol{x})$(which can't be seen in Figure.4.2(a).

In Figure.4.2(b), after the first iteration, 1 samples of MPP point is added in the Kriging model (marked with solid red dot). The mean values of the random variables μ_x is marked with $+$ in the figure, μ_x^0 is the starting point. The first point μ_x^1 is not in the feasible domain, which means the SLA to converge to a wrong point with the poorly trained Kriging.

The final result is shown in Figure.4.2(c), The program converges with 14 iterations, with 18 sample points in total. The history of μ_x and objective function is shown in Figure.4.2(d). The Kriging-SLA method is compared with the SLA result and Chen et al. (2014)'s results [130]. The comparisons are shown in Table 4.5.

From the comparison of Table.4.5, the accuracy of Kriging-SLA is in the same level of SLA results. In fact, other gradient-based RBDO approaches tested for this example by Chen, Qiu, Gao, *et al.* [145] converge to this optimum with reliability index of 1.86. This lack of accuracy is due to the high-nonlinearity of constraint 2. The other methods (LAS, SS) that are converged to the right optimum with checked reliability constraints are based respectively on Monte Carlo and subset simulations, which greatly increase the total computational cost. A

Figure 4.2: Lee and Jung's Example

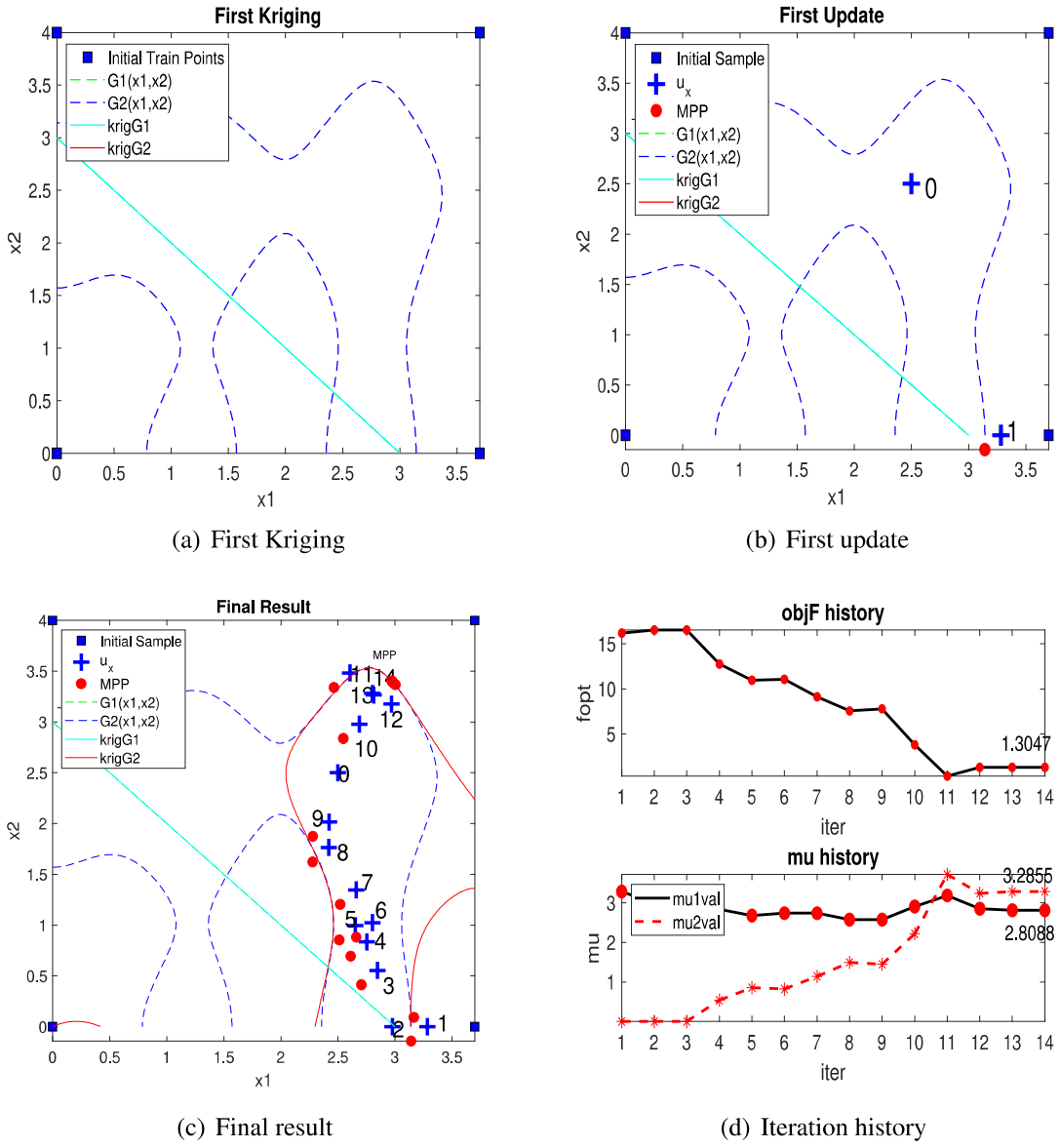

(a) First Kriging

(b) First update

(c) Final result

(d) Iteration history

possible improvement would be by using enhanced single loop approach[146], which promotes the stability of simple SLA.

4.5.5 RBDO of wind turbine tower

Introduction of the problem

This method is used for the optimization of wind turbine tower based on a reference 5MW turbine system given by NREL [3], but with more details in the tower. The simplified turbine structure is shown in Figure.4.3(a).

Table 4.5: Comparison of RBDO results of Lee and Jung's Example

Method	$\boldsymbol{\mu}$	$f(\boldsymbol{\mu})_{(opt)}$	Points	$[\beta^1, \beta^2]$	Error
MCS	[2.8421;3.2320]	1.3259	\	\	
SLA	[2.8162;3.2769]	1.3040	\	[1.86 Inf]	1.65%
Kriging-SLA	[2.8088;3.2855]	1.3047	18	[1.83 Inf]	1.59%
CBS (Chen 2014)	[2.8485;3.2350]	1.3103	45	[1.93 Inf]	1.18%
SS (Chen 2014)	[2.8400;3.2339]	1.3264	29	[2.02 Inf]	0.5%
LAS (Chen 2014)	[2.8408;3.2334]	1.3259	22	[2.00 Inf]	0.04%

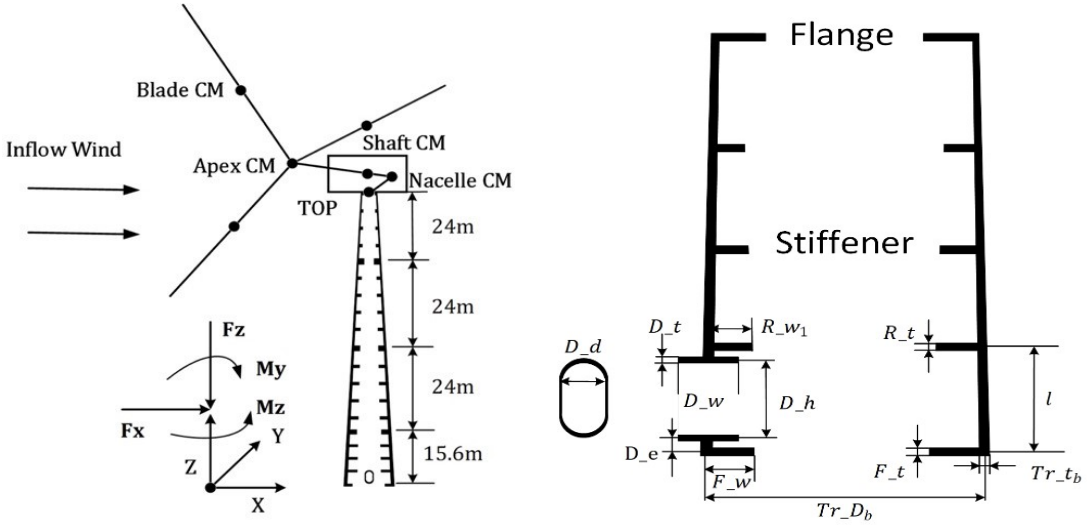

(e) Wind turbine structure

(f) Tower bottom section

Figure 4.3: Wind turbine tower optimization problem

The turbine system is mainly composed of a wind turbine tower, a nacelle, a shaft, an apex, and 3 turbine blades. The mass of the nacelle, shaft, apex, and the blades are approximated with mass points at their correspondent mass center(CM) to calculate the frequency of the entire turbine system. Their coordinates and weights are given in Table 4.6.

The tower is made of material steel, the material properties are given in Table 4.7.

The total tower height H is 87.6 meters, it is a linearly tapering tower, with the diameter at the bottom Tr_{Db} and top Tr_{Dt} are 6 meters and 3.87 meters respectively. The thickness of the tower is also linearly reducing from bottom to top ranging from Tr_{tb} to Tr_{tt}, which are the design variables to be optimized. It is assembled with 4 sections, the length of the bottom section H_b is 15.6 meters, and the other sections H_t are 24 meters. At each end of the sections, there are flanges used for the connection, the flanges are with the same widths F_w (from the middle of tower thickness to the edge of the flange) as 0.16 meters and thicknesses F_t as 0.08

Table 4.6: Properties of nacelle and blades

Parameter Name	Value(kg)	Coordinate Position(m)	Description
$Wt_{nacelle}$	2.4E5	(1.9,0,89.25)	weight of the nacelle
Wt_{shaft}	1.1E5	(0,0,89.46)	weight of the shaft
Wt_{apex}	5.678E4	(-5,0,90)	weight of the apex
Wt_{blade1}	1.744e4	(-4.0415,0,112)	weight of the blade1
Wt_{blade2}	1.744e4	(-7.56,19,79.2)	weight of the blade2
Wt_{blade3}	1.744e4	(-7.56,-19,79.2)	weight of the blade3

Table 4.7: Material properties

Parameter Name	Value	Description
G	210(Gpa)	Young's modulus
P	8.08(Gpa)	Shear modulus
$Density$	7850(kg/m^3)	Steel density

meters. Between the flanges, there are 3 stiffener rings, the widths of the rings R_w are same as 0.12 meters, and the thicknesses of the rings R_t are the same as 0.02 meters.

At the bottom section, there is a door opening at the height of D_e as 0.38m. The height the door D_h is 2 meters and the diameters of the semicircles at both ends D_t are 0.7 meters. Around the opening door, there is a reinforcing stiffener ring, the thickness of the door stiffener D_t is 0.08m and the width of the door stiffener D_w is 0.21m. The constant parameters of the tower are given in Table.4.8.

Table 4.8: Constant geometry parameters

Parameter Name	Value (m)	Description
Tr_{Db}	6	Tower bottom diameter
Tr_{Dt}	3.87	Tower top diameter
D_e	0.38	Opening door height to the base
D_h	2	Opening door height
D_d	0.7	Opening door diameter
D_w	0.21	Opening door stiffener width
D_t	0.08	Opening door stiffener thickness
F_w	0.16	Flange width
F_t	0.08	Flange thickness
R_w	0.12	Ring width
R_t	0.02	Ring thickness

The loads on the top of the tower are considered to be stochastic, they are assumed to follow Normal distribution. They are characterized from simulation results from a 5MW offshore turbine at rated wind speed(11.4m/s, normal turbulence), but are up-scaled to consider more extreme conditions. The coefficient of variation is taken as 20% of the mean values. These are given in Table 4.9.

Table 4.9: Statistical parameters of the random variables

Parameter Name	Distribution	Mean Value	Variance	Description
Fx	Normal	850(kN)	170	Force in direction x
Fz	Normal	-5500(kN)	1100	Force in direction z
My	Normal	22500(kN.m)	4500	Moment in direction y
Mz	Normal	22500(kN.m)	4500	Moment in direction z

Objective and Constraints of RBDO and DO

When the inflow wind speed is higher than the cut in speed v_{in}, the turbine starts to work. To simplify this problem, only 4 stochastic variables and 2 most important design variables are considered. The stochastic variables are 2 forces in the direction x, y: Fx and Fy and 2 moments in direction y, z: My and Mz on the top of the tower, The design variables are the thickness at the bottom Tr_{tb} and thickness at the top Tr_{tt}.

The objective to minimize is the weight of the tower, by ignoring the opening door and the flanges, the geometry of the tower can be very simple, which is a tapering cylinder with constant diameters at bottom and top, so the objective function can be replaced by sum of thicknesses of bottom and top, so $f_{obj} = Tr_{tb} + Tr_{tt}$.

The RBDO constraints for the tower optimization are that the probability of failure should be lower than $1 - \Phi(\beta_t)$. The constraints considered in this paper are:

1. The maximum deflection of the tower d_{max} should be smaller than d_{limit}, taking %1 of the height of the tower, so $d_{limit} = 0.876$.

2. The first eigen-frequency of the tower should higher than 1.2 times the maximum rotating frequency of the blades, taking the maximum rotating speed as $16r/min$, so the frequency limit is taken as 0.32.

3. The first order buckling load factor should be bigger than b_{limit}, to avoid buckling, the minimum buckling factor is 1, so $b_{limit} = 1$.

For RBDO of the wind turbine tower, the problem can be summarized as:

$$
\begin{aligned}
&\min C_{obj} = Tr_{tb} + Tr_{tt} \\
&P_{deflection} = Prob(G_d(\boldsymbol{F}, \boldsymbol{d}) > 0) \leq 1 - \Phi(\beta_t) \\
&P_{freq1} = Prob(G_f(\boldsymbol{F}, \boldsymbol{d}) < 0) \leq 1 - \Phi(\beta_t) \\
&P_{buckling} = Prob(G_b(\boldsymbol{F}, \boldsymbol{d}) < 0) \leq 1 - \Phi(\beta_t)
\end{aligned}
$$

where $\boldsymbol{F}$ is the stochastic loads of forces and moments, $\boldsymbol{d}$ is the design variables which are the thicknesses of the tower. $G_d = d_{max} - d_{limit}$ is the performance function of deflection, $G_f = f_1 - f_{limit}$ is the performance function of frequency, $G_b = b_1 - b_{limit}$ is the performance function of buckling. Two target reliability indices β_t: 3 and 3.5 are considered, which

corresponding to failure probabilities of $1.3e-3$ and $2e-4$.

For deterministic optimization(DO), the empirical rule (3σ rule) is adopted. The forces on top of the tower are set to be $\mu+3\sigma$ of their correspondent Gaussian distributions. It means that the probability of having greater forces than these values $Pr(X > \mu-3\sigma)$ is lower than 0.0013. The loads and limits for DO is given by Table 4.10.

Table 4.10: Deterministic constraints

Name	Fx(kN)	Fz(kN)	My(kN.m)	Mz(kN.m)	d_{limit}(m)	b_{limit}	f_{limit}
Value	1360	-8800	36000	36000	0.876	1	0.32

Simulation and results

The responses of the tower are calculated by finite element method (FEM)byusing ANSYS Academic Research Mechanical, Release 18.1.The displacement response is evaluated by linear static analysis. The eigen-frequency and buck-ling limit states are respectively evaluated by eigenvalue analyses. There is no linear relationship between the input parameters and the output re-ponses. The Finite Element model of the tower is established using Shell element, the mesh of bottom section is show in Figure.4.4. The forces are applied at the top of the tower, at the center with rigid connections with the notes at the top, the tower is fixed at the bottom to the ground.

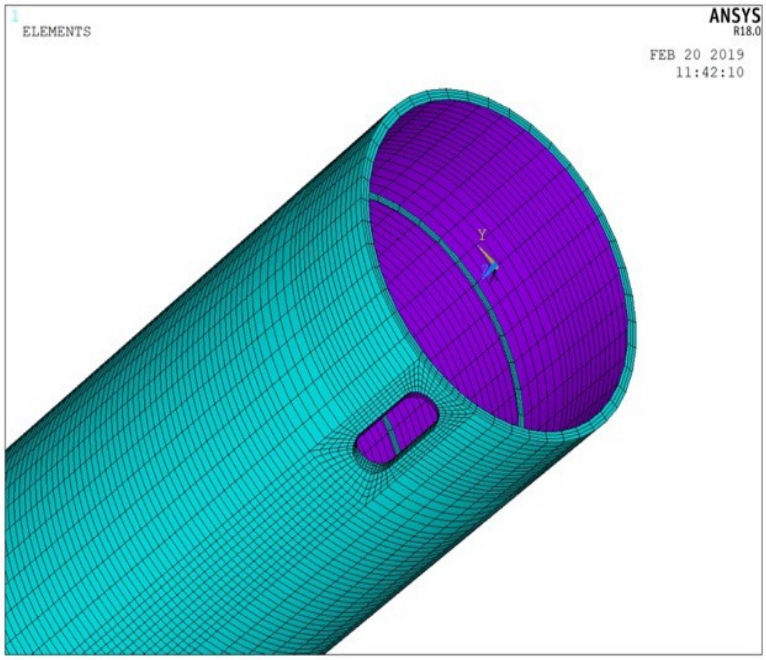

Figure 4.4: Finite element analysis of the wind turbine tower

Analysis show that if the door stiffener is too small, the buckling will happen around the door opening, which will greatly reduce the tower life. To avoid this, the door stiffener is set to be 0.08 meters. In this case, the buckling will happen along the tower, and is constrained by thicknesses of the tower.

For modal analysis, the mass of the nacelle, shaft, apex, blades should be connected to the FEM model, these proprieties are given in Table.4.6, the module shapes of the first and the second order of the tower are The first and the second mode shapes of the tower respectively.

The first Kriging metamodel is built with 64 points sampled by LHS method. The converge criteria ε is set to be $1e-6$. At the optimum point of Kriging-SLA, AK-MCS developed by [137] and implemented in UQLAB codes [97] is used to calculate the reliability indices.

The RBDO and DO results are shown in Table.4.11. At optimum point of SLA, AK-MCS[137] simulation is used to calculate the reliability indices. For DO result, the failure rate is smaller than 1e-7, which becomes even prohibitive for AK-MCS. The constraint values in the table: for RBDO, they represent the performance functions of deflection G_d, frequency G_f, and buckling G_b at Most Probable Point(MPP); For DO, they represent the the deterministic limits of deflection ($d_{max} - d_{limit}$), frequency ($f_1 - f_{limit}$), and buckling factor ($b_1 - b_{limit}$).

The proposed Kriging-SLA method is run for 20 times, and the average value is taken. It

Table 4.11: Comparison of DO and RBDO results

	RBDO(β^t = 3.0)	RBDO(β^t = 3.5)	DO
Optimum design(m)	[0.0418; 0.0114]	[0.0417; 0.0123]	[0.0522; 0.0273]
Cost function(m)	0.0532	0.054	0.0795
Constraint values	[-0.413; 2E-5; 0.022]	[-0.3; 3E-6; 0.111]	[-1e-4; 0.051; 3.598]
AK-MCS	[Inf 3.050 Inf]	[Inf 3.509 Inf]	\

converges with only an averaged 10.6 SLA iterations.

It can be seen that the optimums from Kriging-SLA satisfy the reliability constraints, at optimum points, the reliability indices have reached target reliability β^t. The DO results is much larger than RBDO results in this case, even larger than the design of reliability index of 3.5, which may be too conservative. Another difference is that, for RBDO, the constraint first violated is the frequency constraint, whereas, for DO, the constraint first violated is the maximum deflection.

4.6 Conclusion

Traditional double loop RBDO approaches may become computational prohibitive when facing problems with high dimensions or high target reliability level. In this paper, the single loop approach is combined with Kriging metamodel to solve complex engineering problems. This method uses the gradients from the Kriging metamodel to calculate the MPPs with SLA method. These MPPs are then added to update the Kriging model. In other words, the updating procedure of the Kriging surrogate does not require additional searching points with the learning functions. A very simple but effective stopping criterion is proposed to check the convergence. Three benchmark examples and an practical engineering application are used to validate this method.

The proposed Kriging-SLA method is very efficient compared with other sampling methods. The accuracy of the proposed method is in accordance with the original SLA method without surrogate models. This method needs fewer initial sample points and converges with the minimum number of sample points, as it doesn't seek to globally fit the constraints well, it

seeks to add the best points that are currently available until meeting the convergence criteria. However, this method suffers the same limitations of the gradient-based-method, like SLA or SORA, which are less accurate for highly-nonlinear problems.

Chapter 5

Time-variant reliability-based optimization using double-loop Kriging surrogate

Due to material degradation, stochastic loads or system deterioration with time, the reliability of system become time-dependent. The optimization under this circumstance becomes a time-variant reliability optimization (TvRBDO) problem. The difficulty of TvRBDO lays in the high computational cost for the evaluation of TvR constraints and lack of general form of analytical TvR methods for all situations. This chapter discusses about Time-variant Reliability optimization using Double-Loop Kriging surrogates (TRDLK). The outer-loop conduct TvRBDO, and the so-called Single Loop Kriging (SILK) approach is used to calculate the TvR of inner-loop. In Section.5.1, the background is discussed, in Section.5.2, the time variant reliability method using Single Loop Kriging (SILK) approach is discussed. In Section.5.3, a approach of TvRBDO using double-loop approach is proposed , In Section.5.4, two examples are used to validate the method. Section.5.5 is the conclusion.

5.1 Introduction

Reliability-based design optimization (RBDO) has been widely used in engineering applications [115]. However in many engineering cases, due to degradation, stochastic loads, or system deterioration with time, time-variant reliability (TvR) must be considered [147]. Time-variant reliability is the probability of failure that a product performs under its intended functionality within its serving time. Time-variant reliability-based design optimization

(TvRBDO) is the optimization under time-variant reliability constraints. The general form of TvRBDO can be formulated as:

$$\begin{aligned} &\min C(\boldsymbol{d}, \boldsymbol{\theta}_{X_d}) \\ &st. \begin{cases} \text{Prob}\{G_i(\mathbf{d}, \mathbf{X}_\text{d}, \mathbf{X}_\text{c}, \mathbf{Y}(t), t) < 0\} \leq p_i^* \\ H_j(\mathbf{d}, \boldsymbol{\theta}_{\text{x}_\text{d}}) \leq 0 \end{cases} \\ &i = 1, 2, ...N_p;\ j = 1, 2, ...N_d \end{aligned} \tag{5.1}$$

C is the cost function that can be a combination of deterministic variables $\mathbf{d}$, and statistical moments $\boldsymbol{\theta}$ of random variables $\boldsymbol{X}$. G_i is the ith performance function that may consist in the design variables $\boldsymbol{X}_d$, the random variables $\boldsymbol{X}_c$, the stochastic process $F(t)$ and time t. For each realization d, x_d, and x_c of $\boldsymbol{d}$, $\boldsymbol{X}_d$, and $\boldsymbol{X}_c$, $G_i < 0$ when there exists a time instant $t^{'}$ in the trajectory of t that makes $G_i(d, x_d, x_c, Y(t^{'}), t^{'}) < 0$. The cost function C is minimized under N_p constraints of cumulative probability of failure with respect to $\mathbf{d}$, $\mathbf{X}_\text{d}$, and $\mathbf{X}_\text{c}$, $Prob\{G_i(\mathbf{d}, \mathbf{X}_\text{d}, \mathbf{X}_\text{c})\} < p_i^*$, with p_i^* being the allowable probability of failure and N_d deterministic constraints H_j.

For the evaluation of TvR constraints, existing methods can be classified into two categories: out-crossing methods and extreme value methods [148], [149].

The out-crossing is defined as the events of performance function passing through a failure threshold. The out-crossing methods are based on Rice's formula [150] assuming that the distribution of out-crossing events follows Poisson distribution. Under this assumption, the probability of failure can be bounded by the sum of the initial failure plus the integral of out-crossing rate over time as:

$$P_f(0, T) \leq P_f(0, 0) + \int_0^t v(t) dt \tag{5.2}$$

where $v(t)$ is the out-crossing rate defined as:

$$v(t) = \lim_{\Delta t \to 0} \frac{\text{Probability}(G(t) > 0 \bigcap G(t + \Delta t) \leq 0)}{\Delta t} \tag{5.3}$$

To calculate the out-crossing rate, the most popular method is the PHI2 method [151]. The PHI2 method calculates the outer-crossing rate using two component parallel systems at successive time instants and estimates the bivariate normal integral with FORM method. Later the PHI2 method is improved to integrate the analytical gradient solution of the bivariate normal integral as PHI2+ method [152]. Compared with PHI2 method, the PHI2+ method is less sensitive to the increments of time steps. Though the PHI2 and PHI2+ methods are computationally efficient, their accuracy highly rely on the presumption that the out-crossings are independent. When the reliability is low, or the failure rate is high, there may exist dependence of out-crossings, these two methods may include large errors.

The extreme value based methods try to evaluate the performance functions at the maximum values of each trajectory of the random variables through time. In most cases, there is no analytical solution for the extreme value of the performance functions, so it will become prohibitive for complex engineering problems. In this case, surrogate models are used, for example Zhen Hu(2015)[153] has proposed a mixed-EGO method that uses a Kriging surrogate to approximate the extreme value. The Kriging is first updated with AK-MCS method [137] and then MCS simulations are used to calculate the TvR [153]. Mixed EGO uses double-loop Kriging surrogates with the inner-loop represents the performance functions and outer-loop represents the extreme value of the inner-loop. This double-loop Kriging will amplify the error of the inner-loop and it's computational expensive to identify a new training point. To alleviate these problems, a single-loop Kriging surrogate method (SILK) is proposed [4]. In SILK, the time interval is discretized into small time steps along each random design variable and uses a learning function U to decide whether to update the Kriging surrogate along this variable track.

So far, not many papers have focused on TvRBDO, due to the high computational cost for the evaluation of TvR constraints and lack of accurate analytical TvR methods. Zequn Wang & Pingfeng Wang have proposed a nested extreme response surface method (NERS) which uses a nested EGO approach to conduct TvRBDO. The TvR of NERS is calculated with EGO method from the inner-loop [154]. ZHEN Hu & Xiaoping Du (2016) have expanded the time-independent RBDO method SORA to solve TvR problems [155]. Lara Hawchar & Charbel-Pierre EI Soueidy have based SILK and have proposed a global Kriging surrogate

method that utilizes the Polak-He algorithm [156] to accelerate convergence. For NRES, EGO method itself is a double-loop method, using TvR for TvRBDO may amplify the final error. Though surrogates are used, the evaluation of TvR constraints is still very time-consuming, and the TvRBDO involves multiple iterations of searching in the design space. This will become prohibitive for high reliability problems.

So this work is based on the SILK method and adds another Kriging as the outer-loop to solve TvRBDO problems [157]. In this method, The inner-loop calculates the TvR using SILK, some improvements are made to SILK to consider multiple-constraints; the outer-loop is another Kriging surrogate trained by the results of inner-loop, after the outer-loop is trained, Expected Feasible Function (EFF) is then used to update this outer-Kriging. The time-variant reliability of all sample points of outer-loop are evaluated with the same inner Kriging with SILK method. And after the outer-Kriging is built, the computational cost for TvRBDO is minimal.

5.2 Brief review of time-variant reliability with SILK

In TRDLK, the TvR is calculated with the so-called single-loop Kriging surrogate method (SILK). In this section, the SILK method is reviewed.

5.2.1 Kriging prediction

Kriging (KRG) is a surrogate model based on regression using observed data sets. The Kriging model is discussed in Chapter.2, the prediction of the Kriging surrogate is given as:

$$[\mu_{\widehat{G}(\boldsymbol{X})}, \sigma_{\hat{G}(\mathbf{X})}] \tag{5.4}$$

where $\mu_{\widehat{G}(\boldsymbol{X})}$ is the estimation of input $\mathbf{X}$, $\sigma_{\hat{G}(\mathbf{X})}$ is its corresponding standard deviation.

5.2.2 Modified SILK to consider multiple constraints

The probability of failure in Equation.5.1 can be calculated with Monte Carlo Simulation (MCS):

$$p_f(t_0,t_e) = \text{Probability}\{G(\mathbf{X},t) > 0, \exists t \in [t_0,t_e]\} = \sum_{i=1}^{N} I_t\left(\mathbf{x}^{(i)}\right)/N \tag{5.5}$$

where N is the number of samples, I_t is the indicator for failure for each random $\boldsymbol{x}$ during the time interval of $[t_0,t_e]$:

$$I_t\left(\mathbf{x}^{(i)}\right) = \begin{cases} 1, \text{ if } G\left(\mathbf{x}^{(i)},t\right) > 0, \exists t \in [t_0,t_e], \forall i = 1,2,\cdots,N \\ 0, \text{ otherwise} \end{cases} \tag{5.6}$$

For each random variable, the time is discretized into N_t small time steps, Equation.5.6 becomes:

$$I_t\left(\mathbf{x}^{(i)}\right) = \begin{cases} 1, \text{ if any} I\left(G\left(\mathbf{x}^{(i)},t^{(j)}\right)\right) = 1, \forall j = 1,2,\cdots,N_t \\ 0, \text{ otherwise} \end{cases} \tag{5.7}$$

The fundamental idea of SILK is build a surrogate $\hat{G}(\mathbf{X},t)$ to evaluate Equation.5.5 to Equation.5.7. To make sure the surrogate is accurate for the classification, a U criterion is used:

$$U^{(k)}\left(\mathbf{x}^{(i)},t^{(j)}\right) = \frac{\left|\mu_{\hat{G}^{(k)}}\left(\mathbf{x}^{(i)},t^{(j)}\right)\right|}{\sigma_{\hat{G}^{(k)}}\left(\mathbf{x}^{(i)},t^{(j)}\right)} \tag{5.8}$$

here k is the number of constraints. The probability of making a mistake for the sign of $G\left(\mathbf{x}^{(i)},t^{(j)}\right)$ is given by:

$$P_{\text{error}} = \Phi\left(-U\left(\mathbf{x}^{(i)},t^{(j)}\right)\right) \tag{5.9}$$

In this work, the limit for U is set to be bigger than 2.5, which means the probability of making a error is smaller than 0.62%.

For the kth constraint, Equation.5.7 can then be rewritten as:

$$I_t\left(\mathbf{x}^{(i)}\right)=\begin{cases}1, \text{ if } \hat{G}^{(k)}\left(\mathbf{x}^{(i)},t^{(j)}\right)>0 \text{ and } U^{(k)}\left(\mathbf{x}^{(i)},t^{(j)}\right)\geq 2.5, \exists j=1,2,\cdots,N_t\\ 0, \text{ if } \hat{G}^{(k)}\left(\mathbf{x}^{(i)},t^{(j)}\right)\leq 0 \text{ and } U^{(k)}\left(\mathbf{x}^{(i)},t^{(j)}\right)\geq 2.5, \forall j=1,2,\cdots,N_t\end{cases} \tag{5.10}$$

If a failure is identified in the track of $\boldsymbol{x}^{(i)}$, $U^{(k)}(\boldsymbol{x}^{(i)},:)$, $k=1,....,N_t$ will be replaced with u_e (a value bigger than 2.5), because no more updating is needed in this track of $\boldsymbol{x}^{(i)}$:

$$U_{\min}\left(\mathbf{x}^{(i)}\right)=\begin{cases}u_e\begin{cases}\text{if } \hat{G}^{(k)}\left(\mathbf{x}^{(i)}t^{(j)}\right)>0\\ \text{and } U^{(k)}\left(\mathbf{x}^{(i)},t^{(j)}\right)\geq 2.5, \exists j=1,2,\cdots,N_t\end{cases}\\ \min\limits_{j=1,2,\cdots,N_t}\left\{U^{(k)}\left(\mathbf{x}^{(i)},t^{(j)}\right)\right\}, \text{ otherwise}\end{cases} \tag{5.11}$$

When the surrogate fails to find a accurate point that $\hat{G}^{(k)}(\mathbf{X},t)>0$, or not accurate enough to prove $\hat{G}^{(k)}(\mathbf{X},t)<0$ for all time steps. Points are needed to update the Kriging. The updating points are decided by searching all the random $x^{(i)}$ by minimizing $U(x^{(i)},t^{(j)})$ for each time step t and for each constraint:

$$[i_{\min},j_{\min}]=\min_{i=1,2,\cdots,N}\left\{\min_{j=1,2,\cdots,N_t}\left\{U^{(k)}\left(\mathbf{x}^{(i)},t^{(j)}\right)\right\}\right\} \tag{5.12}$$

To avoid the clustering of new points and current training points, a correlation criterion is added before the searching. If the correlation between the points $\left[x^{(i)},t^{(j)}\right]$ and existing training points are bigger than a limit value, for example 0.95, $U\left(\mathrm{x}^{(i)},t^{(j)}\right)$ will be replaced with a big value, say $U\left(\mathrm{x}^{(i)},t^{(j)}\right)=10$. The correlation is calculated with:

$$\rho_c=\max\left\{(R(\theta,[x^{(i)},t^{(j)}],[\mathbf{x}^s,\mathbf{t}^s]))\right\} \tag{5.13}$$

here R is the correlation function of Kriging, θ is the parameter of current Kriging. $[\mathbf{x}^s,\mathbf{t}^s]$ are the existing training points. The procedures for identifying a new training point are summarized as:

Step 1. Assume the MCS samples as $\boldsymbol{x}^i$, $i=1,2,..,N$, and the time interval $[t_0,t_e]$ is discretized

into N_t time steps.

Step 2. For each sample of MCS sample $\boldsymbol{x}_i$, $i = 1,2,..,N$

(a.) Compute $U(\boldsymbol{x}^i, j)$, and $\rho_c(t^j) = \max\{\rho(\boldsymbol{x}_i^j, \boldsymbol{x}^s)\}$, $j = 1,2,...,N_t$, where $\boldsymbol{x}^s$ are existing training points.

(b.) If there exists a time instant t^j, that any constraint satisfying $\hat{g}^k(\boldsymbol{x}^i, t^j) > 0$ and $U^k(\boldsymbol{x}^i, t^j) \geq 2.5$. Replace $U_{min}(\boldsymbol{x}^i)$ with u_e (a value bigger than 2.5) and jump to Step.3. Otherwise, continue.

(c.) Find the indices d_t that $\rho_c(t^j) \geq 0.95$.

(d.) Replace $U(\boldsymbol{x}^i, d_t)$ with 10.

Step 3. Identify the new training points by Equation.5.12 .

After identifying $i_{\min}$ and $j_{\min}$, a new sample $[x^{(i_{\min})}, t^{j_{\min}}]$ will be added into the current training set . The stop criterion for the updating is that the maximum prediction error is lower than a limit value, 5% for example. The maximum error is calculated as:

$$\varepsilon_r^{\max} = \max_{N_{f_2}^* \in [0, N_2]} \left\{ \frac{\left| N_{f2} - N_{f_2}^* \right|}{N_{f1} + N_{f_2}^*} \times 100\% \right\} \tag{5.14}$$

here N_{f1} is the number of samples for all random $\boldsymbol{x}^i, i = 1, \cdots, N$ and time steps $t^{(j)}, j = 1, \cdots N_t$ that satisfy $U^{(k)}(\mathbf{x}^i, t^{(j)}) \geq 2.5$, which are considered to be accurate; $N_{f2} = N * Nt - N_{f1}$ is the number of the other part of samples.

After the Kriging is built, MCS is used to calculate the reliability.

$$I_t\left(\mathbf{x}^{(i)}\right) = \begin{cases} 1, \begin{cases} \text{if } \hat{G}^{(k)}\left(\mathbf{x}^{(i)} t^{(j)}\right) > 0 \\ \text{and } U^{(k)}\left(\mathbf{x}^{(i)}, t^{(j)}\right) \geq 2.5, \exists j = 1,2,\cdots,N_t \end{cases} \\ 0, \begin{cases} \text{if } \hat{G}^{(k)}\left(\mathbf{x}^{(i)}, t^{(j)}\right) \leq 0 \\ \text{and } U^{(k)}\left(\mathbf{x}^{(i)}, t^{(j)}\right) \geq 2.5, \forall j = 1,2,\cdots,N_t \end{cases} \end{cases} \tag{5.15}$$

Coefficient of variation is used as the stopping criterion of the the calculating of time-variant reliability, taking to be 0.02 in this work:

$$\mathrm{Cov}_{\mathrm{pf}} = \sqrt{\left(1 - p_f(t_0, t_e)\right) / \left(p_f(t_0, t_e)\right) / N_{\mathrm{MCS}}} \tag{5.16}$$

The Flowchart of calculating TvR using SILK is summarized as:

Step 1. Generate initial training points $\boldsymbol{x}$ and evaluate the responses at these training points. Set $Cov_{pf} = 1$. Set $\boldsymbol{x}_{MCS} = []$.

Step 2. Generate N samples of X and add into $\boldsymbol{x}_{MCS}$.

Step 3. Construct the surrogate $\hat{g}(\boldsymbol{x}, t)$.

Step 4. Compute U_{min} using Equation.5.12, and then ε_r^{max} using Equation.5.14.

Step 5. If $\varepsilon_r^{max} > 0.05$, searching new samples to update the Kriging with Equation.5.12 and Equation.5.13 and go back to Step.3.

Step 6. Calculate probability of failure using the the surrogate $\hat{g}(\boldsymbol{X}, t)$ with the samples of $\boldsymbol{x}_{MCS}$.

Step 7. Calculate the coefficient of variation Cov_{pf} with Equation.5.16. N_{MCS} is the number of samples in $\boldsymbol{x}_{MCS}$.

Step 8. If $Cov_{pf} \leq 0.02$, p_f converges, else go to Step.2.

5.3 TvRBDO using double-loop Kriging

This section proposes the TvRBDO using double loop Kriging surrogates. This method consists in building two separate Kriging surrogates, the inner-loop Kriging is used to calculate the TvR with SILK method, the outer-loop Kriging is used to conduct TvRBDO.

5.3.1 Initial Sampling from augmented reliability space for inner loop

In this work, the lower and upper bound for augmented probability density function (PDF) is used [158], which is given as:

$$\begin{cases} q_{X_i}^{-} = \min\limits_{\theta \in D\theta} F_{X_i}^{-1}\left(\Phi\left(-\beta_{0,i}\right)|\theta\right) \\ q_{X_i}^{+} = \max\limits_{\theta \in D\theta} F_{X_i}^{-1}\left(\Phi\left(+\beta_{0,i}\right)|\theta\right) \end{cases} \tag{5.17}$$

where $q_{X_i}^{-}$ and $q_{X_i}^{+}$ are the lower and upper bound respectively, where $F_{X_i}^{-1}$ is the quantile function of the margin of X_i, Φ is the CDF of normal distribution, $\beta_{0,i}$ is the reliability level

the ith constraint. After the bound is calculated, the training samples are drawn uniformly using Latin Hypercube Sampling (LHS), to train the initial inner-loop Kriging. This Kriging is then updated with SILK method reviewed in Section.5.2. After the inner-loop converges, it is then used to calculate time-variant reliability for the outer-loop.

5.3.2 Updating the Kriging for outer-loop optimization

To build the outer-loop Kriging, first LHS sampling is used to train the outer-Kriging, the failure rate is calculated using SILK in the inner loop:

$$p_f = \text{SILK}(\text{d}, \mathbf{X}_\text{d}, t) \tag{5.18}$$

After the outer-loop Kriging is built, expected feasible function (EFF) is used to update the outer-Kriging. The EFF function is re-mentioned here as:

$$\begin{aligned} EF[\widehat{G}(\boldsymbol{x})] = (\mu_{\hat{G}} - \bar{z}) & \left[2\Phi\left(\frac{\bar{z}-\mu_{\hat{G}}}{\sigma_{\hat{G}}}\right) - \Phi\left(\frac{z^- - \mu_{\hat{G}}}{\sigma_{\hat{G}}}\right) - \Phi\left(\frac{z^+ - \mu_{\hat{G}}}{\sigma_{\hat{G}}}\right) \right. \\ & - \sigma_{\hat{G}} \left[2\phi\left(\frac{\bar{z}-\mu_{\hat{G}}}{\sigma_{\hat{G}}}\right) - \phi\left(\frac{z^- - \mu_{\hat{G}}}{\sigma_{\hat{G}}}\right) - \phi\left(\frac{z^+ - \mu_{\hat{G}}}{\sigma_{\hat{G}}}\right) \right] \\ & \left. + \varepsilon \left[\Phi\left(\frac{z^+ - \mu_{\hat{G}}}{\sigma_{\hat{G}}}\right) - \Phi\left(\frac{z^- - \mu_{\hat{G}}}{\sigma_{\hat{G}}}\right) \right] \right] \end{aligned} \tag{5.19}$$

z is taken to be p^* in this case. The updating stops when the maximum EFF is smaller than $1e-6$ or the maximum number of samples is reached. After the outer surrogate is built, it's then used to realize TvRBDO. At each iteration of TvRBDO of the outer-loop, the optimum point of this iteration is added into the outer-loop Kriging training set to update the outer-loop Kriging. The TvRBDO process stops when the change of optimum is smaller than ε.

The Flowchart the TvRBDO can be summarized as:

Step 1. Calculate $q_{X_i}^-$ and $q_{X_i}^+$ from Equation.5.17. After, the inner Kriging is built by drawing sample uniformly from the the bound of $[q_{X_i}^-, q_{X_i}^+]$

Step 2. Draw LHS samples for the design variables $\boldsymbol{X}_d$ from design space $\boldsymbol{\theta}_d$.

Step 3. Calculate the vector of failure rate $\boldsymbol{p}_f$ related $\boldsymbol{X}_d$ with SILK method.

Step 4. Build the outer Kriging with $\boldsymbol{X}_d$ and $\boldsymbol{p}_f$.

Step 5. Update the outer-Kriging by maximize the EFF function of Equation.5.19. The EFF update stops when the maximum EFF is smaller than $1e-6$ or the maximum number of samples are added.

Step 6. Conduct optimization using the outer-Kriging, the optimum design are added into the outer-Kriging data set in Step.4.

Step 7. The optimization stops when the change of optimum design is lower than ε .

5.4 Example and Results

In this section, two examples are used to validate the proposed method.

5.4.1 A two-variable example

The first example is a numerical example that consists in two random variables: $X_1 \sim N(\mu_1, 0.6)$ and $X_2 \sim N(\mu_2, 0.6)$. The design variables are the mean values of the two variables. The time interval for this problem is set to be $[0,5]$. The objective function and constraints are summarized as follows:

$$\begin{aligned} &\min \mathrm{C}(\mu_1,\mu_2) = \mu_1 + \mu_2 \\ &st. \begin{cases} \mathrm{Prob}\{G_1(X_1,X_2,t) < 0\} \le p_i^* & ,i = 1,2,3 \\ 0 \le \mu_j \le 10 & ,j = 1,2 \end{cases} \end{aligned} \tag{5.20}$$

The limit failure rate p^* is set to be 0.1 for all probability constraints. The performance functions are given as:

$$\begin{cases} G_1(X_1,X_2,t) = X_1^2 X_2 - 5X_1 t + (X_2+1)t^2 - 20 \\ G_2(X_1,X_2,t) = (X_1+X_2-0.1t-5)^2/30 + (X_1-X_2+0.2t-12)^2/120 - 1 \\ G_3(X_1,X_2,t) = 90/\left((X_1+0.05t)^2 + 8(X_2+0.1t) - \sin(t) + 5\right) - 1 \end{cases} \tag{5.21}$$

The three performance functions with different time instants are shown in Figure.5.1.

Figure 5.1: Performance functions with different time instants

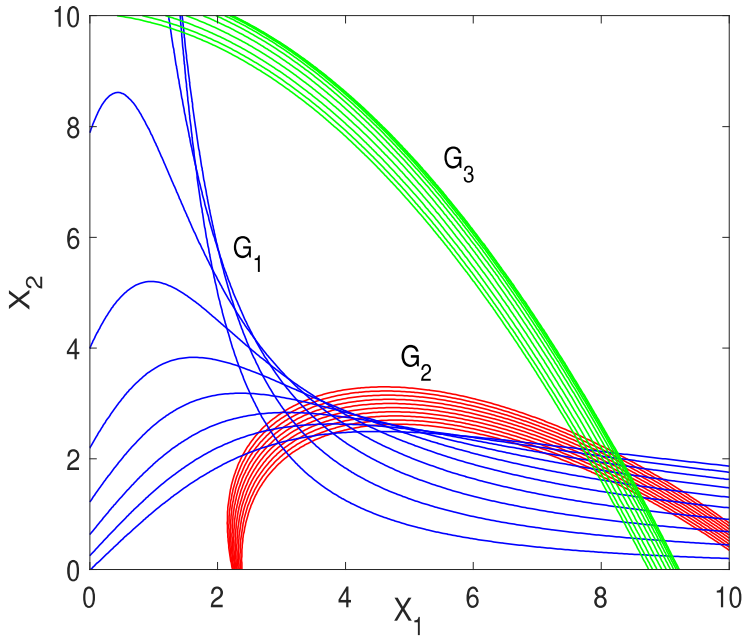

The program starts by sampling 64 LHS samples $[\boldsymbol{x}_1^{\text{outer}}, \boldsymbol{x}_2^{\text{outer}}]$ for outer-loop and 36 LHS samples $[\boldsymbol{x}_1^{\text{Inner}}, \boldsymbol{x}_2^{\text{Inner}}, \boldsymbol{t}]$ for inner-loop from the augmented PDF. The failure rates $\boldsymbol{f}$ of the samples of outer-Kriging are evaluated with SILK method from the inner-loop Kriging, then the failure rates and the outer-loop samples are used to train the outer-Kriging. Before the TvRBDO optimization, the outer-loop is first updated with points that maximize EFF function, the maximum number for updating outer-loop is set to be 50. After the EFF updating of the outer-loop, this outer-Kriging is used to conduct TvRBDO.

The optimum results from each iteration of TvRBDO of the outer-loop is also added into the outer-loop Kriging training sets. The TvRBDO optimization stops when the change between iterations smaller than 1e-6. The final results are shown in Table.5.1.

The Time-variant Reliability-based optimization using Double-Loop Kriging (TRDLK) proposed in this work converges with less function evaluations (137) than NERS (which is based on the extreme value of the double-loop EGO TvR method). This advantage comes from the advantage of SILK. TRDLK uses more function evaluations and iterations to converge, but compared with NERS, it should be noted that, after the outer-loop Kriging is built, the computational cost for TvRBDO will be minimal.

Table 5.1: Comparison of Results with NERS and TRDLK

	NERS	TRDLK
Initial Design	[2.5000, 4.3555]	[0,0]
Optimal Design	[3.6390, 4.0352]	[3.6243 4.1553]
Optimal Cost	7.6642	7.7797
$P_f^1(0,5)$	0.1216	0.0983
$P_f^2(0,5)$	0.0836	0.0580
$P_f^3(0,5)$	0	0
N_{func}	336	137
N_{iter}	4	9

5.4.2 Two-bar frame structure

Another example is a two-bar frame structure subject to stochastic force $F(t)$ taken from Hu & Du[155] as shown in Figure.5.2. The two distances of O_1O_3 and O_1O_2 are random variables

Figure 5.2: A two-bar frame structure

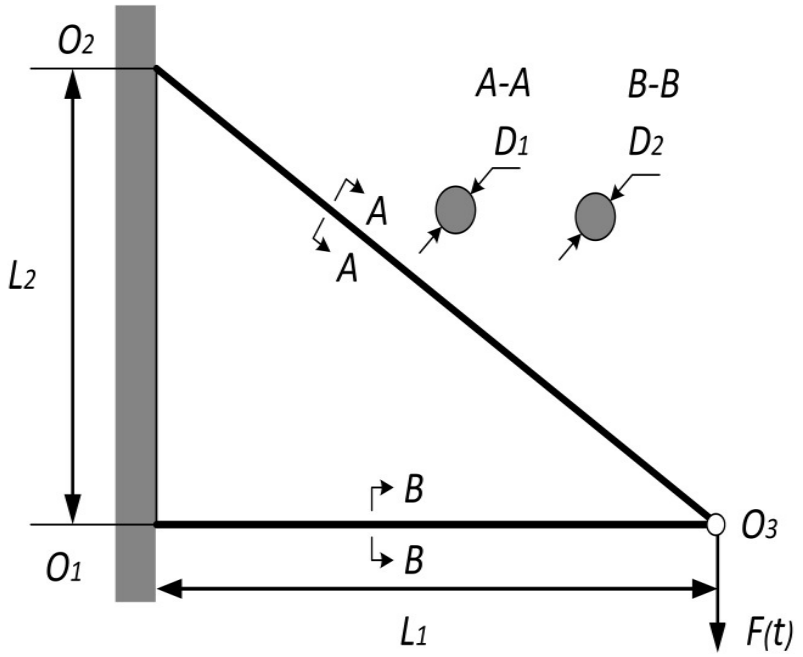

denoted as L_1 and L_2. Failure occurs when the maximum stresses in either bars are larger than their material yield stress S_1 and S_2. The design variables are the diameters of the two bars D_1 and D_2. The distribution parameters of the random variables are listed in Table.5.2.

$F(t)$ is considered as a stationary Gaussian process with exponential square auto-correlation

Table 5.2: Random parameters of two-bar frame structure

Parameters	Distribution	Mean	Standard deviation
D_1	Normal	μ_{D_1}	1e-3
D_2	Normal	μ_{D_2}	1e-3
L_1	Normal	0.4m	1e-3
L_2	Normal	0.3m	1e-3
S_1	Log-normal	1.7e8Pa	1.7e7Pa
S_2	Log-normal	1.7e8Pa	1.7e7Pa

function given by:

$$\rho_F\left(t_i,t_j\right)=\exp\left(-\left(\frac{t_j-t_i}{0.1}\right)^2\right) \tag{5.22}$$

The mean value and standard deviation of the Gaussian process are stationary as $\mu_F=2.2e6$ and $\sigma_F=2.0e5$. The problem can be summarized as:

$$\begin{aligned}&\min C\left(\mu_{D_1},\mu_{D_2}\right)=\pi\mu_{L_1}\mu_{D_1}^2/4+\pi\sqrt{\mu_{L_1}^2+\mu_{L_2}^2}\mu_{D_3}^2/4\\ &st.\begin{cases}\text{Prob}\left\{G_i\left(\mathbf{X}_1,F(t),t\right)<0\right\}\le p_i^* & ,i=1,2\\ 0.07\le\mu_{D,}\le 0.25 & ,j=1,2\end{cases}\end{aligned} \tag{5.23}$$

The limit failure rate p_i^* for two performance functions are set to be 0.01 and 0.001 that are given as:

$$\begin{aligned}G_1(\mathbf{X},t)&=\pi D_1^2S_1/4-\sqrt{L_1^2+L_2^2}F(t)/L_2\\ G_2(\mathbf{X},t)&=\pi D_2^2S_2/4-L_1F(t)/L_2\end{aligned} \tag{5.24}$$

Similar to example 1, the TvRBDO is started by 64 LHS samples $[\boldsymbol{x}_d^{\text{outer}},\boldsymbol{x}_c^{\text{outer}}]$ for outer-loop Kriging and 64 LHS samples $[\boldsymbol{x}_d^{\text{inner}},\boldsymbol{x}_c^{\text{inner}},\boldsymbol{F}_t^{\text{inner}}]$ for inner-loop. The stochastic process F_t is discretized over 10 intervals. The final results are shown in Table.5.3. As shown from the results, this method uses fewer function evaluations than t-SORA[155] and the accuracy is similar.

Table 5.3: Comparison of Results with t-SORA and TRDLK

	t-SORA	TRDLK	Analytical
Optimal Design	[0.2102 0.1964]	[0.2017 0.1886]	[0.2027 0.1894]
Optimal Cost	0.0290	0.0267	0.0270
$P_f^1(0,5)$	0.0094	0.0102	0.01
$P_f^2(0,5)$	0.0009	0.0009	0.001
N_{func}	715	471	\

5.5 Conclusion

This chapter proposed a double-loop Kriging surrogate method to conduct time-variant reliability optimization. This method consists in two separate Kriging surrogates, the inner-loop Kriging evaluates the time-variant reliability using SILK method, and the outer-loop Kriging is trained with the results of the inner-loop. After the out-loop Kriging is built, it is then updated with EFF function at allowable failure rate . Two examples are used to validate the effectiveness of the method. Compared to other existing methods, this method is simple, accurate and easy to implement. The computational cost mainly comes from the searching of points to update the inner-Kriging. After the outer-Kriging is built, the computational cost for optimization will be minimal. However, due to Kriging is less competent for high-linear problems and high-dimensional problems, this method may be less effective for such problems. Also the inner-loop Kriging error will be accumulated to outer-loop Kriging, it's recommended to use a smaller Coefficient of variation (Cov) value, while this will inevitably increase the total computational cost.

Conclusion and Perspective

In this thesis, the subjects around the uncertainty quantification for wind turbine tower are discussed. Wind turbine is a complex system, and the working environment includes multiple sources of uncertainties. The thesis try to cover wide aspects from the fundamental mechanical theories to applications of reliability-based design optimization. This final chapter gives a summary about what are mentioned in the whole thesis.

Conclusions

During the lifespan of wind turbines, there exist multiple failure scenarios caused by the existence of uncertainties. In Chapter.1, the fundamental theories of the structure dynamics of wind turbine system and the design requirements of wind turbine structure are introduced , from the fundamental theories of BEM method to the structure Kinetic modeling of Kane's equations. With the help of these theories and simulation tools, many researchers try to optimize the design of wind turbine structures considering different installation sites and design load cases. Two types of methodologies :safety-factor-based and reliability-based methodologies are compared. Reliability-based design optimization has the advantage of balancing cost and reliability, avoiding risky or over-conservative designs.

Due to the uncertainties mentioned in Chapter.1, uncertainty propagation methods widely used in wind energy are summarized in Chapter.2, covering simulation methods, surrogate models, sensitivity analysis and reliability analysis. To carry out reliability analysis or sensitivity analysis, the most straightforward way is using simulation methods. However simulation methods are time-consuming when facing complex engineering problems. So surrogate models are widely used to replace the complex engineering models. Currently,

different surrogate models are available, the choice for surrogate is very problem- oriented, this is further discussed in Chapter.3.

In Chapter.3, the uncertainty propagation of inflow wind is discussed. 6 surrogate models mentioned in Chapter.3 are firstly compared with several mathematical problems, the results shown the capacities of each surrogate model , among which Kriging surrogate has shown its adaptation to various problems. For the probabilistic characterization of loads on top of wind turbine tower, it's shown that the mean, maximum of the load responses can be approximated with Normal distribution and Extreme distribution respectively. Then the surrogate models are used for the propagation of inflow wind uncertainties. The results show that, it's possible to build a relationship between input wind uncertainties to the statistical characteristics of response loads on top of the tower. The surrogate comparison shows KRG can achieve lower generalized relative error e_R, and smaller Kullback-Leibler divergence d_{KL} for the wind uncertainty propagation problem. Once again Kriging has shown superiority in aspects of e_R and d_{KL} criteria.

In Chapter.4, the RBDO problems is discussed, the SLA method is coupled with Kriging surrogate, the design points of each RBDO optimization is used to update the Kriging surrogate. The proposed Kriging-SLA method is very efficient compared with other sampling methods. The accuracy of the proposed method is in accordance with the original SLA method without surrogate models. This method needs fewer initial sample points and converges with the minimum number of sample points. However, this method suffers the same limitations of the gradient-based-method, like SLA or SORA, which are less accurate for highly-nonlinear problems.

In Chapter.5, a method of TvRBDO using double-loop Kriging surrogates is proposed. This method consists in two separate Kriging surrogates. The inner-loop evaluates the time-variant reliability using SILK method, and the outer-loop Kriging is trained with the results of the inner-loop. Before conduct TvRBDO, the outer-loop is firstly updated with EFF function at allowable failure rate before TvRBDO. Two examples are used to validate the effectiveness of the method. The method is simple, accurate and easy to implement. The computational cost mainly comes from the searching of points to update the inner-Kriging, after the outer-Kriging is build, the computational cost for optimization is minimal. However, due to Kriging is

less competent for high-linear problems and high-dimensional problems, this method may be less effective for such problems. Also the inner-loop Kriging error will be accumulated to outer-loop Kriging. It's recommended to use a smaller coefficient of variation value, however this will inevitably increase the total computational cost.

Perspective

This paper focuses on the reliability-based design optimization of wind turbine tower, various subjects are discussed. However the author thinks there exist several issues needed future work.

Firstly, for the uncertainty propagation of wind turbine loads, besides prediction of the probabilistic characteristics of responses, further study can be focused on the sensitivity of inputs, the fatigue prediction of components, for example fatigue prediction of blade, tower, etc.

Secondly, for the RBDO using SLA, this method is less effective for high-dimensional or high-linearity problems. Additional work may ameliorate these drawbacks, for example using gradient enhanced-Kriging [159] for the constraints or enhanced-SLA method [146].

Thirdly, for the TvRBDO, suitable engineering problems can be added, for example the TvRBDO of wind turbine components considering fatigue and erosion. However, the TvRBDO for wind turbine components is monochrome decreasing problem, so setting the objective function as life cost or profit would be more interesting.

Bibliography

[1] E. Lantz, M. Hand, and R. Wiser, "Past and future cost of wind energy", National Renewable Energy Lab.(NREL), Golden, CO (United States), Tech. Rep., 2012.

[2] B. Iooss and P. Lemaître, "A review on global sensitivity analysis methods", in *Uncertainty management in simulation-optimization of complex systems*, Springer, 2015, pp. 101–122.

[3] J. Jonkman, S. Butterfield, W. Musial, and G. Scott, "Definition of a 5-mw reference wind turbine for offshore system development", National Renewable Energy Lab.(NREL), Golden, CO (United States), Tech. Rep., 2009.

[4] Z. Hu and S. Mahadevan, "A single-loop kriging surrogate modeling for time-dependent reliability analysis", *Journal of Mechanical Design*, vol. 138, no. 6, 2016.

[5] GWEC, *Global installed capacity in 2018*, https://gwec.net/51-3-gw-of-global-wind-capacity-installed-in-2018/, 2018.

[6] BP, *Bp global:wind energy*, https://www.bp.com/en/global/corporate/energy-economics/statistical-review-of-world-energy/renewable-energy, 2018.

[7] WindEurope, *Wind power supplied 15% of the electricity consumed in europe in 2019*, https://business.devilhunter.net/2020/02/wind-power-supplied-15-of-electricity.html, Feb. 2020.

[8] W. E. C. GLOBAL, "Global wind report 2018", *Bruxelas:[sn]*, 2019.

[9] P. K. Chaurasiya, V. Warudkar, and S. Ahmed, "Wind energy development and policy in india: A review", *Energy Strategy Reviews*, vol. 24, pp. 342–357, 2019.

[10] M. Junginger, A. Louwen, N. G. Tuya, D. de Jager, E. van Zuijlen, and M. Taylor, "Offshore wind energy", in *Technological Learning in the Transition to a Low-Carbon Energy System*, Elsevier, 2020, pp. 103–117.

[11] M. O. L. Hansen, J. N. Sørensen, S. Voutsinas, N. Sørensen, and H. A. Madsen, "State of the art in wind turbine aerodynamics and aeroelasticity", *Progress in aerospace sciences*, vol. 42, no. 4, pp. 285–330, 2006.

[12] H. Glauert, "Airplane propellers", in *Aerodynamic theory*, Springer, 1935, pp. 169–360.

[13] R. F. Mikkelsen and J. N. Sørensen, "Actuator disc methods applied to wind turbines", 2004.

[14] B. A. Mulugeta and A. Gerawork, "Aerodynamic design of horizontal axis wind turbine blades", *FME Transactions*, vol. 45, no. 4, pp. 647–660, 2017.

[15] J. M. Jonkman, "Modeling of the UAE wind turbine for refinement of FAST_AD", National Renewable Energy Lab., Golden, CO (US), Tech. Rep., 2003.

[16] R. E. Wilson, P. B. Lissaman, and S. N. Walker, *Aerodynamic performance of wind turbines*. Oregon State University Corvallis, Oregon, 1976.

[17] T. R. Kane and D. A. Levinson, *Dynamics, theory and applications*. McGraw Hill, 1985.

[18] J. M. Jonkman, M. L. Buhl Jr, *et al.*, "Fast user's guide", *National Renewable Energy Laboratory, Golden, CO, Technical Report No. NREL/EL-500-38230*, 2005.

[19] J. M. Jonkman, "Dynamics modeling and loads analysis of an offshore floating wind turbine", National Renewable Energy Lab.(NREL), Golden, CO (United States), Tech. Rep., 2007.

[20] T. J. Larsen and A. M. Hansen, "How 2 hawc2, the user's manual", 2007.

[21] E. Bossanyi, "Gh bladed user manual", *Garrad Hassan and Partners Ltd*, vol. 701, 2009.

[22] B. EN, "61400-1: 2005+ a1: 2010: Wind turbines—design requirements", *British Standards Institution: London, UK*, 2006.

[23] J. Mann, "The spatial structure of neutral atmospheric surface-layer turbulence", *Journal of fluid mechanics*, vol. 273, pp. 141–168, 1994.

[24] J. C. Kaimal, J. Wyngaard, Y. Izumi, and O. Coté, "Spectral characteristics of surface-layer turbulence", *Quarterly Journal of the Royal Meteorological Society*, vol. 98, no. 417, pp. 563–589, 1972.

[25] B. J. Jonkman and M. L. Buhl Jr, "Turbsim user's guide", National Renewable Energy Lab.(NREL), Golden, CO (United States), Tech. Rep., 2006.

[26] F. Spinato, P. J. Tavner, G. J. Van Bussel, and E. Koutoulakos, "Reliability of wind turbine subassemblies", *IET Renewable Power Generation*, vol. 3, no. 4, pp. 387–401, 2009.

[27] E. Echavarria, B. Hahn, G. Van Bussel, and T. Tomiyama, "Reliability of wind turbine technology through time", *Journal of Solar Energy Engineering*, vol. 130, no. 3, 2008.

[28] P. Tavner, J. Xiang, and F. Spinato, "Reliability analysis for wind turbines", *Wind Energy: An International Journal for Progress and Applications in Wind Power Conversion Technology*, vol. 10, no. 1, pp. 1–18, 2007.

[29] P. Tavner, C. Edwards, A. Brinkman, and F. Spinato, "Influence of wind speed on wind turbine reliability", *Wind Engineering*, vol. 30, no. 1, pp. 55–72, 2006.

[30] M. Grigoriu, *Stochastic systems: uncertainty quantification and propagation*. Springer Science & Business Media, 2012.

[31] W. Hu, *Advanced wind turbine technology*. Springer, 2018.

[32] A. Seebregts, L. Rademakers, and B. Van Den Horn, "Reliability analysis in wind turbine engineering", *Microelectronics Reliability*, vol. 35, no. 9-10, pp. 1285–1307, 1995.

[33] J. D. Sørensen, "Reliability analysis of wind turbines exposed to dynamic loads", in *9th International Conference on Structural Dynamics*, European Association for Structural Dynamics (EASD), 2014, pp. 39–46.

[34] J. W. Holmes, B. F. Sørensen, and P. Brøndsted, "Reliability of wind turbine blades: An overview of materials testing", *Proceedings of the Wind Power Shanghai*, 2007.

[35] H. S. Toft and J. D. Sørensen, "Reliability-based design of wind turbine blades", *Structural Safety*, vol. 33, no. 6, pp. 333–342, 2011.

[36] R. Bakhshi and P. Sandborn, "The effect of yaw error on the reliability of wind turbine blades", in *ASME 2016 10th International Conference on Energy Sustainability collocated with the ASME 2016 Power Conference and the ASME 2016 14th International Conference on Fuel Cell Science, Engineering and Technology*, American Society of Mechanical Engineers Digital Collection, 2016.

[37] W. Yang and B. Attaf, "Testing and condition monitoring of composite wind turbine blades", *Recent Advances in Composite Materials for Wind Turbine Blade*, pp. 147–169, 2013.

[38] H. S. Toft, K. Branner, P. Berring, and J. D. Sørensen, "Defect distribution and reliability assessment of wind turbine blades", *Engineering Structures*, vol. 33, no. 1, pp. 171–180, 2011.

[39] Z. Hu and X. Du, "Reliability analysis for hydrokinetic turbine blades", *Renewable Energy*, vol. 48, pp. 251–262, 2012.

[40] K. Smolders, H. Long, Y. Feng, and P. Tavner, "Reliability analysis and prediction of wind turbine gearboxes", in *European Wind Energy Conference and Exhibition 2010, EWEC 2010*, Sheffield, vol. 4, 2010, pp. 2660–2682.

[41] M. P. Barrett and J. Stover, "Understanding oil analysis: How it can improve the reliability of wind turbine gearboxes", *Gear Technology: Elk Grove Village, IL, USA*, pp. 104–111, 2013.

[42] B. LIU and Z. An, "System reliability analysis of wind turbine gearbox considering component life dependency [j]", *Journal of Mechanical Engineering*, vol. 51, no. 10, pp. 164–171, 2015.

[43] W. LaCava, W. LaCava, and B. McNiff, "Gearbox reliability collaborative: Test and model investigation of sun orbit and planet load share in a wind turbine gearbox", in *53rd AIAA/ASME/ASCE/AHS/ASC Structures, Structural Dynamics and Materials Conference 20th AIAA/ASME/AHS Adaptive Structures Conference 14th AIAA*, 2012, p. 1418.

[44] Y. Hsu, W.-F. Wu, and Y.-C. Chang, "Reliability analysis of wind turbine towers", *Procedia Engineering*, vol. 79, pp. 218–224, 2014.

[45] T. H. H. Jin-Hak Yi, "Reliability analysis on wind turbine tower structures with composite section", *Journal of the Korean Society of Hazard Mitigation*, vol. 16, no. 4, pp. 185–194, 2016.

[46] R. Rackwitz and B. Flessler, "Structural reliability under combined random load sequences", *Computers & Structures*, vol. 9, no. 5, pp. 489–494, 1978.

[47] B. Low, "Form, sorm, and spatial modeling in geotechnical engineering", *Structural Safety*, vol. 49, pp. 56–64, 2014.

[48] K. Breitung, "Asymptotic approximations for multinormal integrals", *Journal of Engineering Mechanics*, vol. 110, no. 3, pp. 357–366, 1984.

[49] P. M. McKay, R. Carriveau, D. S.-K. Ting, and J. L. Johrendt, "Global sensitivity analysis of wind turbine power output", *Wind Energy*, vol. 17, no. 7, pp. 983–995, 2014.

[50] C.-C. Zhu, X.-Y. Xu, and H.-J. Wang, "Modal prediction and sensitivity analysis of wind-turbine planetary gear system with flexible planet pin", *Advanced Science Letters*, vol. 4, no. 3, pp. 1219–1224, 2011.

[51] M. Kubik, P. J. Coker, and C. Hunt, "Using meteorological wind data to estimate turbine generation output: A sensitivity analysis", in *World Renewable Energy Congress-Sweden; 8-13 May; 2011; Linköping; Sweden*, Linköping University Electronic Press, 2011, pp. 4074–4081.

[52] R. Martin, I. Lazakis, S. Barbouchi, and L. Johanning, "Sensitivity analysis of offshore wind farm operation and maintenance cost and availability", *Renewable Energy*, vol. 85, pp. 1226–1236, 2016.

[53] L. C. T. Overgaard and E. Lund, "Structural design sensitivity analysis and optimization of vestas v52 wind turbine blade", in *Proc. 6th world congress on structural and multidisciplinary optimization*, 2005.

[54] C. Pradhan and C. N. Bhende, "Frequency sensitivity analysis of load damping coefficient in wind farm-integrated power system", *IEEE Transactions on Power Systems*, vol. 32, no. 2, pp. 1016–1029, 2016.

[55] M. D. Morris, "Factorial sampling plans for preliminary computational experiments", *Technometrics*, vol. 33, no. 2, pp. 161–174, 1991.

[56] I. M. Sobol, "Global sensitivity indices for nonlinear mathematical models and their monte carlo estimates", *Mathematics and computers in simulation*, vol. 55, no. 1-3, pp. 271–280, 2001.

[57] S. Marelli, C. Lamas, K. Konakli, C. Mylonas, P. Wiederkehr, and B. Sudret, "UQLab user manual – Sensitivity analysis", Chair of Risk, Safety & Uncertainty Quantification, ETH Zurich, Tech. Rep., 2019, Report # UQLab-V1.2-106.

[58] K. Binder, D. Heermann, L. Roelofs, A. J. Mallinckrodt, and S. McKay, "Monte carlo simulation in statistical physics", *Computers in Physics*, vol. 7, no. 2, pp. 156–157, 1993.

[59] R. M. Neal, "Annealed importance sampling", *Statistics and computing*, vol. 11, no. 2, pp. 125–139, 2001.

[60] J. H. Friedman *et al.*, "Multivariate adaptive regression splines", *The annals of statistics*, vol. 19, no. 1, pp. 1–67, 1991.

[61] G. E. Box and K. B. Wilson, "On the experimental attainment of optimum conditions", *Journal of the Royal Statistical Society: Series B (Methodological)*, vol. 13, no. 1, pp. 1–38, 1951.

[62] N. Wiener, "The homogeneous chaos", *American Journal of Mathematics*, vol. 60, no. 4, pp. 897–936, 1938.

[63] S. Marelli and B. Sudret, "UQLab user manual – Polynomial chaos expansions", Chair of Risk, Safety & Uncertainty Quantification, ETH Zurich, Tech. Rep., 2019, Report # UQLab-V1.2-104.

[64] D. Xiu and G. E. Karniadakis, "The wiener–askey polynomial chaos for stochastic differential equations", *SIAM journal on scientific computing*, vol. 24, no. 2, pp. 619–644, 2002.

[65] M. Eldred and J. Burkardt, "Comparison of non-intrusive polynomial chaos and stochastic collocation methods for uncertainty quantification", in *47th AIAA aerospace sciences meeting including the new horizons forum and aerospace exposition*, 2009, p. 976.

[66] G. H. Golub and J. H. Welsch, "Calculation of gauss quadrature rules", *Mathematics of computation*, vol. 23, no. 106, pp. 221–230, 1969.

[67] J. Sacks, W. J. Welch, T. J. Mitchell, and H. P. Wynn, "Design and analysis of computer experiments", *Statistical science*, pp. 409–423, 1989.

[68] C. E. Rasmussen, "Gaussian processes in machine learning", in *Summer School on Machine Learning*, Springer, 2003, pp. 63–71.

[69] A. Forrester, A. Sobester, and A. Keane, *Engineering design via surrogate modelling: a practical guide*. John Wiley & Sons, 2008.

[70] C. Cortes and V. Vapnik, "Support-vector networks", *Machine learning*, vol. 20, no. 3, pp. 273–297, 1995.

[71] A. J. Smola and B. Schölkopf, "A tutorial on support vector regression", *Statistics and computing*, vol. 14, no. 3, pp. 199–222, 2004.

[72] M. Moustapha, C. Lataniotis, S. Marelli, and B. Sudret, "UQLab user manual – Support vector machines for regression", Chair of Risk, Safety & Uncertainty Quantification, ETH Zurich, Tech. Rep., 2019, Report # UQLab-V1.2-111.

[73] V. Vapnik, *The nature of statistical learning theory*. Springer science & business media, 2013.

[74] J. Mercer, *Functions of positive and negative type and their connection with the theory of integral equations, philosophical transsaction of the royal society of london, ser*, 1909.

[75] R. L. Hardy, "Theory and applications of the multiquadric-biharmonic method 20 years of discovery 1968–1988", *Computers & Mathematics with Applications*, vol. 19, no. 8-9, pp. 163–208, 1990.

[76] J. MacQueen *et al.*, "Some methods for classification and analysis of multivariate observations", in *Proceedings of the fifth Berkeley symposium on mathematical statistics and probability*, Oakland, CA, USA, vol. 1, 1967, pp. 281–297.

[77] A. Géron, *Hands-on machine learning with Scikit-Learn and TensorFlow: concepts, tools, and techniques to build intelligent systems*. " O'Reilly Media, Inc.", 2017.

[78] D. P. Kingma and J. Ba, "Adam: A method for stochastic optimization", *arXiv preprint arXiv:1412.6980*, 2014.

[79] L. Rokach and O. Z. Maimon, *Data mining with decision trees: theory and applications*. World scientific, 2008, vol. 69.

[80] P. J. Schubel and R. J. Crossley, "Wind turbine blade design", *Energies*, vol. 5, no. 9, pp. 3425–3449, 2012.

[81] K. J. Smith and D. Griffin, "Supersized wind turbine blade study: R&d pathways for supersized wind turbine blades", 2019.

[82] W. Xudong, W. Z. Shen, W. J. Zhu, J. N. Sørensen, and C. Jin, "Shape optimization of wind turbine blades", *Wind Energy: An International Journal for Progress and Applications in Wind Power Conversion Technology*, vol. 12, no. 8, pp. 781–803, 2009.

[83] P. Fuglsang and H. A. Madsen, "Optimization method for wind turbine rotors", *Journal of Wind Engineering and Industrial Aerodynamics*, vol. 80, no. 1-2, pp. 191–206, 1999.

[84] I. Lavassas, G. Nikolaidis, P. Zervas, E. Efthimiou, I. Doudoumis, and C. Baniotopoulos, "Analysis and design of the prototype of a steel 1-mw wind turbine tower", *Engineering structures*, vol. 25, no. 8, pp. 1097–1106, 2003.

[85] H. M. Negm and K. Y. Maalawi, "Structural design optimization of wind turbine towers", *Computers & Structures*, vol. 74, no. 6, pp. 649–666, 2000.

[86] M. Muskulus and S. Schafhirt, "Design optimization of wind turbine support structures-a review", *Journal of Ocean and Wind Energy*, vol. 1, no. 1, pp. 12–22, 2014.

[87] F. D. Bianchi, H. De Battista, and R. J. Mantz, *Wind turbine control systems: principles, modelling and gain scheduling design*. Springer Science & Business Media, 2006.

[88] A. D. Hansen, C. Jauch, P. E. Sørensen, F. Iov, and F. Blaabjerg, "Dynamic wind turbine models in power system simulation tool digsilent", 2004.

[89] T. Sebastian and M. Lackner, "Characterization of the unsteady aerodynamics of offshore floating wind turbines", *Wind Energy*, vol. 16, no. 3, pp. 339–352, 2013.

[90] W. J. Veloz, H. Zhang, H. Bai, Y. Aoues, and D. Lemosse, "Uncertainty propagation in wind turbine blade loads", in *International Symposium on Uncertainty Quantification and Stochastic Modeling*, Springer, 2020, pp. 337–346.

[91] J. P. Murcia, P.-E. Réthoré, N. Dimitrov, A. Natarajan, J. D. Sørensen, P. Graf, and T. Kim, "Uncertainty propagation through an aeroelastic wind turbine model using polynomial surrogates", *Renewable energy*, vol. 119, pp. 910–922, 2018.

[92] J. Velarde, C. Kramhøft, and J. D. Sørensen, "Global sensitivity analysis of offshore wind turbine foundation fatigue loads", *Renewable energy*, vol. 140, pp. 177–189, 2019.

[93] J. Quick, P. E. Hamlington, R. King, and M. A. Sprague, "Multifidelity uncertainty quantification with applications in wind turbine aerodynamics", in *AIAA Scitech 2019 Forum*, 2019, p. 0542.

[94] V. Keshavarzzadeh, R. G. Ghanem, and D. A. Tortorelli, "Shape optimization under uncertainty for rotor blades of horizontal axis wind turbines", *Computer Methods in Applied Mechanics and Engineering*, vol. 354, pp. 271–306, 2019.

[95] I. TC88-MT, "Iec 61400-3: Wind turbines–part 1: Design requirements", *International Electrotechnical Commission, Geneva*, vol. 64, 2005.

[96] G. Jekabsons, "Areslab: Adaptive regression splines toolbox for matlab/octave (ver. 1.10. 3)", *Institute of Applied Computer Systems Riga Technical University, Latvia. Available from: http://www. cs. rtu. lv/jekabsons/Files/ARESLab. pdf*, 2016.

[97] S. Marelli and B. Sudret, "Uqlab: A framework for uncertainty quantification in matlab", in *Vulnerability, uncertainty, and risk: quantification, mitigation, and management*, 2014, pp. 2554–2563.

[98] F. Pedregosa, G. Varoquaux, A. Gramfort, V. Michel, B. Thirion, O. Grisel, M. Blondel, P. Prettenhofer, R. Weiss, V. Dubourg, J. Vanderplas, A. Passos, D. Cournapeau, M. Brucher, M. Perrot, and E. Duchesnay, "Scikit-learn: Machine learning in Python", *Journal of Machine Learning Research*, vol. 12, pp. 2825–2830, 2011.

[99] M. Abadi, P. Barham, J. Chen, Z. Chen, A. Davis, J. Dean, M. Devin, S. Ghemawat, G. Irving, M. Isard, *et al.*, "Tensorflow: A system for large-scale machine learning", in *12th {USENIX} Symposium on Operating Systems Design and Implementation ({OSDI} 16)*, 2016, pp. 265–283.

[100] M. Rosenblatt, "Remarks on a multivariate transformation", *The annals of mathematical statistics*, vol. 23, no. 3, pp. 470–472, 1952.

[101] H. Adeli, *Advances in design optimization*. CRC press, 1994.

[102] H. O. Madsen, S. Krenk, and N. C. Lind, *Methods of structural safety*. Courier Corporation, 2006.

[103] M. Mayer, " Die Sicherheit der Bauwerke und ihre Berechnung nach Grenzkräften anstatt nach zulässigen Spannungen.Verlag Springer.", *ZAMM - Journal of Applied Mathematics and Mechanics / Zeitschrift für Angewandte Mathematik und Mechanik*, vol. 6, no. 5, pp. 421–421, 1926.

[104] A. M. Freudenthal, "The Safety of Structures", *Transactions of the American Society of Civil Engineers*, vol. 112, no. 1, pp. 125–159, 1947. [Online]. Available: https://cedb.asce.org/CEDBsearch/record.jsp?dockey=0293546.

[105] ——, "Safety and the Probability of Structural Failure", *Transactions of the American Society of Civil Engineers*, vol. 121, no. 1, pp. 1337–1375, 1956. [Online]. Available: https://cedb.asce.org/CEDBsearch/record.jsp?dockey=0293031.

[106] M. Lemaire, A. Chateauneuf, and J.-C. Mitteau, *Fiabilité des structures: Couplage mécano-fiabiliste statique*. Hermès Science Publications, 2005.

[107] A. Chateauneuf, "Principles of reliability-based design optimization", *Structural design optimization considering uncertainties*, pp. 3–31, 2008.

[108] H. Hilton and M. Feigen, "Minimum weight analysis based on structural reliability", *Journal of the Aerospace Sciences*, vol. 27, pp. 641–652, 1960.

[109] F. Moses and D. Kinser, "Optimum structural design with failure probability constraints", *AIAA Journal*, vol. 5, no. 6, pp. 1152–1158, 1967.

[110] D. M. Frangopol, "Structural optimization using reliability concepts", *Journal of Structural Engineering*, vol. 111, no. 11, pp. 2288–2301, 1985.

[111] A. T. Beck, R. K. Tessari, and H. M. Kroetz, "System reliability-based design optimization and risk-based optimization: A benchmark example considering progressive collapse", *Engineering Optimization*, vol. 51, no. 6, pp. 1000–1012, 2019.

[112] T. Lee and B. Kwak, "A reliability-based optimal design using advanced first order second moment method", *Mechanics of Structures and Machines*, vol. 15, no. 4, pp. 523–542, 1987.

[113] I. Enevoldsen and J. Sørensen, "Reliability-based optimization in structural engineering", *Structural Safety*, vol. 15, no. 3, pp. 169–196, 1994, ISSN: 0167-4730. DOI: https://doi.org/10.1016/0167-4730(94)90039-6. [Online]. Available: http://www.sciencedirect.com/science/article/pii/0167473094900396.

[114] J. Tu, K. K. Choi, and Y. H. Park, "A new study on reliability-based design optimization", *Journal of mechanical design*, vol. 121, no. 4, pp. 557–564, 1999.

[115] Y. Aoues and A. Chateauneuf, "Benchmark study of numerical methods for reliability-based design optimization", *Structural and multidisciplinary optimization*, vol. 41, no. 2, pp. 277–294, 2010.

[116] M. A. Valdebenito and G. Schuëller, "A survey on approaches for reliability-based optimization", *Structural and Multidisciplinary Optimization*, vol. 42, no. 5, pp. 645–663, 2010.

[117] E. Johnson, C. Proppe, B. Spencer, L. Bergman, G. Székely, and G. Schuëller, "Parallel processing in computational stochastic dynamics", *Probabilistic Engineering Mechanics*, vol. 18, no. 1, pp. 37–60, Jan. 2003, ISSN: 0266-8920. DOI: 10.1016/S0266-8920(02)00041-3. [Online]. Available: https://www.sciencedirect.com/science/article/pii/S0266892002000413.

[118] M. Moustapha and B. Sudret, "Surrogate-assisted reliability-based design optimization: a survey and a unified modular framework", *Structural and Multidisciplinary Optimization*, pp. 1–20, May 2019, ISSN: 1615-147X. DOI: 10.1007/s00158-019-02290-y.

[119] T. H. Lee and J. J. Jung, "A sampling technique enhancing accuracy and efficiency of metamodel-based rbdo: Constraint boundary sampling", *Computers & Structures*, vol. 86, no. 13-14, pp. 1463–1476, 2008.

[120] A. M. Hasofer and N. C. Lind, "Exact and invariant second-moment code format", *Journal of the Engineering Mechanics division*, vol. 100, no. 1, pp. 111–121, 1974.

[121] M. Rashki, M. Miri, and M. Azhdary Moghaddam, "A new efficient simulation method to approximate the probability of failure and most probable point", *Structural Safety*, vol. 39, pp. 22–29, Sep. 2012, ISSN: 01674730. DOI: 10.1016/j.strusafe.2012.06.003.

[122] M. Rashki, M. Miri, and M. A. Moghaddam, "A simulation-based method for reliability based design optimization problems with highly nonlinear constraints", *Automation in Construction*, vol. 47, pp. 24–36, Sep. 2014, ISSN: 09265805. DOI: 10.1016/j.autcon.2014.07.004.

[123] N. M. Okasha, "An improved weighted average simulation approach for solving reliability-based analysis and design optimization problems", *Structural Safety*, vol. 60, pp. 47–55, May 2016, ISSN: 01674730. DOI: 10.1016/j.strusafe.2016.01.005.

[124] H. Madsen and P. F. Hansen, "A comparison of some algorithms for reliability based structural optimization and sensitivity analysis", in *Reliability and Optimization of Structural Systems' 91*, Springer, 1992, pp. 443–451.

[125] J. Liang, Z. P. Mourelatos, and J. Tu, "A single-loop method for reliability-based design optimization", in *ASME 2004 international design engineering technical conferences and computers and information in engineering conference*, American Society of Mechanical Engineers, 2004, pp. 419–430.

[126] X. Du and W. Chen, "Sequential optimization and reliability assessment method for efficient probabilistic design", in *ASME 2002 International Design Engineering Technical Conferences and Computers and Information in Engineering Conference*, American Society of Mechanical Engineers, 2002, pp. 871–880.

[127] G. Cheng, L. Xu, and L. Jiang, "A sequential approximate programming strategy for reliability-based structural optimization", *Computers & structures*, vol. 84, no. 21, pp. 1353–1367, 2006.

[128] B. Hyeon Ju and B. Chai Lee, "Reliability-based design optimization using a moment method and a kriging metamodel", *Engineering Optimization*, vol. 40, no. 5, pp. 421–438, 2008.

[129] Z. Chen, H. Qiu, L. Gao, X. Li, and P. Li, "A local adaptive sampling method for reliability-based design optimization using kriging model", *Structural and Multidisciplinary Optimization*, vol. 49, no. 3, pp. 401–416, 2014.

[130] V. Dubourg and B. Sudret, "Meta-model-based importance sampling for reliability sensitivity analysis", *Structural Safety*, vol. 49, pp. 27–36, 2014.

[131] Z. Lv, Z. Lu, and P. Wang, "A new learning function for kriging and its applications to solve reliability problems in engineering", *Computers & Mathematics with Applications*, vol. 70, no. 5, pp. 1182–1197, 2015.

[132] J. Zhang, M. Xiao, and L. Gao, "An active learning reliability method combining kriging constructed with exploration and exploitation of failure region and subset simulation", *Reliability Engineering & System Safety*, 2019.

[133] F. Li, T. Wu, A. Badiru, M. Hu, and S. Soni, "A single-loop deterministic method for reliability-based design optimization", *Engineering Optimization*, vol. 45, no. 4, pp. 435–458, 2013.

[134] V. Ho-Huu, T. Le-Duc, L. Le-Anh, T. Vo-Duy, and T. Nguyen-Thoi, "A global single-loop deterministic approach for reliability-based design optimization of truss structures with continuous and discrete design variables", *Engineering Optimization*, vol. 50, no. 12, pp. 2071–2090, 2018.

[135] H. Zhang, Y. Aoues, H. Bai, D. Lemosse, and E. S. de Cursi, "Kriging-based reliability-based design optimization using single loop approach", in *World Congress on Global Optimization*, Springer, 2019, pp. 991–1000.

[136] B. J. Bichon, M. S. Eldred, L. P. Swiler, S. Mahadevan, and J. M. McFarland, "Efficient global reliability analysis for nonlinear implicit performance functions", *AIAA journal*, vol. 46, no. 10, pp. 2459–2468, 2008.

[137] B. Echard, N. Gayton, and M. Lemaire, "Ak-mcs: An active learning reliability method combining kriging and monte carlo simulation", *Structural Safety*, vol. 33, no. 2, pp. 145–154, 2011.

[138] Z. Wang and P. Wang, "A maximum confidence enhancement based sequential sampling scheme for simulation-based design", *Journal of Mechanical Design*, vol. 136, no. 2, p. 021 006, 2014.

[139] M. K. Sadoughi, M. Li, C. Hu, C. A. MacKenzie, S. Lee, and A. T. Eshghi, "A high-dimensional reliability analysis method for simulation-based design under uncertainty", *Journal of Mechanical Design*, vol. 140, no. 7, 2018.

[140] X. Li, H. Qiu, Z. Chen, L. Gao, and X. Shao, "A local kriging approximation method using mpp for reliability-based design optimization", *Computers & Structures*, vol. 162, pp. 102–115, 2016.

[141] D. R. Jones, M. Schonlau, and W. J. Welch, "Efficient global optimization of expensive black-box functions", *Journal of Global optimization*, vol. 13, no. 4, pp. 455–492, 1998.

[142] B. J. Bichon, "Efficient surrogate modeling for reliability analysis and design", PhD thesis, Vanderbilt University, 2010.

[143] T. Cho and B. Lee, "Reliability-based design optimization using convex linearization and sequential optimization and reliability assessment method", *Structural Safety*, vol. 33, no. 1, pp. 42–50, 2011.

[144] I. Lee, K. Choi, L. Du, and D. Gorsich, "Dimension reduction method for reliability-based robust design optimization", *Computers & Structures*, vol. 86, no. 13-14, pp. 1550–1562, 2008.

[145] Z. Chen, H. Qiu, L. Gao, L. Su, and P. Li, "An adaptive decoupling approach for reliability-based design optimization", *Computers & Structures*, vol. 117, pp. 58–66, 2013.

[146] B. Keshtegar and P. Hao, "Enhanced single-loop method for efficient reliability-based design optimization with complex constraints", *Structural and Multidisciplinary Optimization*, vol. 57, no. 4, pp. 1731–1747, 2018.

[147] A. Singh, Z. P. Mourelatos, and J. Li, "Design for lifecycle cost using time-dependent reliability", *Journal of Mechanical Design*, vol. 132, no. 9, 2010.

[148] C. Gong and D. M. Frangopol, "An efficient time-dependent reliability method", *Structural Safety*, vol. 81, p. 101 864, 2019.

[149] Y. Wang, S. Zeng, and J. Guo, "Time-dependent reliability-based design optimization utilizing nonintrusive polynomial chaos", *Journal of Applied Mathematics*, vol. 2013, 2013.

[150] S. O. Rice, "Mathematical analysis of random noise", *Bell System Technical Journal*, vol. 23, no. 3, pp. 282–332, 1944.

[151] C. Andrieu-Renaud, B. Sudret, and M. Lemaire, "The phi2 method: A way to compute time-variant reliability", *Reliability Engineering & System Safety*, vol. 84, no. 1, pp. 75–86, 2004.

[152] B. Sudret, "Analytical derivation of the outcrossing rate in time-variant reliability problems", *Structure and Infrastructure Engineering*, vol. 4, no. 5, pp. 353–362, 2008.

[153] Z. Hu and X. Du, "Mixed efficient global optimization for time-dependent reliability analysis", *Journal of Mechanical Design*, vol. 137, no. 5, 2015.

[154] Z. Wang and P. Wang, "A nested extreme response surface approach for time-dependent reliability-based design optimization", *Journal of Mechanical Design*, vol. 134, no. 12, 2012.

[155] Z. Hu and X. Du, "Reliability-based design optimization under stationary stochastic process loads", *Engineering Optimization*, vol. 48, no. 8, pp. 1296–1312, 2016.

[156] E. Polak, *Optimization: algorithms and consistent approximations*. Springer Science & Business Media, 2012, vol. 124.

[157] H. Zhang, Y. Aoues, D. Lemosse, H. Bai, and E. S. De Cursi, "Time-variant reliability-based optimization with double-loop kriging surrogates", in *International Symposium on Uncertainty Quantification and Stochastic Modeling*, Springer, 2020, pp. 436–446.

[158] V. Dubourg, "Adaptive surrogate models for reliability analysis and reliability-based design optimization", PhD thesis, 2011.

[159] B. A. Lockwood and M. Anitescu, "Gradient-enhanced universal kriging for uncertainty propagation", *Nuclear Science and Engineering*, vol. 170, no. 2, pp. 168–195, 2012.

Appendix A

Blade Element Momentum theory

A.1 Rankine-Froude actuator disc theory and Betz limit

The classical Rankine-Froude theory considers the balance of axial-momentum far-up and downstream of the rotor for a uniformly loaded disc, the theory is established under the following assumptions[13]–[15]:

1. The air is stable, homogeneous, in-compressible without friction.
2. There are infinite number of blades.
3. There is no rotational component of the flow.
4. The velocity through the disc is continuous.
5. The pressure per unit over the disc is constant.

The model is shown in Figure.A.1.

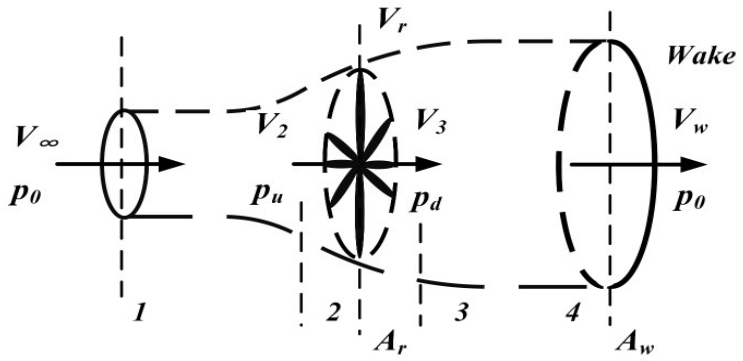

Figure A.1: Idealized flow through a wind turbine modeled by an actuator disc

In the Figure.A.1, p, V are the pressure and speed at different locations, from far-up, to far-wake.

For a 1D, uncompressed, steady flow, by applying the balance of axial momentum from

far-up and downstream of rotor, the force of wind on the turbine, the thrust T, can be expressed as:

$$T = \dot{m}(V_\infty - V_w) \tag{A.1}$$

where $\dot{m} = \rho A_r V_r$ is the air flow rate through the disk, A_r is the area at rotor, ρ is density of air, using the mass conservation and uncompressed presumption, $A_r V_r = A_w V_w$.

Considering the conservation of kinetics, the Bernoulli function for each side of the rotor are given:

$$\begin{aligned} p_0 + \tfrac{1}{2}\rho V_\infty^2 &= p_u + \tfrac{1}{2}\rho V_r^2 \\ p_d + \tfrac{1}{2}\rho V_r^2 &= p_0 + \tfrac{1}{2}\rho V_w^2 \end{aligned} \tag{A.2}$$

The pressure decrease at the rotor, $\Delta p = p_u - pd$ is calculated from Equation.A.2:

$$\Delta p = \frac{1}{2}\rho \left(V_\infty^2 - V_w^2\right) \tag{A.3}$$

The thrust also be expressed by the decrease of pressure with the area at the rotor:

$$T = \Delta p A_r \tag{A.4}$$

By equating Equation.A.1 and Equation.A.4, also considering $\dot{m} = \rho A_r V_r$, the air speed at rotor plane is:

$$V_r = \frac{V_\infty + V_w}{2} \tag{A.5}$$

An axial induction factor a is defined as the ratio between the fractional speed decrease at the rotor plane and far downstream:

$$a = \frac{V_\infty - V_r}{V_\infty} \tag{A.6}$$

The power output equal to the thrust times the flow speed at rotor:

$$P = T V_r \tag{A.7}$$

Combining Equation.A.3 $\sim$ Equation.A.7, the resultant thrust force and power output are

given as:

$$\begin{aligned} T &= 2\rho A_r a(1-a)V_\infty^2 \\ P &= 2\rho A_r a(1-a)^2 V_\infty^3 \end{aligned} \tag{A.8}$$

Dividing the thrust force and power output in Equantion.A.8 by $0.5\rho A_r V_\infty^2$ and $0.5\rho A_r V_\infty^3$ respectively, the thrust force and power output are expressed in dimensionless coefficients C_T and C_P:

$$\begin{aligned} C_T &= 4a(1-a) \\ C_P &= 4a(1-a)^2 \end{aligned} \tag{A.9}$$

Note that thrust coefficient C_P has a global optimum C_P^{max} at $a = 1/3$. This C_P^{max} is called Betz limit, indicating the maximum theoretical power output from a wind turbine tower.

A.1.1 Generalized momentum theory

The Rankine-Froude actuator disc theory is generalized to include effect of wake rotation of wind turbine rotor as shown in FigureA.2: R is the radius at the rotor tip. The flow behind the rotor rotates in the opposite direction of the rotor, while the axial component of the velocity remains constant. The angular velocity the air relative to the blade increases from Ω to $\Omega + \omega$, where ω is the speed imparted by the rotor. Similar to Equation.A.3, the pressure decrease $\Delta p'$ can be calculated as:

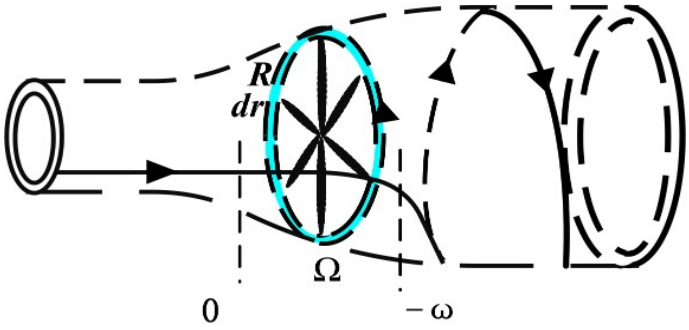

Figure A.2: Effect of wake rotation

$$\Delta p' = \frac{1}{2}\rho((\Omega+\omega)^2 - \Omega^2)r^2 \tag{A.10}$$

where r is the radius of the disc as shown in Figure.A.2.

Then the thrust introduced by angular momentum can be calculated by:

$$T = \Delta p' A_r \tag{A.11}$$

A similar angular induction factor a' is defined as:

$$a' = \omega/2\Omega \tag{A.12}$$

The thrust can then be expressed as:

$$dT = 4a'\left(1+a'\right)\frac{1}{2}\rho\Omega^2 r^2 2\pi r dr \tag{A.13}$$

Applying the conservation of angular momentum, the torque exerted on the rotor dQ can be expressed by the change in angular momentum of the wake:

$$dQ = \Delta m \omega r^2 = \rho V_R 2\pi r dr \omega r^2 \tag{A.14}$$

The power of each blade element dP can be calculated as:

$$dP = \Omega dQ \tag{A.15}$$

A.2 Blade Element method

The blade element method is another method of analyzing the forces of blades based on the geometry of the blade. As shown in Figure.A.3, along the blade, it is divided into small independent sections, with the width of the section being dr, the length of the section being c. α is the angle between the inflow and the chord line, θ is the sum of pitch angle and blade twist angle, ϕ is the angle between inflow with respect to plane rotation, which is the sum of θ and α .

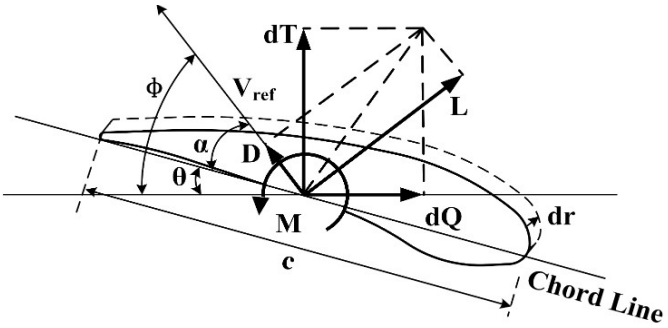

Figure A.3: Blade element geometry

On an airfoil, the forces are resolved into two forces: drag force F_D , and lift force F_L , and one moment M. These forces are then expressed as coefficients:

$$\begin{aligned} C_L &= \frac{F_L/Element}{0.5\rho V_{rel}^2 c} \\ C_D &= \frac{F_D/Element}{0.5\rho V_{rel}^2 c} \end{aligned} \tag{A.16}$$

Here V_{ref} is the incoming flow velocity relative to the airfoil, which can be derived from geometry relationship and Equation.A.6 :

$$\begin{aligned} V_{ref} &= V_\infty(1-a)/\sin(\phi) \\ \tan(\phi) &= \frac{V_\infty(1-a)}{\Omega r(1+a')} \end{aligned} \tag{A.17}$$

For a wind turbine rotor consists of B rotors, the differential thrust dT and differential torque dQ can be expressed as:

$$\begin{aligned} dT &= B\tfrac{1}{2}\rho V_{rel}^2 \left[C_L\cos(\phi) + C_D\sin(\phi)\right] cdr \\ dQ &= B\tfrac{1}{2}\rho V_{rel}^2 \left[C_L\sin(\phi) - C_D\cos(\phi)\right] crdr \end{aligned} \tag{A.18}$$

A.3 Blade element momentum theory

As the name indicates, the blade element momentum theory (BEM) is established by combining the thrust and torque equations from momentum theory and blade element theory (Equation.A.13, Equation.A.14, Equation.A.18). Before applying BEM theory, the thrust and torque of Equation.A.13 and Equation.A.14 are multiplied by a tip-loss factor F that is summarized by Wilson[16] to account for the finite number of blades and finite radius of

blades.

$$F = \left(\frac{2}{\pi}\right)\cos^{-1}\left[e^{-\frac{B(R-r)}{2r\sin(\phi)}}\right] \tag{A.19}$$

Then the equations results in:

$$\left(\frac{a}{1-a}\right)\left[\frac{\sin^2(\phi)}{\cos(\phi)}\right] = \left(\frac{Bc}{2\pi r}\right)\left(\frac{C_L}{4F}\right)\left[1+\frac{C_D\sin(\phi)}{C_L\cos(\phi)}\right] \tag{A.20}$$

$$\left(\frac{\Omega r}{V_0}\right)\left[\frac{\sin(\phi)}{\cos(\phi)}\right]\left(\frac{a'}{1-a}\right) = \left(\frac{Bc}{2\pi r}\right)\left(\frac{C_L}{4F}\right)\left[\frac{1}{\cos(\phi)}-\frac{C_D}{C_L\sin(\phi)}\right] \tag{A.21}$$

To the equations above for the induction factor a and a', the drag coefficient C_D is set to zero to simplify the problem, which according to Welson[16], this will add negligible errors. The final results that after algebraic manipulation, considering $C_D = 0$ and Equation.A.15, Equation.A.17 is summarized as:

$$C_L = \frac{4F\sin(\phi)}{\sigma}\frac{(\cos(\varphi)-\sin(\phi))}{(\sin(\phi)+\lambda_r\cos(\phi))} \tag{A.22}$$

$$C_P = \frac{8}{\lambda^2}\int_{\lambda_h}^{\lambda}\left[\begin{array}{c} F\sin^2(\phi)\,(\cos(\phi)-\lambda_r\sin(\phi))\,(\sin(\phi) \\ +\lambda_r\cos(\phi)\left[1-\frac{C_D\cos(\phi)}{C_L\sin(\phi)}\right]\lambda_r^2 \end{array}\right] d\lambda_r \tag{A.23}$$

Here $\sigma = Bc/2\pi r$ is the solidity radio, $\lambda = \Omega R/V_\infty$ is tip speed radio, $\lambda_r = \lambda r/R$ is the local speed ratio.

The lift coefficient and power coefficient are functions of angle attack α, annular radius r, wind speed V_0, number of blades B, blade radius R, pitch, twist, chord distribution c, and rotation speed Ω. These are used for calculating the response of wind turbine system and optimizing the performance of wind turbine tower.